DOE/ID/13104--1

# ELECTROLYSIS OF NEODYMIUM OXIDE

**Final Report for the Period**
**August 19, 1991 through February 28, 1997**

**R. Keller**
**K. T. Larimer**

**May 1997**

**Work Performed Under Contract No. FC07-91ID13104**

**For**
**U.S. Department of Energy**
**Assistant Secretary for**
**Energy Efficiency and Renewable Energy**
**Washington, DC**

**By**
**EMEC Consultants**
**Export, PA**

MASTER

DISTRIBUTION OF THIS DOCUMENT IS UNLIMITED

DISCLAIMER

Portions of this document may be illegible in electronic image products. Images are produced from the best available original document.

## DISCLAIMER

This report was prepared as an account of work sponsored by an agency of the United States Government. Neither the United States Government nor any agency thereof, nor any of their employees, makes any warranty, express or implied, or assumes any legal liability or responsibility for the accuracy, completeness, or usefulness of any information, apparatus, product, or process disclosed, or represents that its use would not infringe privately owned rights. Reference herein to any specific commercial product, process, or service by trade name, trademark, manufacturer, or otherwise does not necessarily constitute or imply its endorsement, recommendation, or favoring by the United States Government or any agency thereof. The views and opinions of authors expressed herein do not necessarily state or reflect those of the United States Government or any agency thereof.

**DOE/ID/13104**
**Distribution Category UC-1419**

# ELECTROLYSIS OF NEODYMIUM OXIDE

Final Report for the Period
August 19, 1991 through February 28, 1997

RECEIVED
AUG 29 1997
OSTI

Rudolf Keller
Kirk T. Larimer

May 1997

Work Performed Under Contract No. FC07-91ID13104

Prepared for the
U.S. Department of Energy
Assistant Secretary for
Energy Efficiency and Renewable Energy
Washington, DC

Prepared by
EMEC Consultants
Export, PA 15632

# FOREWORD

This Final Report was submitted by EMEC Consultants to the Department of Energy according to the reporting requirements of Cooperative Agreement No. DE-FC07-91ID13104. It describes and discusses the project activities during the period 19 August 1991 to 28 February 1997.

The following members of EMEC Consultants' staff contributed to this report: D. L. Anthony (supporting experimentation), W. C. Cochran (Chemical Hygiene Officer), D. G. Gatty (main experimentation), D. M. Hydock (materials studies), R. Keller (Principal Investigator), K. T. Larimer (Research Engineer conducting and coordinating main experimentation), and D. B. Stofesky (flow modeling). In addition, C. N. Cochran and C. O. Bounds contributed an economic/benefit analysis in the Phase I part.

C. N. Cochran and W. E. Haupin participated as consultants, and H. E. Smith as a laboratory assistant on temporary assignment. The experimental work was performed in EMEC Consultants' laboratory in New Kensington, Pennsylvania.

The effort benefitted from the cooperation with Rhône-Poulenc Basic Chemicals Company which provided the cost share. Dr. Charles O. Bounds, Director of R&D, Rare Earths and Gallium, Cranbury, New Jersey, made the interactions particularly productive and enjoyable.

Mr. J. Donald Talbot, Consultant, provided appreciated support in estimating costs.

We gratefully acknowledge the support of the DOE Idaho Operations Office, with Mr. D. W. Robertson and Mr. J. Yankeelov serving as Project Managers. We thank Mr. J. V. Anderson and Dr. Charles Mohr, Idaho National Engineering Laboratory, who served as Technical Monitors, for their interest and advice, also Mr. J. O. Lee, Ms. K. Stallman, Ms. L. A. Hallum, and Ms. C. L. Bruns for negotiating and administering the agreement. We also owe thanks, in particular, to Mr. M. J. McMonigle, DOE Office of Industrial Technologies, Washington, D.C., for his interest, support, and stimulating discussions, as well as his successors, Dr. Larry Boxall and Dr. Sarah Dillich.

This report is structured in two separately paginated parts, according to the two phases of the three-phase program that were actually conducted; the planned progression into pilot scale studies was cancelled by the Department of Energy.

The total project costs were approximately as budgeted and approved:

| | | |
|---|---|---|
| Phase I | $ 524,803.39 | total |
| | $ 42,113.39 | cost share |
| | $ 482,690.00 | Federal share |
| Phase II (projected) | $ 948,843.00 | total |
| | $ 189,773.00 | cost share |
| | $ 759,070.00 | Federal share |
| Total (projected) | $ 1,473,646.39 | total |
| | $ 231,886.39 | cost share |
| | $ 1,241,176.00 | Federal share |

EMEC Consultants submitted a patent application to the United States Office of Patents and Trademarks. It covers proprietary aspects of this report in its entirety.

This report was prepared as an account of work sponsored by an agency of the United States Government. Neither EMEC Consultants, its owner, nor any of its employees or consultants makes any warranty, expressed or implied, or assumes any legal liability or responsibility for the accuracy, completeness, or usefulness of any information, apparatus, product, or process disclosed, or represents that its use would not infringe privately owned rights. Reference herein to any specific commercial product, process or service by trade name, trademark, manufacturer, or otherwise, does not necessarily constitute or imply its endorsement, recommendation, or favoring by EMEC Consultants, by the United States Government, or by any agency thereof.

# SUMMARY

## STATEMENT OF OBJECTIVES

The objective of this research was to develop an electrolytic process for the continuous and economic production of neodymium metal and neodymium alloys from neodymium oxide.

Phase I was to select an electrolyte for efficient operation (electrical conductivity, and metal and oxide solubilities) relatively free from envisioned problems (anode effect and cathode scum), and to perform an economic and energy-savings assessment of the process and the end-use motor applications.

The objectives of Phase II were to demonstrate achievement of critical process parameters at laboratory-scale, to establish preferred operating conditions, and to define the boundaries of acceptable operation for subsequent design of a pilot cell. Goals included: development of continuous feeding, metal siphoning, and off-gas treating strategies; cell operations for periods of 100 hours with current efficiencies greater than 50 % at a high level of neodymium oxide utilization; establishment of electrode wear rates and patterns in representative geometrical arrangements; and achievement of favorable metal quality.

Phase III (cancelled by DOE) was to demonstrate this technology at pilot-scale.

## USE AND PRODUCTION OF NEODYMIUM

Neodymium is one of the dominant rare earth elements, typically occurring in rare earth ores at concentrations of about 10 to 15 wt%. Correspondingly, it is a major component of misch metal (mixture of rare-earth metals, in naturally occurring or processed composition). Recently, neodymium has found increased use as constituent in advanced permanent magnets; with the composition $Nd_2Fe_{14}B$ as a basis, extremely high field strengths have been demonstrated. Neodymium also is receiving attention as a component in alloys for metal hydride battery electrodes.

The application of primary interest in this effort is the use in magnets for high-efficiency electric motors. Based on an analysis of cost benefits and potential energy savings presented in the Phase I part of the report, it has been projected that annual energy savings of 1.7 quadrillion Btu could result from implementation of new technology involving

neodymium-containing permanent magnets; part of the savings are to be achieved by higher efficiency of electric motors, a smaller fraction by weight reductions in the transportation sector.

Neodymium presently is mainly produced by calciothermic reduction in a batch process. Electrolysis would have the advantage of continuous operation and actually has been implemented with neodymium halides as feed material. These halides are manufactured from the oxide or from solutions. A direct electrolysis of neodymium oxide, essentially the chemical form occurring naturally, would be more cost-effective. The total reduction of operating costs in the production of neodymium by substituting an efficient neodymium oxide electrolysis for the calciothermic production is estimated to exceed 30 percent.

## NEODYMIUM OXIDE ELECTROLYSIS

Neodymium oxide is the neodymium compound most readily available for the production of neodymium metal or alloys. The oxide, $Nd_2O_3$, can be electrolyzed to obtain the metal:

$$2\ Nd_2O_3 + 3\ C \longrightarrow 4\ Nd + 3\ CO_2\ .$$

This process is analogous to the electrolysis of aluminum oxide in Hall-Héroult cells and is also conducted in fluoride-based molten salt electrolyte with carbon anodes. Investigations by the Bureau of Mines have shown promising possibilities for the production of neodymium by such an electrolytic process. It was the main objective of the present work to refine the approach, identify and overcome obstacles, and to develop a commercially attractive process to the pilot stage.

## EXPERIMENTAL INVESTIGATIONS

Phase I investigations focused on

- the selection of electrolyte compositions and determination of electrolyte properties;
- the study of electrode reactions and sludge formation at the metal-electrolyte interface;
- electrolysis experiments on a 5 to 20 A scale.

Early experiments were conducted in the $CaF_2$-LiF-CaO-$Nd_2O_3$ system. High oxide contents were expected to eliminate anode effect problems. Excessive solubility of reactive metal was found and made it advisable to switch to the $NdF_3$-LiF-$Nd_2O_3$ system.

The phase diagram for $NdF_3$-LiF shows a eutectic composition of 64.6 wt% $NdF_3$ / 35.4 wt% LiF at a eutectic temperature of about 720 °C. Electrolysis in the temperature range of 800 to 900 °C is readily possible in this system. Although no liquid neodymium (pure) metal can be deposited at such temperatures, liquid Fe-Nd alloys are obtained using iron cathodes.

When Nd-Fe alloy was exposed to eutectic $NdF_3$-LiF electrolyte, with and without oxide additions, the formation of a dark viscous layer in the electrolyte above the metal-bath interface was observed. After solidification, neodymium metal was found in this layer, in amounts that were about tenfold higher in the presence of neodymium oxide. It is postulated that the oxide content fosters the formation of subvalent neodymium species, thus the dissolution of reactive metal, and that this leads to the formation of the dark viscous layer.

This then evidenced the following dilemma: while a high oxide content is desirable to electrolyze oxide without anode effect, it leads to current efficiency losses due to high metal dissolution and reoxidation. This was confirmed in electrolysis experiments. Operational conditions, however, were found that yielded high current efficiencies with smooth operation at the anode. In a 20-A cell, current efficiencies of up to 87 % were achieved at cell voltages of 5 to 6.5 V.

Electrolysis experiments were conducted in a closed Inconel vessel that permitted operation with an inert atmosphere and collection of off-gases for analysis. It was observed that the best results were achieved in a regime that produced carbon tetrafluoride ($CF_4$) as a component in the off-gas, typically at a content of about 20 mole%. Experimental studies showed that $CF_4$ can be converted to $CO_2$ by reaction with neodymium oxide at elevated temperatures. Off-gas treatment with cell feed and recuperation of fluoride values appeared to be a potentially viable option.

Phase II investigations that followed focused on

- achieving consistently good results at the 10-20-A level;
- validating a modified concept assuring the absence of perfluorinated carbon compounds (PFCs) in the off-gases;
- scaling-up to the 100-A cell level;
- identifying critical parameters to be considered for large-scale cell design;
- operating a 100-A cell consistently for an extended time period of 96 hours.

While electrolysis experiments to produce appreciable amounts of neodymium-iron alloy at high quality and with acceptable current efficiency and utilization efficiency for the oxide occupied center stage, supporting research yielded increased knowledge on metal solubility,

oxide dissolution, anode effect occurrence, electrolyte flow conditions, and materials preparation.

Operating with a current of 20 A, conditions were identified at which operation proceeded smoothly and yielded good results. No anode effects interrupted the production, but the off-gases contained significant amounts of perfluorinated carbon compounds ($CF_4$ and $C_2F_6$). It was discovered that under certain conditions an electrolysis regime exists at relatively high voltage, in which high currents can be maintained with only partial occurrence of an oxide-related anode effect that manifests itself, however, by the anodic formation of PFCs. Subsequent efforts focusing on an electrolysis in a low-voltage regime, where no undesirable perfluorinated carbon compounds are emitted, were successful. Experiments were carried into the 100-A scale where good-quality alloy was produced in 96-hour experiments at current efficiencies exceeding 60 percent; only CO and $CO_2$ were present in the off-gases.

Details to be considered in cell construction and operation were discovered. It is important that the oxide concentration of electrolyte contacting metal product and cathodes is as low as possible. Reoxidation of neodymium, furthermore, can be minimized by reducing mass transport rates in the cathode region, also by eliminating opportunities for corrosive action provided by the contact of metal product with other metallic components of the cell.

Preliminary plans for a pilot cell were made. As Phase II goals were met, a logical continuation will involve the construction and operation of a pilot or prototype cell.

## ENVIRONMENTAL IMPLICATIONS

Other sources have patented or are practicing a neodymium oxide electrolysis. There are indications that in all cases the electrolysis is conducted in a high-voltage regime in which substantial amounts of perfluorinated carbon compounds are emitted. Based on our results, we estimate that an annual production of 2,000 t of neodymium potentially may produce as much or more of the undesirable greenhouse gases as the entire domestic aluminum industry. A costly treatment of the cell off-gases to remove the chemically unreactive compounds $CF_4$ and $C_2F_6$ seems inevitable; avoiding their formation is clearly more attractive.

## RECOMMENDATIONS

The essential goals of Phases I & II were met. A concept for a cost-effective, energy-efficient and environmentally acceptable process was established, based on experimental results on the scale of up to 100 A. A continuation into pilot cell experimentation in the planned Phase III was recommended to the Department of Energy, but refocussing of the program at the Office of Industrial Technologies eliminated any funding for such a continuation.

An opportunity may have been lost. An aggressive progression into a pilot scale campaign may have led to establishing a technology in the United States that would have given the domestic industry a competitive advantage. With lower-risk technological alternatives and foreign sources for neodymium available, it appears likely that the technology successfully developed by this program will not be utilized. On the other hand, global restrictions in the emission of greenhouse gases may re-establish interest in our technology.

Aside from neodymium for magnetic materials, misch metal is a related rare earth product that is rapidly gaining importance. It is recommended that the prospects of cost-reduction by adapting our concept to the production of misch metal be examined.

## PUBLICATIONS

R. Keller and K. T. Larimer, "Anode Effect in Neodymium Oxide Electrolysis", in Rare Earths, Science, Technology and Applications, Vol. III, edited by R. G. Bautista, C. O. Bounds, T. W. Ellis and B. T. Kilbourn, published by TMS, pp. 175-180 (1997).

R. Keller, "Electrolytic Production of Neodymium -- With and Without Emission of Greenhouse Gases", accepted for presentation and publication of extended abstract for the 1997 Joint International Meeting of The Electrochemical Society and the International Society of Electrochemistry, Paris, September 1997.

# Neodymium Oxide Electrolysis

**PHASE I FINAL REPORT**

**For the Period 19 August 1991 - 30 March 1994**

Principal Authors:

Rudolf Keller
Kirk T. Larimer

Contributing Authors:

Charles O. Bounds, Rhône-Poulenc, Inc.
C. Norman Cochran, Consultant

3 August 1994

Work Performed Under Cooperative Agreement DE-FC07-91ID13104

For
U.S. Department of Energy
Office of Industrial Technologies

By
EMEC Consultants
Export, PA 15632

# ELECTROLYSIS OF NEODYMIUM OXIDE

**Final Report**
**for the Period 19 August 1991 - 30 March 1994**

Rudolf Keller
Kirk T. Larimer

3 August 1994

EMEC Consultants
4221 Roundtop Road
Export, PA 15632

Work Performed Under Cooperative Agreement No. DE-FC07-91ID13104

Prepared for
the U.S. Department of Energy
Office of Industrial Technologies

# FOREWORD

This Final Report was submitted by EMEC Consultants to the Department of Energy according to the reporting requirements of Cooperative Agreement No. DE-FC07-91ID13104. It describes and discusses the project activities during the period 19 August 1991 to 30 March 1994.

The following members of EMEC Consultants' staff contributed to this report: D. L. Anthony, W. C. Cochran, D. G. Gatty, D. M. Hydock, R. Keller, K. T. Larimer, and D. B. Stofesky. In addition, C. N. Cochran and W. E. Haupin participated as consultants, and H. E. Smith as a laboratory assistant on temporary assignment. The experimental work was performed in EMEC Consultants' laboratory in New Kensington, Pennsylvania.

The effort benefitted from the cooperation with Rhône-Poulenc Basic Chemicals Company which provided the cost share. Dr. Charles O. Bounds, Director of R&D, Rare Earths and Gallium, Cranbury, New Jersey, made the interactions particularly productive and enjoyable.

We gratefully acknowledge the support of the DOE Idaho Operations Office, with Mr. D. W. Robertson serving as Project Manager. We thank Mr. J. V. Anderson, EG&G Idaho, who was the Technical Monitor, for his interest and advice, also Mr. J. O. Lee, Ms. K. Stallman, Ms. L. A. Hallum, and Ms. C. L. Bruns for negotiating and administering the agreement. We also owe thanks to Mr. M. J. McMonigle, DOE Office of Industrial Technologies, Washington, D.C., for his interest, support, and stimulating discussions.

This report was prepared as an account of work sponsored by an agency of the United States Government. Neither EMEC Consultants, its owner, nor any of its employees or consultants makes any warranty, expressed or implied, or assumes any legal liability or responsibility for the accuracy, completeness, or usefulness of any information, apparatus, product, or process disclosed, or represents that its use would not infringe privately owned rights. Reference herein to any specific commercial product, process or service by trade name, trademark, manufacturer, or otherwise, does not necessarily constitute or imply its endorsement, recommendation, or favoring by EMEC Consultants, by the United States Government, or by any agency thereof.

# SUMMARY


## USE AND PRODUCTION OF NEODYMIUM

Neodymium is one of the dominant rare earth elements, typically occurring in rare earth ores at concentrations of about 10 to 15 wt%. Correspondingly, it is a major component of mischmetal. Recently, neodymium has found increased use as constituent in advanced permanent magnets; with the composition $Nd_2Fe_{14}B$ as a basis, extremely high field strengths have been demonstrated. Neodymium also is receiving attention as a component in alloys for metal hydride battery electrodes.

The application of primary interest in this effort is the use in magnets for high-efficiency electric motors. An analysis of cost benefits and potential energy savings is presented in this report. It is projected that annual energy savings of 1.7 quadrillion Btu could result from implementation of new technology involving neodymium-containing permanent magnets, part of the savings achieved by higher efficiency of motors, a smaller fraction by weight reductions in the transportation sector.

Neodymium presently is mainly produced by calciothermic reduction in a batch process. Electrolysis would have the advantage of continuous operation and actually has been implemented with neodymium halides as feed material. These halides are manufactured from the oxide, and a direct electrolysis of neodymium oxide would be more cost-effective. A techno-economic comparison of electrolytic and calciothermic reduction is presented in this report. The total reduction of operating costs in the production of neodymium is estimated to exceed 30 percent if an efficient neodymium oxide electrolysis process can be implemented.

## NEODYMIUM OXIDE ELECTROLYSIS

Neodymium oxide is the neodymium compound most readily available for the production of neodymium metal or alloys. The oxide, $Nd_2O_3$, can be electrolyzed to obtain the metal:

$$2\ Nd_2O_3 + 3\ C \ \text{----}> \ 4\ Nd + 3\ CO_2\ .$$

This process is analogous to the electrolysis of aluminum oxide in Hall-Héroult cells and is also conducted in fluoride-based molten salt electrolyte with carbon anodes. Investigations by the Bureau of Mines have shown promising possibilities for the production of neodymium by an electrolytic process. It is the main objective of the present work to refine the approach and to develop it to the pilot stage.

## EXPERIMENTAL INVESTIGATIONS

The present investigations focused on

- the selection of electrolyte compositions and determination of electrolyte properties
- the study of electrode reactions and sludge formation at the metal-electrolyte interface
- electrolysis experiments on a 5 to 20 A scale.

Early experiments were conducted in the $CaF_2$-LiF-CaO-$Nd_2O_3$ system. High oxide contents were expected to eliminate anode effect problems. Excessive solubility of reactive metal was found and made it advisable to switch to the $NdF_3$-LiF-$Nd_2O_3$ system.

The phase diagram for $NdF_3$-LiF shows a eutectic composition of 64.6 wt% $NdF_3$ / 35.4 wt% LiF at a eutectic temperature of about 720 °C. Electrolysis in the temperature range of 800 to 900 °C is readily possible in this system. Although no liquid neodymium (pure) metal can be deposited at such temperatures, liquid iron-neodymium alloys are obtained using iron cathodes.

When Nd-Fe alloy was exposed to eutectic $NdF_3$-LiF electrolyte, with and without oxide additions, the formation of a dark viscous layer in the electrolyte above the metal-bath interface was observed. After solidification, neodymium metal was found in this layer, in amounts that were about tenfold higher in the presence of neodymium oxide. It is postulated that the oxide content fosters the formation of subvalent neodymium species, thus the dissolution of reactive metal, and that this leads to the formation of the dark viscous layer.

This then evidenced the following dilemma: while a high oxide content is desirable to electrolyze oxide without anode effect, it leads to current efficiency losses due to high metal dissolution and reoxidation. This was confirmed in electrolysis experiments. Operational conditions, however, were found that yielded high current efficiencies with smooth operation at the anode. In a 20-A cell, current efficiencies of up to 87 % were achieved at cell voltages of 5 to 6.5 V.

Electrolysis experiments were conducted in a closed Inconel vessel, as shown in Figure 1. The bottom of the vessel containing the electrolytic cell was placed in a crucible furnace, to be kept at the desired high temperature. Electrical connections were made through the water-cooled top. The sealed system permitted operation with an inert atmosphere and collection of off-gases for analysis.

It was observed that the best results were achieved in a regime that produced carbon tetrafluoride ($CF_4$) as a component in the off-gas, typically at a content of about 20 mole%. Experimental studies showed that $CF_4$ can be converted to $CO_2$ by reaction with neodymium

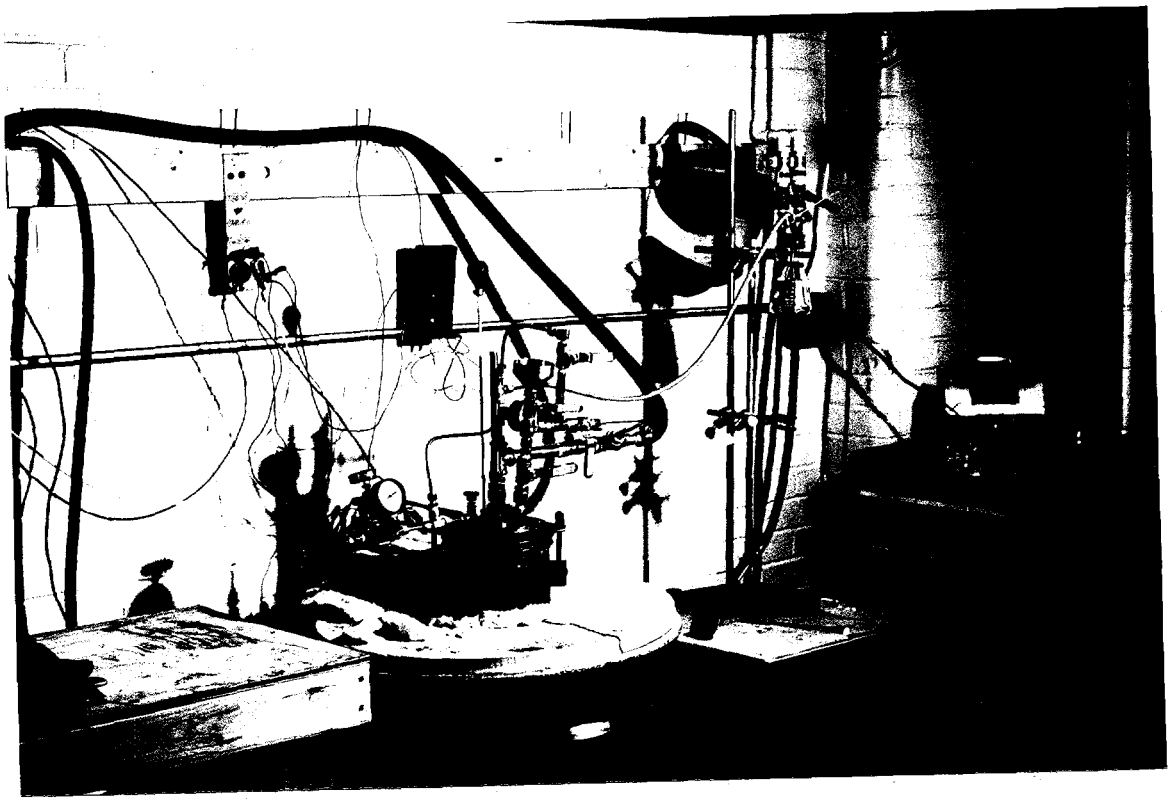

**Figure 1** Electrolysis Arrangement with Closed Inconel Vessel

oxide at elevated temperatures. Off-gas treatment with cell feed and recuperation of fluoride values appears to be a viable option.

## RECOMMENDATIONS AND FUTURE WORK

Prospects for an electrolytic production of iron-neodymium alloy with neodymium oxide as the feed are good. It is recommended to pursue further process development.

While current efficiencies exceeding 50 percent have been achieved regularly in 20-A experiments, some inconsistencies in cell operation persisted. Future work should focus on this point, examining in more detail the anode reaction, with emphasis on off-gas analysis. Scale-up to the 100-A level then should follow.

# CONTENTS

## LIST OF FIGURES

## LIST OF TABLES

# INTRODUCTION

## USE AND PRODUCTION OF NEODYMIUM

Neodymium is a rare earth metal. In ores it is usually associated with the more dominant lanthanum. The metal has a bright silvery metallic luster. Neodymium is one of the more reactive rare earth metals and tarnishes in air, forming an adherent or non-adherent, protective or non-protective oxide.

Neodymium oxide ($Nd_2O_3$) is used in specialty glasses and as a colorant for enamels. The metal, in conjunction with iron and boron, has been found to yield permanent magnets with very high field strength. Recently it is also receiving attention as a component in alloys for metal hydride battery electrodes.

The application of primary interest in this effort is the use in magnets for high-efficiency electric motors. With the composition $Nd_2Fe_{14}B$ as a basis, field strengths of up to 38-45 MOe have been demonstrated. Such material is being used in small compact electric motors for special applications. A broader user in high-efficiency motors could lead to substantial energy savings.

Neodymium can be produced by reducing its halides such as neodymium fluoride with a reactive metal such as calcium. An alternative approach is electrolysis. In an approach developed at General Motors, the electrolysis of calcium has been combined with the subsequent reduction of neodymium. This "NEOCHEM" process and other major processes have been reviewed by Sharma [1].

At the present time, most commercial neodymium is produced by reduction of its fluoride with calcium by the following reaction:

$$3\ Ca + 2\ NdF_3 \longrightarrow 3\ CaF_2 + 2\ Nd\ .$$

This is a somewhat cumbersome batch process and requires the preparation of calcium metal by electrolysis of calcium chloride.

Rare earth metals are frequently produced by the electrolysis of their anhydrous chlorides. The electrolyte consists of the rare earth chloride and alkali or alkaline-earth chlorides. Typical temperatures are 800 to 900 °C. These temperatures are below the melting point of neodymium (1020 to 1050 °C). Generally it is difficult in molten salt electrolysis to deposit and collect a solid metal, i.e. a metal deposited at a temperature below its melting point. If an iron-

neodymium (Fe-Nd) alloy is the required product, it is possible to recover the neodymium as component of a liquid alloy. According to the iron-neodymium phase diagram [2] (see Figure 3, p. 14), this permits one to operate at lower temperatures.

Electrolysis of neodymium metal was studied by the Bureau of Mines. While the electrolysis of neodymium chloride received some attention [3], several reports were published dealing with the electrolysis of rare earth oxides. An effort to produce lanthanum metal [4] preceded the electrolysis work on neodymium. This electrolysis was conducted with an electrolyte composed of 70 wt% $LaF_3$ / 20 wt% $BaF_2$ / 10 wt% LiF, which separated into two phases. The $La_2O_3$ solubility in the electrolyte was about 2 wt% at an operating temperature of 975 °C. Three bath compositions were employed in studies to produce neodymium [5]:

90 wt% $NdF_3$ / 10 wt% LiF
80 wt% $NdF_3$ / 20 wt% LiF
74 wt% $NdF_3$ / 26 wt% LiF

The solubility of $Nd_2O_3$ in these baths was determined to be about 2 wt%. The electrolysis produced a current efficiency of 78 %, an oxide utilization of about 60 %, and an atmosphere in the cell chamber of 7 mole% CO, 3 mole% $CO_2$, and 0.5 mole% $CF_4$, in helium. To achieve high current efficiency (CE), a thermal gradient cell was used, collecting the metal product at a lower temperature (740 °C) than the average electrolyte temperature (1198 °C). This work was extended to electrowinning of liquid rare-earth ferroalloys [6]. A samarium-iron alloy was of particular interest. Later rare-earth-cobalt alloys were studied because of their potential use as permanent magnet materials [7]. Cobalt-neodymium alloy was prepared with a CE of 73 %. Discussions about more recent, unpublished work, which included the exploration of composite anodes, were held with Bureau of Mines personnel in Reno [8].

Chinese authors reported short-term experiments to electrowin Nd-Fe alloy from $NdF_3$-LiF and $NdF_3$-LiF-$BaF_2$ melts [9]. They observed maximum current efficiency over a temperature range of 990 - 1020 °C, and a negative effect on current efficiency when samarium and europium impurities were present.

An electrolysis process is expected to yield a pure metal whose quality is essentially governed by the purity of the feed materials (including carbon anodes). It is, furthermore, possible to co-deposit alloy components.

## ELECTROLYSIS OF NEODYMIUM OXIDE AND GOALS OF THE PRESENT EFFORT

Neodymium oxide is the most readily available compound for the production of neodymium metal or alloys. The oxide, $Nd_2O_3$, can be electrolyzed to obtain the metal:

$$2\ Nd_2O_3 + 3\ C \ ----> \ 4\ Nd + 3\ CO_2\ ,$$

by the following electrochemical reactions:
at the cathode:

$$Nd_2O_3 + 6\ e^- \ ----> \ 2\ Nd + 3\ O^{2-}$$

and at the anode:

$$Nd_2O_3 + 3\ C \ ----> \ 2\ Nd^{3+} + 3\ CO_2 + 6\ e^-\ .$$

These equations represent overall reactions and do not reflect details of the reaction mechanism.

The approach is similar to the Hall-Héroult process to produce primary aluminum. Carbon anodes are employed and minimal metallic contaminants are introduced by the anode.

It is conceivable to conduct the electrolysis with oxygen-evolving anodes, employing a technology that is being developed for aluminum production with the support of the Department of Energy:

$$2\ Nd_2O_3 \ ----> \ 4\ Nd + 3\ O_2\ .$$

Very likely, however, the use of such anodes would lead to undesirable impurities in the electrolyte and, consequently, in the metal. An iron-oxide based anode could be an exception, if iron-containing neodymium alloys are produced.

The present effort contributes to the development of a cost-effective neodymium oxide electrolysis process, yielding a high-quality product. Critical aspects were examined on the small laboratory scale. Main issues were the selection of electrolyte composition, including determination of electrolyte properties, and the study of reactions and sludge formation at the metal-electrolyte interface. Based on the experimental results of these studies, conditions were chosen to conduct electrolysis experiments at the 5 to 20 A scale. The major goal of these experiments was to achieve a high current efficiency at smooth cell operation, without anode effect problems and without excessive build-up of sludge.

# EXPERIMENTAL RESULTS

## OVERVIEW

The effort was started with a study of electrolyte properties. It was hoped that a suitable electrolyte composition with a high oxide concentration could be found for neodymium deposition to avoid the occurrence of anode effects. The concentration of neodymium compounds would not necessarily have to be as high as in traditionally selected electrolyte compositions. In previous work [10], the system $CaF_2$-LiF-CaO showed promise for the dissolution and electrolytic reduction of various oxides. Properties of such melts, with neodymium compounds added, were determined, but electrolysis experiments showed that the approach had severe shortcomings.

Electrolysis experiments were subsequently performed with electrolytes based on the system $NdF_3$-LiF-$Nd_2O_3$. Two cells to operate in sealed Inconel containers were constructed, one for currents of 5 to 10 A, the other for 20 A. The focus of the electrolysis experiments was primarily on achieving high current efficiencies. To reduce reactive metal activities in the electrolyte, low operating temperatures were stressed, and cathodic formation of iron-neodymium alloy was favored over the deposition of pure neodymium. Current efficiencies of up to 87 % were achieved, but inconsistencies plagued the experimentation.

Study of interactions between the metal product and the electrolyte was emphasized in a special study. It was found that high oxide concentrations fostered the formation of scum above the metal surfaces. This formation evidently was associated with the formation of lower-valent species. Moisture in start-up electrolyte and in neodymium oxide feed was found to increase the tendency for scum formation and to critically lower current efficiencies.

## 1. ELECTROLYTE PROPERTIES

### 1.1. Selection of Electrolyte Compositions

The system $CaF_2$-LiF-CaO was investigated initially. Relatively high oxide solubilities have been found for this system [10]. This should be beneficial in avoiding anode effects. The solubility of neodymium oxide, however, remained to be established.

The following ratios of $CaF_2$ to LiF were selected for the base electrolyte:

70 wt% $CaF_2$ / 30 wt% LiF at 1040 °C <1>
46 wt% $CaF_2$ / 54 wt% LiF at 850 °C <2>
46 wt% $CaF_2$ / 54 wt% LiF at 950 °C <3>
64 wt% $CaF_2$ / 36 wt% LiF at 950 °C <4>

These conditions are marked in the phase diagram of Figure 2.

The above compositions were selected based on the following considerations: (1) the melting point of neodymium at 1024 °C [11]; (2) the phase diagram for the system $CaF_2$-LiF; and (3) experiences in the electrolysis of oxides in previous work [10].

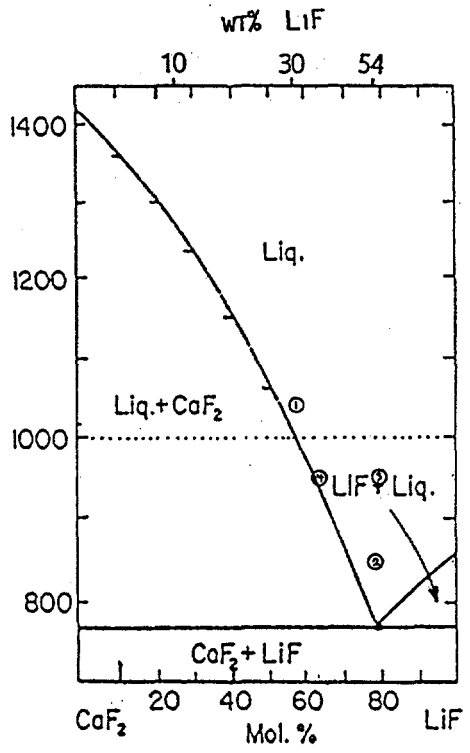


**Figure 2** Phase Diagram for the System $CaF_2$-LiF

Previous experience has shown that a high $CaF_2$ content in the $CaF_2$-LiF system fosters the dissolution of oxides. The liquidus temperature for a mixture of 70 wt% $CaF_2$ and 30 wt% LiF is about 1000 °C. This composition was selected for operation at temperatures of 1040-1050 °C, at which neodymium is deposited as a liquid. The melt contained as much $CaF_2$ as possible, with some margin to avoid undesirable solidification during imperfect cell operation.

Operating temperatures can be lowered and a liquid cathode product can still be obtained if a Fe-Nd cathode is selected (see Nd-Fe phase diagram of Figure 3). In this case, selection of the eutectic composition of 46 wt% $CaF_2$ / 54 wt% LiF may permit electrolysis at temperatures as low as 850 °C. Our experiments then were to reveal if oxide solubility is adequate under these conditions. Perhaps the solubility may have to be enhanced by operating at somewhat higher temperature; testing for oxide contents at 950 °C, thus, was included. If such higher temperatures are required, one may also consider an electrolyte composition of higher calcium fluoride content, i.e. 64 wt% $CaF_2$ / 36 wt% LiF at 950 °C.

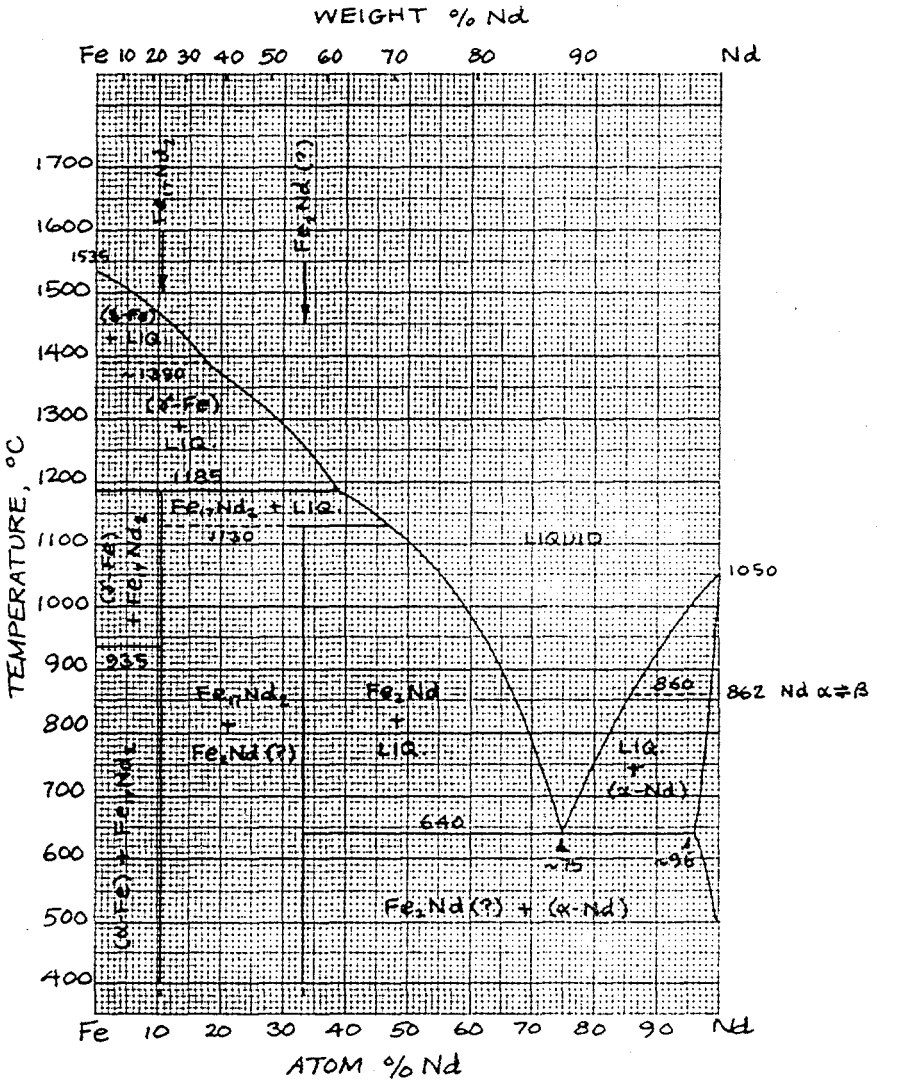


RUSSIAN METALLURGY (METALLY), 1965, No. 3, P.50 (ENGL)

**Figure 3** Phase Diagram for Neodymium - Iron

After electrolysis experiments yielded unsatisfactory results with the above electrolytes and the presence of calcium was suspected to be detrimental, calcium fluoride and calcium oxide contents were reduced to zero and neodymium fluoride became a major component. Figure 4 shows the phase diagram of the $NdF_3$-LiF system, with a eutectic composition of 64.6 wt% $NdF_3$ / 35.4 wt% LiF at a eutectic temperature of 710 - 720 °C.

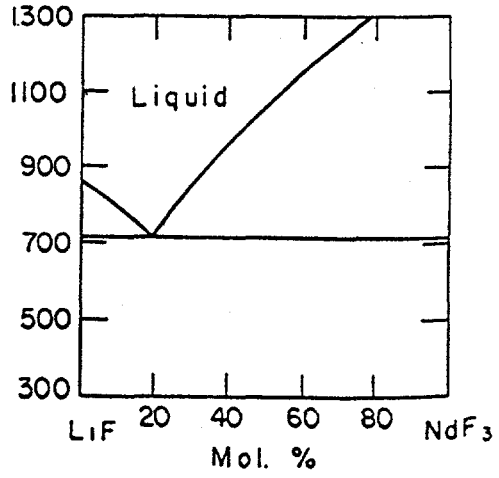


**Figure 4** Phase Diagram for the System $NdF_3$-LiF

## 1.2. Oxide Solubilities

Several methods were used to determine the solubility limits of oxides in molten salts. In one method, oxide additions are observed visually; when the melt remains cloudy after an incremental addition, the solubility limit had been exceeded. Preparation of a saturated melt and chemical analysis of the oxide content was another possibility.

### 1.2.1. Determinations by an Electrochemical Method

Technique. A convenient electrochemical technique to determine oxide contents has been studied by several authors for cryolitic melts. Reynolds Metals Company authors published repeatedly on the development of such a method for use with industrial aluminum electrolysis cells [12] [13] [14]. The method involves polarization of a graphite sensor electrode up to a critical current at which an anode effect occurs. The value of this critical current can be taken as a measure of the oxide content. In a recent contract, EMEC Consultants applied the method to other fluoride melts [10].

When using the electrode design of Figure 5 that had been used successfully in cryolitic melts, we noticed a deterioration of the boron nitride (BN) material. A reaction occurred that was accompanied by gas bubble formation and was accelerated by increased calcium content of the melt. Although thermodynamic calculations do not indicate a reactivity between CaO and BN, a reaction may occur in the presence of hydroxide.

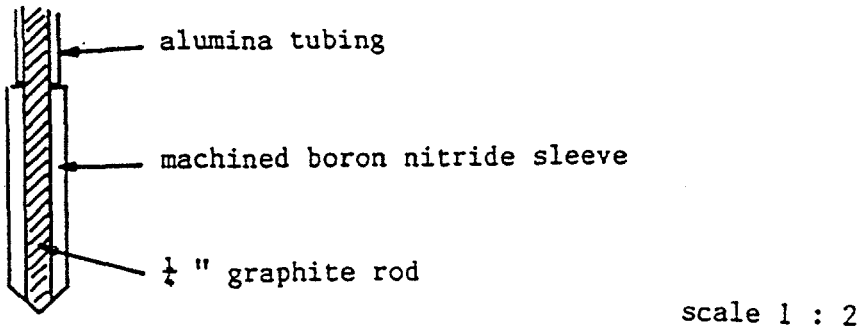


**Figure 5** Construction of Oxide Sensor Electrode

As this effect led to erroneous results, the design of the sensor electrode was modified. An unshielded graphite cone was immersed into the electrolyte, as shown in Figure 6. Immersion depth was 3.20 mm, immersing the electrode by this amount into the melt from the point where the tip of the electrode established electrical contact with the melt. Current scans were applied to unshielded electrodes and reproducible and consistent results were obtained.

Contents of dissolved oxide were determined for selected electrolyte systems. Oxides were added incrementally to the fluoride melt. It then was determined whether the critical current increased by an amount corresponding to full dissolution, or the critical current increased to a lesser extent, indicating only partial dissolution.

Oxide Determinations. A series of initial measurements were conducted with melts containing 70 wt% $CaF_2$ and 30 wt% LiF, plus oxide additions.

Addition of calcium oxide, CaO, produced the results of Figure 7. Three runs in which incremental amounts of CaO were added to the fluoride melt at 1040 °C are shown. Critical current values were rather reproducible at CaO contents of up to 4 wt% CaO. At 5 wt% CaO and higher concentrations, values started to diverge. The solubility limit in a 70 wt% / 30 wt% LiF melt, according to Experiment # Nd-1-04, is about 6 wt% CaO (critical current at 6 wt% CaO: 12.4 A, at 7 wt% CaO: 12.2 A).

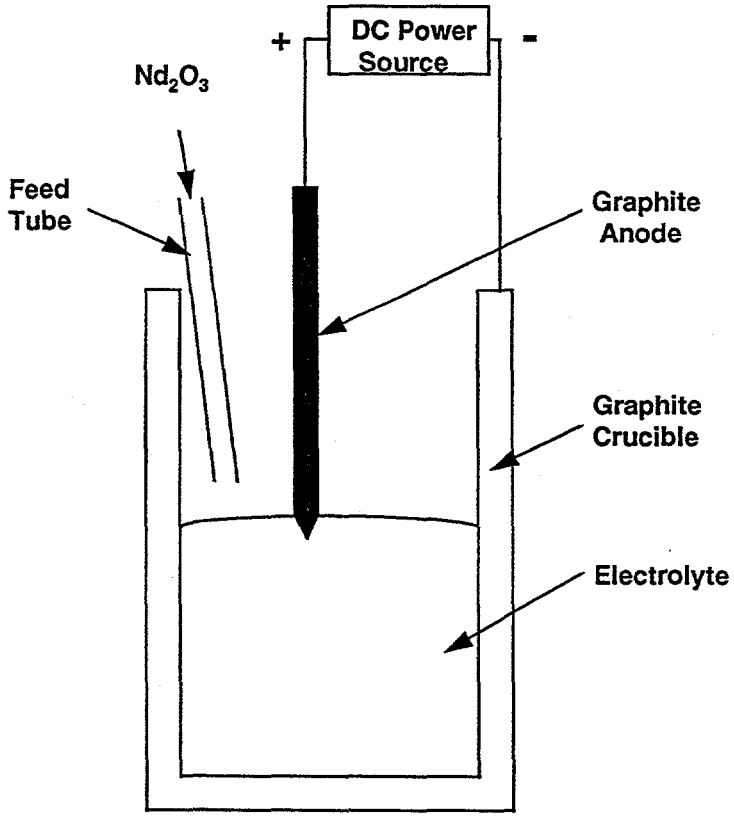


**Figure 6** Modified Oxide Sensor Electrode

Figure 8 presents results obtained with neodymium oxide additions, in addition to CaO additions. In Experiment # Nd-1-07, 2 wt% $Nd_2O_3$ was added initially, and another 2 wt% as a second increment. Two calcium oxide additions were made subsequently. The critical current reached with 2 wt% $Nd_2O_3$ added was about 75 percent of a value typically reached with 1 wt% CaO. CaO contains about twice as much oxygen per unit weight as $Nd_2O_3$, since the formula weight for $Nd_2O_3$ (336.48) is six times greater than that of CaO (56.08). This reduced critical current appears to indicate incomplete dissolution of the neodymium oxide, which is confirmed by the marginal increase observed after a second addition of $Nd_2O_3$. Calcium oxide added subsequently, however, dissolved regularly. In Experiment # Nd-1-08, $Nd_2O_3$ was added after 2 wt% CaO had been dissolved in the melt. Again, an increase in critical current was observed, although somewhat less pronounced (about 1 wt% $Nd_2O_3$ may have dissolved in this case). Addition of neodymium oxide to a melt containing 4 wt% CaO, in Experiment # Nd-1-09, resulted in somewhat erratic readings which seemed to indicate incomplete dissolution of neodymium oxide.

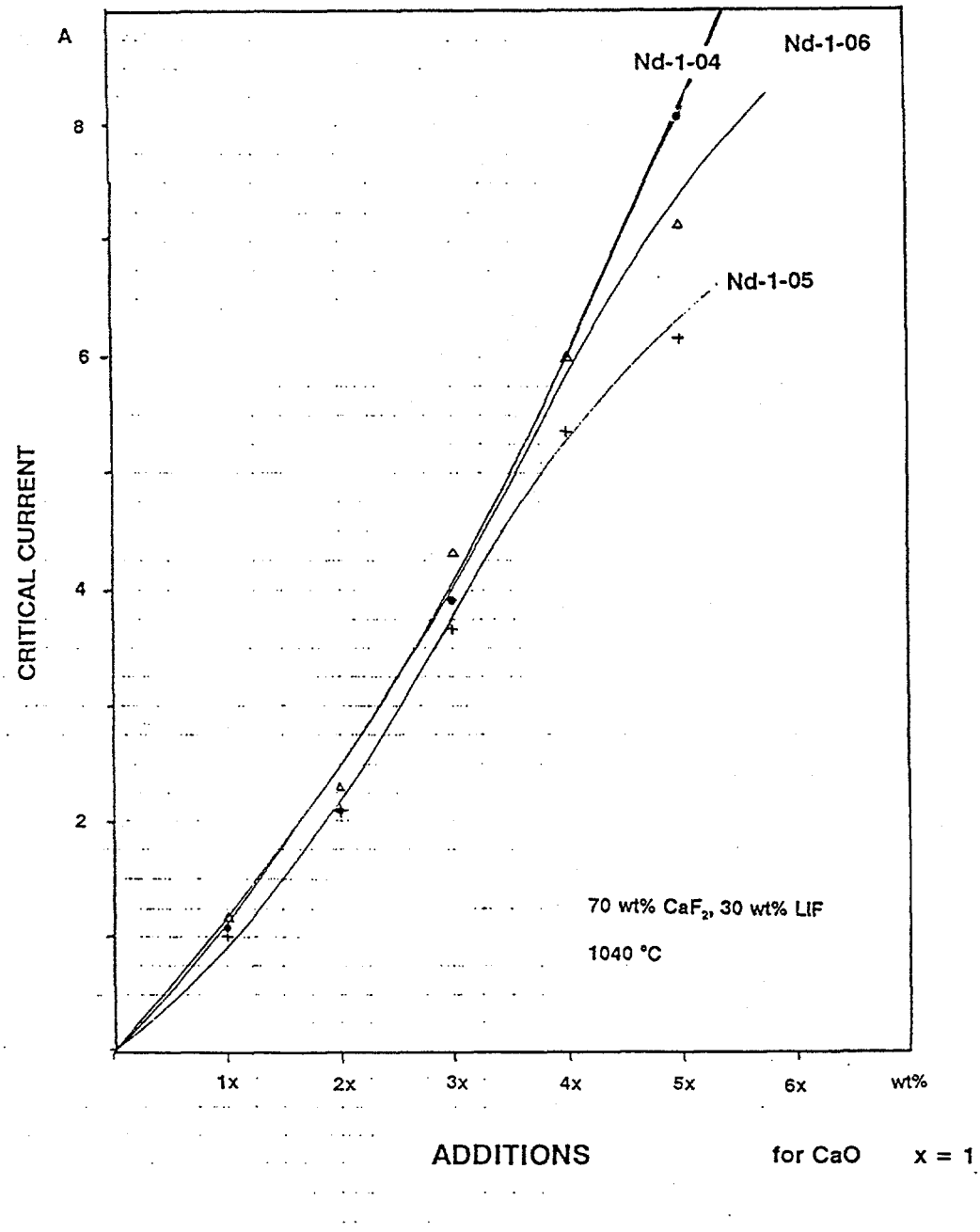


**Figure 7** Critical Currents with 70 wt% $CaF_2$ / 30 wt% LiF, and CaO Additions

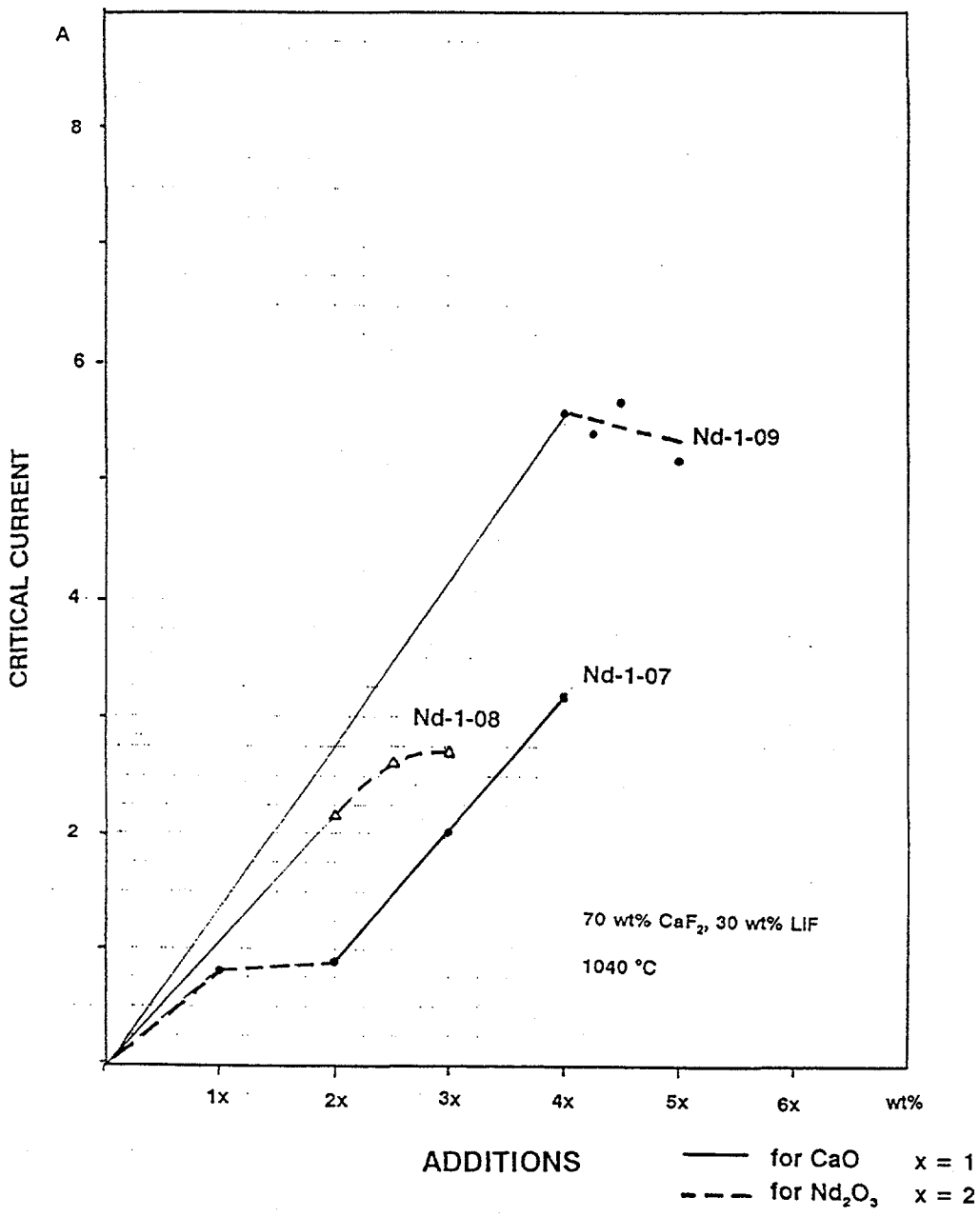


**Figure 8** Critical Currents Obtained with $Nd_2O_3$ Additions to $CaF_2$-LiF Melts Containing CaO

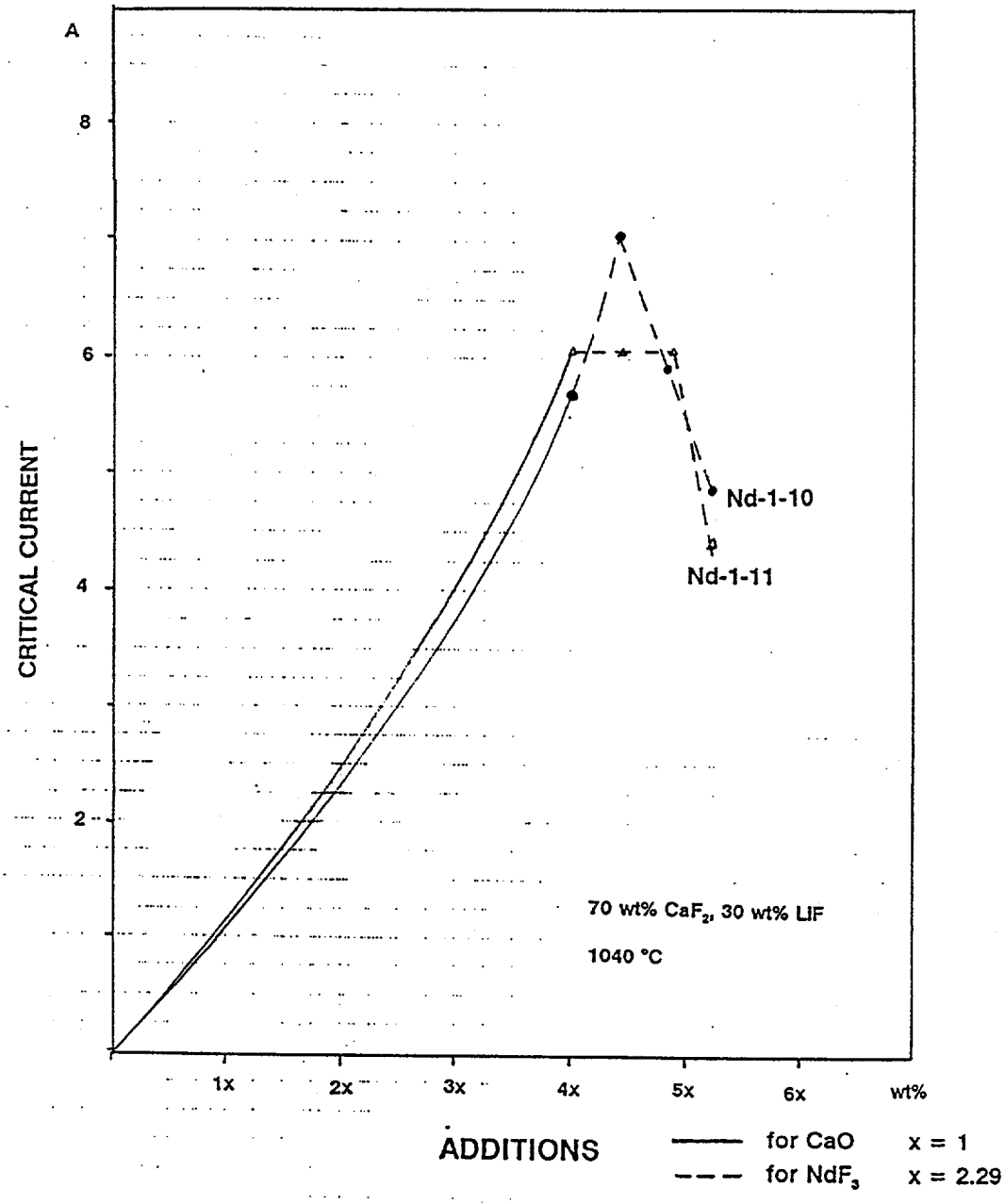


**Figure 9** Critical Currents Obtained with $NdF_3$ Additions to $CaF_2$-LiF Melts Containing CaO

In the two experiments represented in Figure 9, neodymium fluoride was added to $CaF_2$-LiF melt containing CaO. Fluoride additions should not affect the critical currents significantly, unless they affect the oxide content of the melt. This is the case if neodymium oxide precipitates when its solubility limit is exceeded:

$$3\ CaO + 2\ NdF_3 \quad ----> \quad 3\ CaF_2 + Nd_2O_3$$

In Experiment # Nd-1-11, two additions of 1 wt% $NdF_3$ did not affect the critical current, but a third addition appears to indicate essentially quantitative neodymium oxide formation. The dissolution of 0.42 wt% $NdF_3$ corresponds to a content of 0.5 wt% dissolved $Nd_2O_3$ or 1 wt% CaO, respectively. Similar results were obtained in Experiment # Nd-1-10, but an increase of the critical current upon the first addition of $NdF_3$ was recorded, an observation that we cannot easily explain.

Synopsis. From these results we could expect a solubility of 1 to 1.75 wt% $Nd_2O_3$ in the electrolytes considered for electrolysis of neodymium oxide at 1040 °C. The upper numbers approached the approximate value of 2 wt% given in the literature for neodymium fluoride-rich electrolyte. The dissolution of an additional 4 wt% CaO, however, indicated a considerably higher oxide content. This was expected to support a much smoother anode reaction.

### 1.2.2. Oxygen Analysis of the Electrolyte

The solubilities of neodymium oxide in $CaF_2$-$NdF_3$ electrolyte systems were determined by oxygen analysis of electrolyte samples. Electrolytes rich in neodymium and calcium fluoride, with lithium fluoride as the second component, were melted with substantial quantities of oxide added to the melt. The electrolyte was agitated for three hours with argon gas bubbling from a molybdenum tube. The molybdenum bubbler tube was removed and electrolyte was allowed to settle for an additional 3 hours. A sample was extracted from the top of the melt with a alumina tube. The solidification of the sample was immediate and therefore contamination of oxide from the alumina tube was insignificant. The sample was removed from the alumina tube and analyzed by Rhône-Poulenc for oxygen content.

Two electrolyte systems were studied, and neodymium oxide solubilities were determined for the compositions 70 wt% $CaF_2$ / 30 wt% LiF and 64.6 wt% $NdF_3$ / 35.4 wt% LiF. Table I contains the electrolyte composition, temperature, and neodymium oxide solubility values.

The first composition of 70 wt% $CaF_2$ / 30 wt% LiF, with oxide additions at temperatures between 1040 °C and 1050 °C, contained between 0.33 wt% and 0.66 wt% neodymium oxide in solution. The second electrolyte composition of 64.6 wt% $NdF_3$ / 35.4 wt% LiF, with neodymium oxide additions at 800 °C, contained approximately 2 wt% dissolved neodymium oxide. This solubility is consistent with results published by the U.S. Bureau of Mines [5].

**Table I** Solubility of Neodymium Oxide, as Determined by Analysis of Electrolyte Samples

| Electrolyte Composition | Temperature (°C) | Neodymium Oxide Solubility |
|---|---|---|
| 70 wt% $CaF_2$ / 30 wt% LiF + 2 wt% $Nd_2O_3$ | 1044 °C | 0.55 wt% $Nd_2O_3$ |
| 70 wt% $CaF_2$ / 30 wt% LiF + 6 wt% $Nd_2O_3$ + 5 wt% CaO | 1040 °C | 0.37 wt% $Nd_2O_3$ |
| 70 wt% $CaF_2$ / 30 wt% LiF + 5 wt% $Nd_2O_3$ + 3 wt% CaO | 1047 °C | 0.33 wt% $Nd_2O_3$ |
| 70 wt% $CaF_2$ / 30 wt% LiF + 10 wt% $Nd_2O_3$ + 6 wt% CaO | 1040 °C | 0.60 wt% $Nd_2O_3$ |
| 64.6 wt% $NdF_3$ / 35.4 wt% LiF + 5 wt% $Nd_2O_3$ | 800 °C | 2.07 wt% $Nd_2O_3$ |
| 64.6 wt% $NdF_3$ / 35.4 wt% LiF + 5 wt% $Nd_2O_3$ | 800 °C | 1.95 wt% $Nd_2O_3$ |

## 1.3. Electrolyte Conductivities

### 1.3.1. Introduction

High electrolyte conductivity is desirable to minimize ohmic losses and, thus, energy consumption. While specific conductances of 2 $ohm^{-1}cm^{-1}$ are typical for electrolytes employed in Hall-Héroult electrolysis, somewhat higher values can be expected for electrolytes with high lithium ion content, as in the compositions under consideration for neodymium oxide electrolysis.

It was not the purpose of the conductivity measurements to establish accurate conductivity values, but rather to verify favorable conditions for the employment of the electrolytes under consideration.

### 1.3.2. Experimental Procedure

To select a material for the construction of a conductivity probe, several candidates were tested for their reactivity with 70 wt% $CaF_2$ / 30 wt% LiF baths. The selection of candidates was limited because only nonconducting materials could be utilized. Alumina and boron nitride were tested. During material testing, boron nitride reacted with the electrolyte, while alumina showed no dimensional changes. A double bore alumina tube with platinum wire set at a fixed distance from the end was employed as the conductivity probe. A YSI resistance meter was used to determine the resistance of the melt. The experimental arrangement is shown in Figure 10.

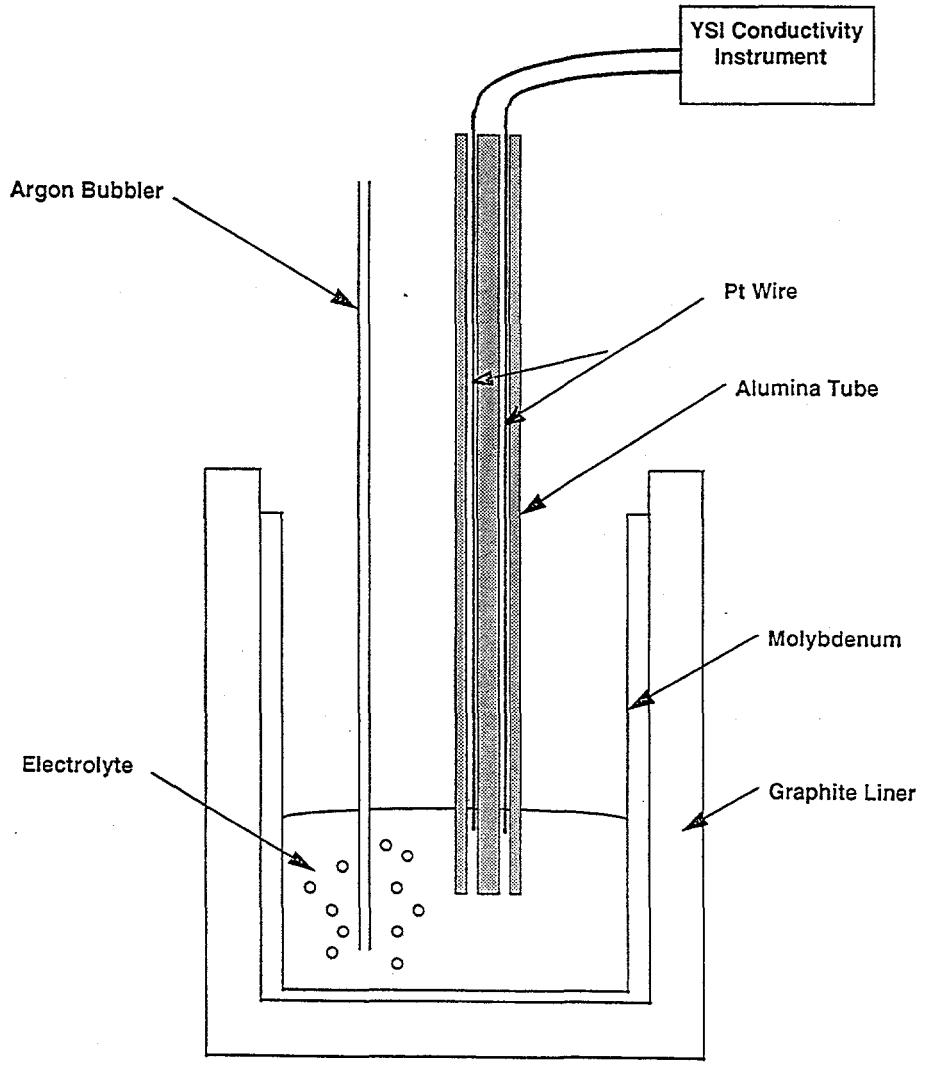


**Figure 10** Experimental Arrangement to Determine Electrolyte Conductivity

For use with a composition of 64.6 wt% $NdF_3$ / 35.4 wt% LiF, two probes constructed from alumina and boron nitride were tested. Both materials proved to be stable in the material tests that were performed. The boron nitride probe, however, was not wetted by the electrolyte so readings could not be obtained. On the other hand, the alumina probe functioned properly, allowing several resistance readings to be recorded.

### 1.3.3. Results and Discussion

The conductivity of 70 wt% $CaF_2$ / 30 wt% LiF at 1040°C was determined to be between 4 to 6 $ohm^{-1}cm^{-1}$.

A conductivity of the 64.6 wt% $NdF_3$ / 35.4 wt% LiF salt was determined at two temperatures. Conductivities of 4.75 $ohm^{-1}cm^{-1}$ at 805 °C and 4.57 $ohm^{-1}cm^{-1}$ at 826 °C were obtained.

## 1.4. Metal Solubilities

### 1.4.1. Introduction

Reactive metals are often soluble in their salt melts, which may serve as useful electrolytes. This solubility can lead to electronic conductance of the electrolyte, or, more frequently or more extensively, to the formation of subvalent species, $AlF^+$ and $Na_2^+$ being examples. Dissolution of metallic cathode product into the electrolyte and subsequent oxidation by anode products, electrochemically at the anode, or by air lead to current efficiency losses. Even though such losses occur, successful operation of electrometallurgical processes is possible, as the Hall-Héroult process clearly illustrates.

Neodymium has some solubility in melts containing $NdF_3$. Dworkin and Bredig [15] measured a relatively low solubility of 0.1 to 0.5 mol% for Nd in $NdF_3$ by examining melting point depressions. As discussed below, low solubility values were confirmed by our measurements, but they may be higher in the presence of oxide because of the formation of subvalent oxides.

Metal solubilities generally increase with increasing temperature and depend on the activity of the metal present. Alloying with iron reduces the activity of neodymium and can be expected to lead to lower current efficiency losses.

### 1.4.2. Experimental Procedure

Weighed electrolyte charges were placed into a molybdenum crucible along with Nd or Nd-Fe metal to be reacted. Once the electrolyte reached the set temperature, an argon flow through a molybdenum bubbler tube was used to agitate the melt for 6 hours. A sample of the electrolyte was taken at the end of the test with an alumina tube. The content of reactive metal in the electrolyte was determined by hydrogen evolution. In several other experiments, the metal solubility was calculated from the metal weight loss. The experimental arrangement is shown below in Figure 11.

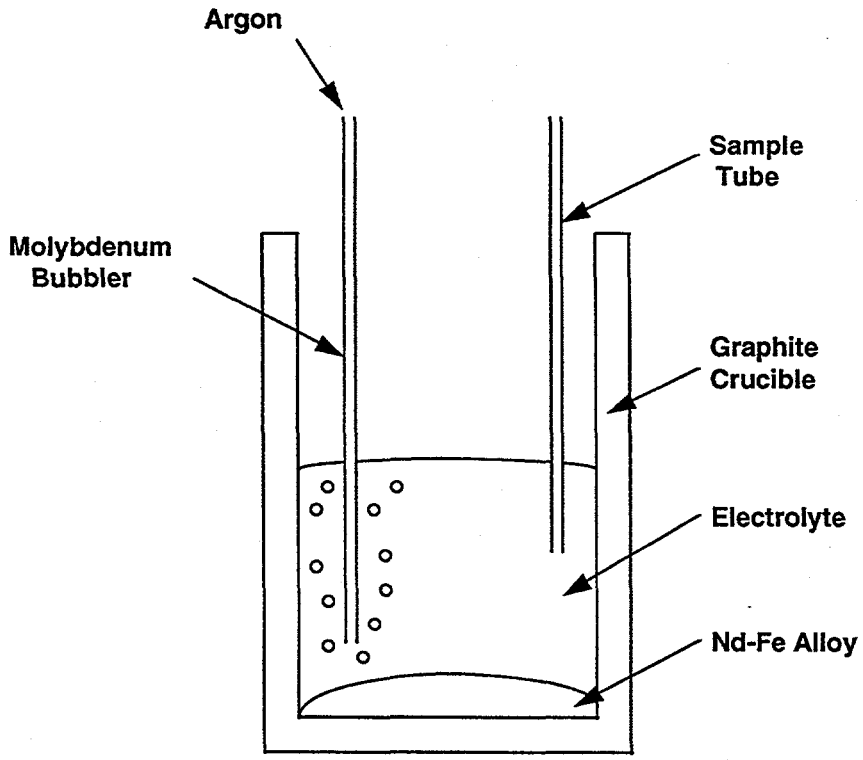


**Figure 11** Experimental Arrangement to Determine Solubility of Neodymium Oxide

### 1.4.3. Results

The results of the metal solubility experimentation are presented in Table II. Electrolyte composition, reactive metal, temperature, methods of determination and metal solubility are

shown. While analysis of electrolyte samples by hydrogen evolution did not take into account buildup of reactive metal in the dark layer above the metal, experiments in which metal solubilities were determined by weight loss took into account metal loss into electrolyte as well as metal contained in the dark layer. Such a dark layer was present in all experiments.

**Table II** Solubility of Reactive Metal in the Electrolyte

| Electrolyte Composition | Reactive Metal | Temp. ( °C) | Method of Determination | Metal Solubility |
|---|---|---|---|---|
| 70 wt% $CaF_2$ / 30 wt% LiF + 1 wt% $Nd_2O_3$ | Nd | 1030-1040 | $H_2$ evolution | 0.66 wt% Nd |
| 70 wt% $CaF_2$ / 30 wt% LiF + 1 wt% $Nd_2O_3$ | Nd | 1030-1040 | $H_2$ evolution | 0.67 wt% Nd |
| 64.6 wt% $NdF_3$ / 35.4 wt% LiF + 1 wt% $Nd_2O_3$ | Nd-Fe alloy | 805 | $H_2$ evolution | 0.0 wt% Nd from sample tube; 0.7 - 1.4 wt% Nd from solidified dark layer |
| 64.6 wt% $NdF_3$ / 35.4 wt% LiF | Nd-Fe alloy | 800 | $H_2$ evolution | 0.17 wt% Nd |
| 64.6 wt% $NdF_3$ / 35.4 wt% LiF + 1 wt% $Nd_2O_3$ | Nd-Fe alloy | 800 | $H_2$ evolution | 0.1 wt% Nd |
| 41.7 wt% $NdF_3$ / 41.7 wt% LiF / 16.6 wt% $CaF_2$ / + 2 wt% $Nd_2O_3$ | Nd-Fe alloy | 900 | weight loss | 0.84 wt% Nd |
| 41.7 wt% $NdF_3$ / 41.7 wt% LiF / 16.6 wt% $BaF_2$ / + 2 wt% $Nd_2O_3$ | Nd-Fe alloy | 900 | weight loss | 0.25 wt% Nd |

The solubility of neodymium in calcium-neodymium fluoride melts were well within the realm for acceptable electrochemical performance. The solubility of aluminum in cryolite in industrial Hall-Héroult cells is typically 0.1 wt%. When the atomic weights of neodymium and aluminum are considered (144.24 g/mole vs 26.98 g/mole) the highest solubility observed in Table II of 0.84 wt% is equivalent to only 0.16 wt% aluminum dissolved in cryolite. Solubilities calculated by weight loss tend to be higher than by hydrogen evolution, as they also take into account neodymium trapped in the dark viscous layer above the metal, not only neodymium dissolved into the melt (as seen by hydrogen evolution).

## 2. ELECTRODE REACTIONS

### 2.1. Products of Metal-Electrolyte Interaction

#### 2.1.1. Introduction

Sludge or scum formation has hampered previous attempts to electrolyze rare earths. Products of interactions between neodymium metal and electrolyte were studied, because we suspected that such interactions affect sludge formation.

Nd-Fe alloy was reacted, in the absence of electrolysis, with eutectic $NdF_3$-LiF electrolyte with and without oxide additions. A dark viscous layer was observed in most experiments when oxide was present. The solidified layer was examined by EDX at the Materials Characterization facility of Carnegie Mellon University. Samples obtained with electrolyte containing neodymium oxide showed approximately 10 times the amount of neodymium metal present in the dark layer when compared to samples with no neodymium oxide added.

#### 2.1.2. Experimental Procedure

In Experiment # DOE-Nd-1-122, eutectic electrolyte containing 64.6 wt% $NdF_3$ (387.6 g) / 35.4 wt% LiF (212.4 g) / + 5 wt% $Nd_2O_3$ (30.0 g) was charged into a molybdenum crucible, along with Nd-Fe eutectic alloy (113.0 g). The crucible containing the charge was placed in the inert-atmosphere vessel which was evacuated and backfilled with argon several times. The charge was then heated to approximately 900 °C. The electrolyte was agitated with dried argon through a molybdenum bubbler tube into the electrolyte about 1/2 inch above the metal. After six hours, the bubbler tube was removed and the melt was allowed to cool. The entire crucible and content was sectioned and photographed. The sample was examined by EDX at Carnegie Mellon University.

The same procedure was followed in Experiment # DOE-Nd-1-123 for electrolyte containing no oxide. Conditions were as previously described, with the following exceptions: the Nd-Fe eutectic alloy weighed 126.39 g, no neodymium oxide was added.

#### 2.1.3. Experimental Results

Photographic documentation of Experiment # DOE-Nd-1-122 and 123 is shown in Figure 12. A dark layer, approximately 1.5 cm thick, was observed above the metal in Experiment # DOE-Nd-1-122. A dark purple layer approximately 0.8 cm thick was measured in Experiment # DOE-Nd-1-123. The thickness and color of the layer seemed to be affected by the presence of

DOE-Nd-1-122
(5 wt% $Nd_2O_3$ Added)

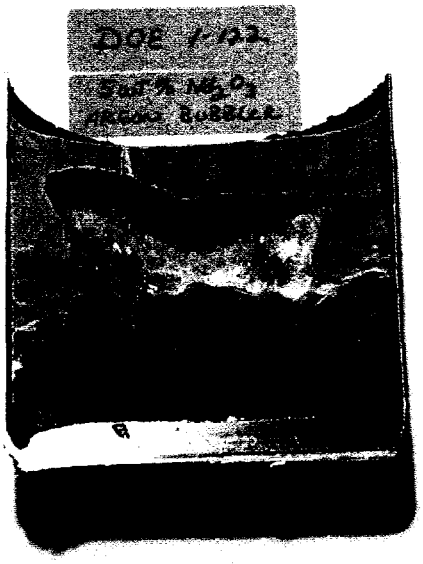


DOE-Nd-1-123
(No $Nd_2O_3$ Added)

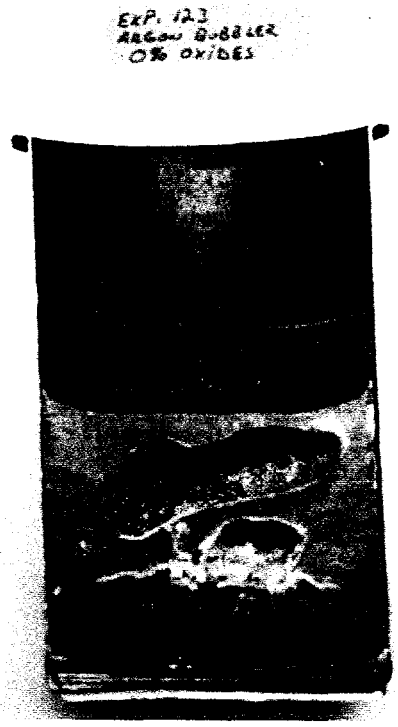


**Figure 12** Solidified Electrolyte After Exposure to Nd-Fe Eutectic Metal

neodymium oxide. Also the wetting characteristics of the Nd-Fe alloy with the molybdenum crucible were different in the two cases. In Experiment # DOE-Nd-1-122, the Nd-Fe alloy did not fully wet the crucible indicating that the layer in this case was probably more viscous than in Experiment # DOE-Nd-1-123. The bulk electrolyte in both cases was similar in color.

The electrolyte samples were mounted, polished and then taken to Carnegie Mellon University and examined under EDX. The EDX micrograph and energy dispersion patterns at various points on the sample are shown in Figures 13 and 14 for Experiment # DOE-Nd-1-122.

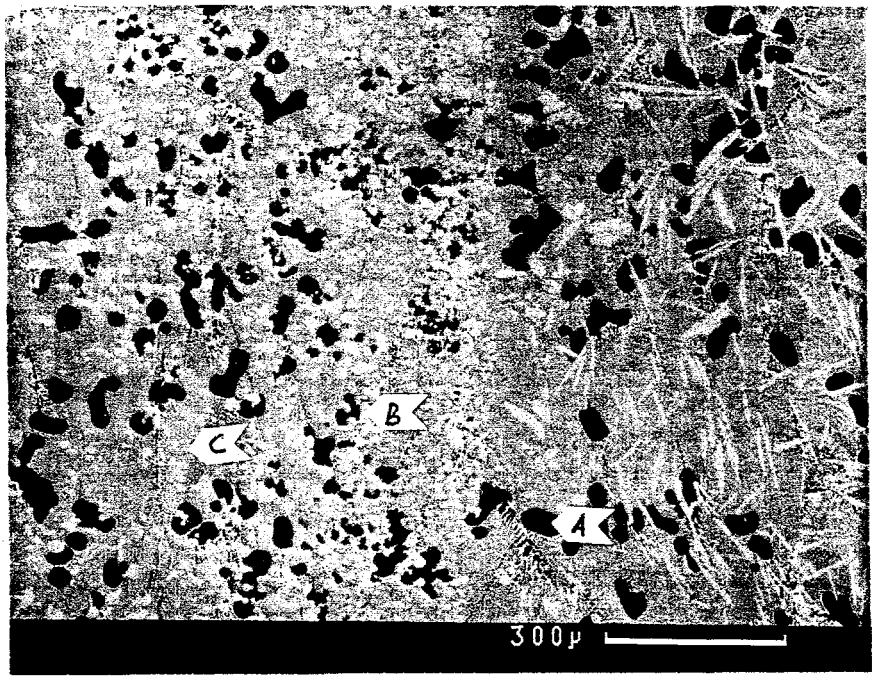


**Figure 13** EDX Micrograph of Electrolyte Sample (Experiment # DOE-Nd-1-122)

The micrograph for Experiment # DOE-Nd-1-122 illustrates three distinctly different regions. Area A (dark region) was concluded not to be holes in the sample but pockets of LiF because relatively high background energy was observed. Area B (bright region) contained pure neodymium metal with no iron present. Area C (mixed region) was speculated to contain a mixture of neodymium oxide and electrolyte.

EDX micrograph and energy dispersion patterns at various points of a second sample (Experiment # DOE-Nd-1-123) are shown in Figures 15 and 16.

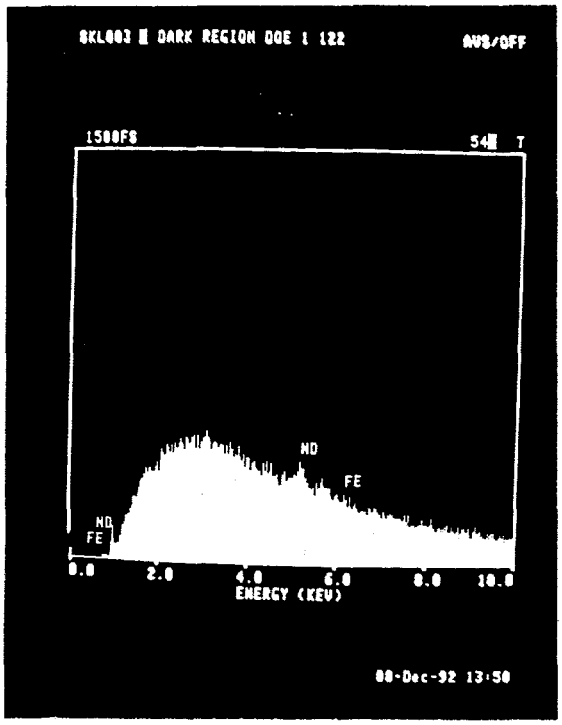


Area A

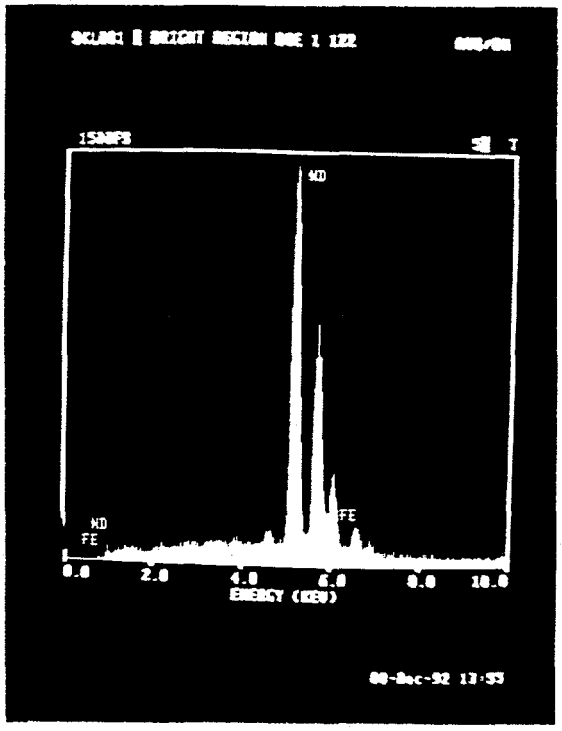


Area B

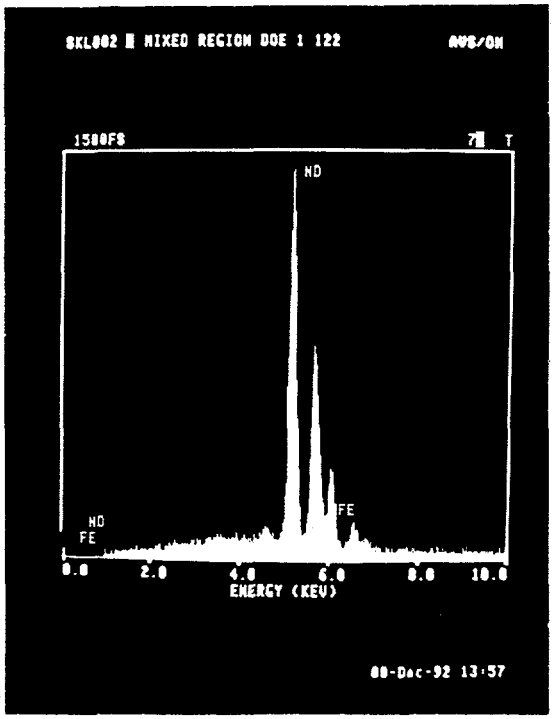


Area C

**Figure 14** Energy Dispersion Patterns for Electrolyte Sample (Experiment # DOE-Nd-1-122)

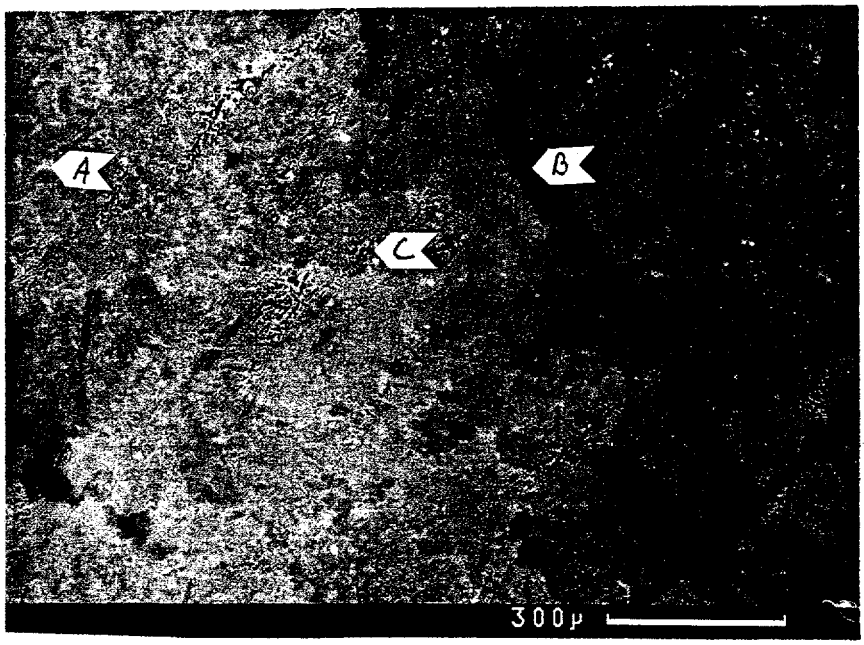


**Figure 15** EDX Micrograph of Electrolyte Sample (Experiment # DOE-Nd-1-123)

The micrograph for Experiment # DOE-Nd-1-123 illustrates three distinctly different regions. The same conclusions were made about the three contrasting areas. Area A (bright region) contained pure neodymium metal, Area B (mixed region) contained a mixture of neodymium oxide and electrolyte, Area C (dark region) contained pockets of LiF.

### 2.1.3. Discussion of Results

The thickness of the dark layer was doubled when Nd-Fe alloy was exposed to neodymium oxide. Formation of subvalent species containing oxide possibly fostered the dissolution of neodymium metal. Approximately 10 times the amount of neodymium metal was observed in the layer above the metal when neodymium oxide was present in the electrolyte. The bulk electrolyte in Experiment # DOE-Nd-1-122 (5 wt% oxide) contained copious amounts of neodymium metal, whereas little or no neodymium metal was found in the electrolyte in Experiment # DOE-Nd-1-123 (no oxide). Neodymium metal of the dark layer or bulk electrolyte did not contain any iron. The neodymium metal, therefore, must have dissolved or reacted with electrolyte and oxide; a dispersion of the Nd-Fe alloy by agitation can be ruled out.

### 2.1.4. Conclusions

Operating a cell with lower concentrations of neodymium oxide would be beneficial in reducing the formation of the dark viscous layer. Metal solubility in the bulk electrolyte would also be reduced.

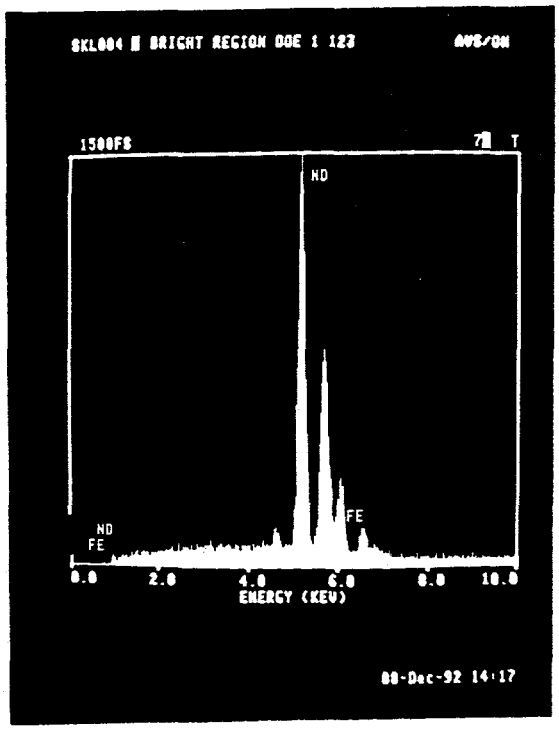


Area A

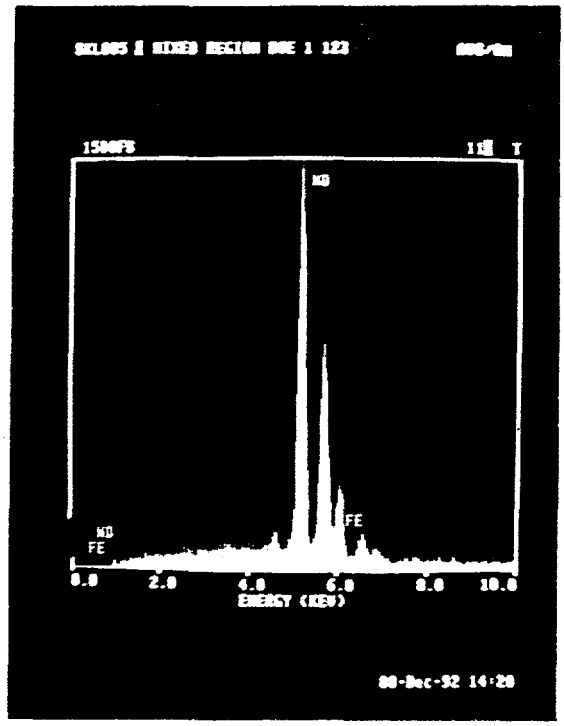


Area B

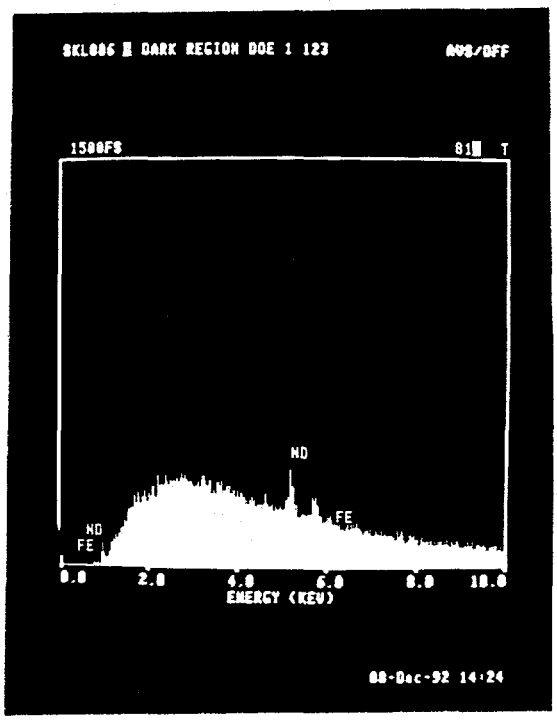


Area C

**Figure 16** Energy Dispersion Patterns for Electrolyte Sample (Experiment # DOE-Nd-1-123)

## 2.2. Investigation of the Formation of a Dark Layer

### 2.2.1. Introduction

The formation of a detrimental dark viscous layer in the electrolyte at the cathode metal interface and the build-up of scum or sludge have been observed in neodymium electrolysis. To elucidate this phenomenon further, a series of experiments were initiated in which $NdF_3$-LiF electrolytes containing neodymium oxide were exposed to liquid Nd-Fe alloy and the tendency to form a dark layer was examined.

### 2.2.2. Experimental Procedure

The basic non-electrolysis experimental set-up used is shown in Figure 17. A graphite liner supporting a molybdenum crucible containing the melt was placed in an Inconel vessel that could be sealed and operated with a controlled atmosphere. Electrolyte was mixed with neodymium oxide and placed on top of Nd-Fe eutectic alloy. An argon bubbler of molybdenum, a sampling tube of alumina, and a thermocouple were inserted through the lid of the vessel, which was sealed, evacuated, and backfilled with argon three to five times. The charge was heated to a desired temperature of 800 to 1000 °C. Dried argon was bubbled through the molten charge for 5 hours to promote the formation of the dark layer. After bubbling, the electrolyte was allowed to settle for two hours. The alumina sampling tube was lowered into the electrolyte to 1 inch from the bottom and suction was applied to extract a sample. The alumina tube was removed from the electrolyte. The inert atmosphere vessel was lifted out of the furnace to allow the sample and the charge to cool. After cooling, the sample was removed from the alumina tube and sent to Rhône-Poulencin Phoenix for oxygen analysis. The crucible was sectioned with a diamond saw and photographed. Procedures were modified according to the special purpose of the experiment.

Solid Oxide in Contact With Metal: Solid oxide was allowed to contact the liquid metal, as shown in Figure 17. Sufficient oxide was added to exceed the solubility limit of neodymium oxide.

Solid Oxide Not in Contact With Metal: The experimental arrangement was modified, as shown in Figure 18. The metal was contained in a Tribocor® crucible. The neodymium oxide was so added that undissolved oxide rested on the bottom around the Tribocor® crucible. Only dissolved oxide contacted the metal. Otherwise, the same experimental procedure as previously described was followed. No samples of the electrolyte were taken.

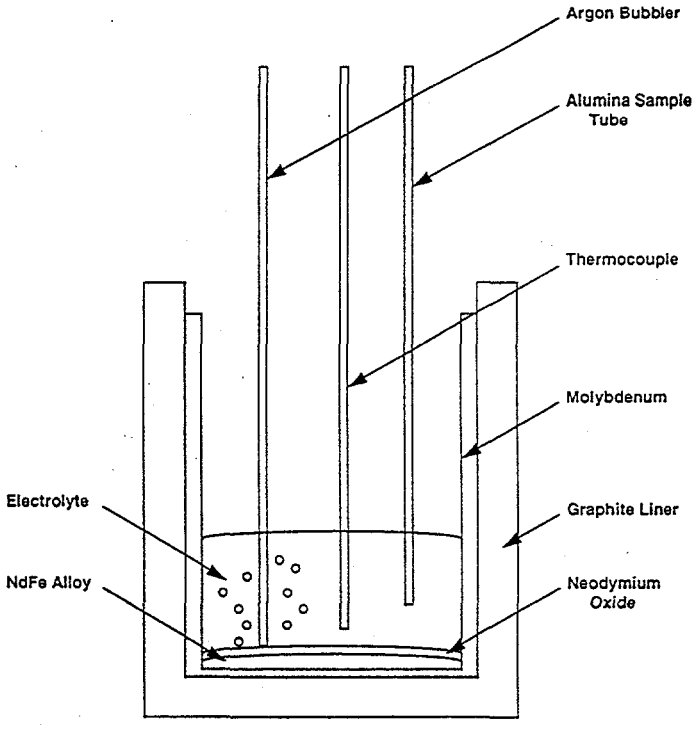


**Figure 17** Experimental Arrangement

Moisture Added to Argon Stream: The experimental arrangement used to study the effect of moisture is that shown in Figure 17. The only difference was that the argon was first bubbled through water before entering the cell. Otherwise, the same experimental procedure was used as described previously.

Metal Polarization: Figure 19 shows the experimental arrangement modified to study the effect on the dark layer formation of polarization of the Nd-Fe alloy. The experimental procedure remained the same, with the exception that the Nd-Fe alloy was electrically polarized.

Dark Layer Conductivity: The experimental arrangement used to determine the conductivity of the dark layer is shown in Figure 20. Electrolyte mixed with 5 wt% $Nd_2O_3$ was melted in the inert atmosphere vessel and brought to temperature (900 to 1000 °C). A conductivity probe constructed from an alumina tube and an Inconel sheathed thermocouple was used. The conductivity was first determined before any argon was bubbled through the melt. After five hours of bubbling to form a dark layer, the conductivity was measured again and compared to the previous reading.

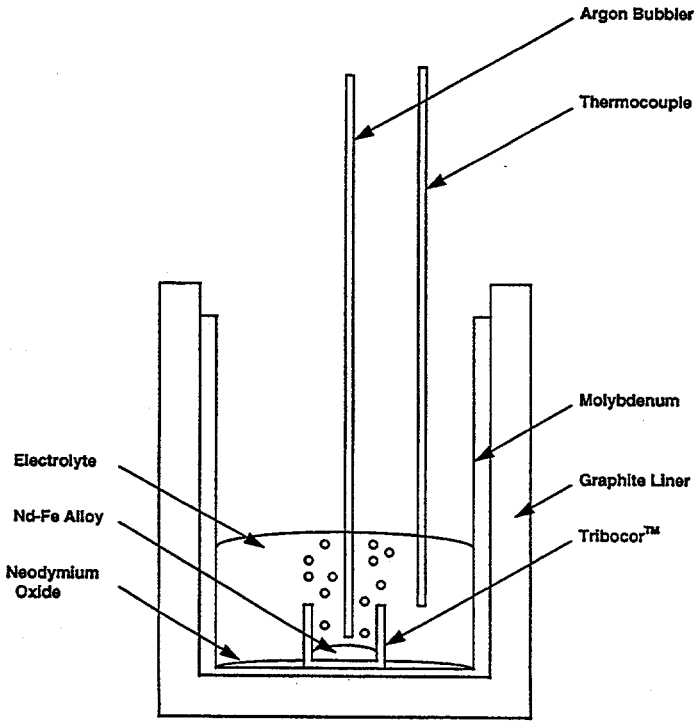


**Figure 18** Experimental Arrangement, Modified to Avoid Contact of Solid, Undissolved Oxide With Metal

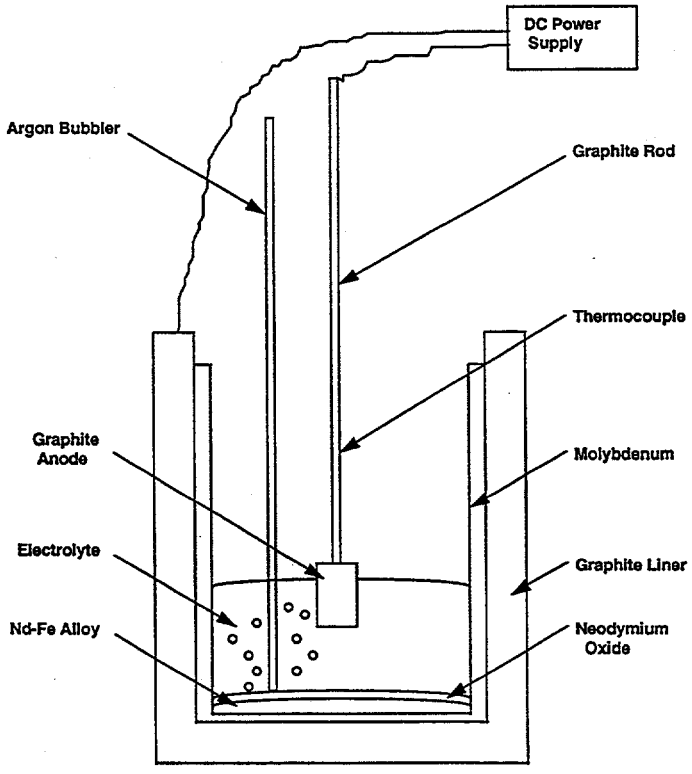


**Figure 19** Experimental Arrangement With Cathodic Polarization of the Metal

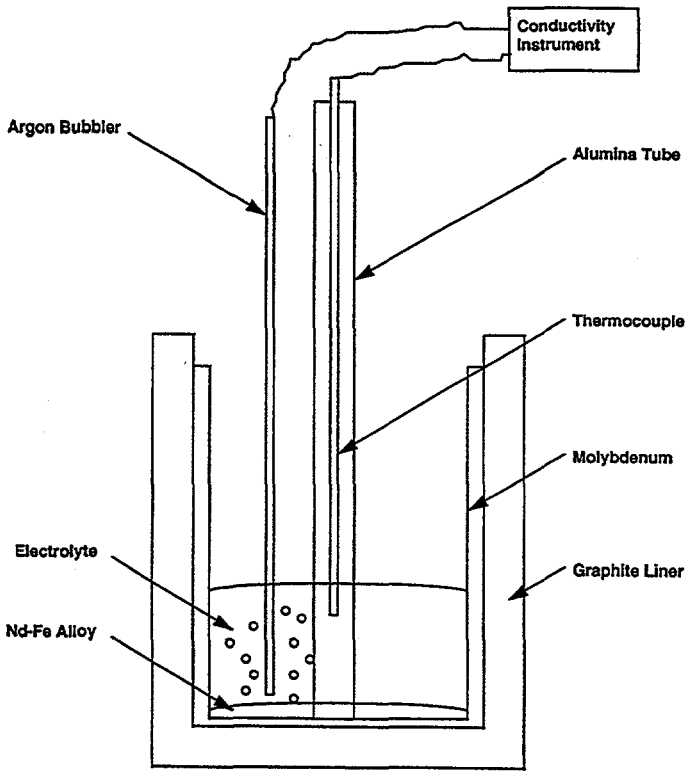


**Figure 20** Experimental Arrangement (Conductivity of Dark Layer)

### 2.2.3. Experimental Results

Table III lists the results of the experiments with and without water added to the argon. The composition of the electrolyte in weight percent is given for each test. An amount of 5 wt% $Nd_2O_3$ was added to the electrolyte in all cases, except in Experiments # DOE-Nd-1-159 and 160. Argon stirring was employed, except in Experiments # DOE-Nd-1-159 and 161. In two experiments, the composition of the bubbler gas was varied. In Experiment # DOE-Nd-1-176, moisture was added to the argon stream, and in Experiment # DOE-Nd-1-180 argon contained 2 wt% oxygen. Temperature was varied between 800 °C and 1000 °C, with most experiments being conducted at 900 °C. After bath solidification, each crucible was sectioned. The degree of dark layer formation was evaluated visually; results are noted in the column Relative Dark Layer Formation (10 worst, i.e. highest degree of formation, to 0 being the best). The thickness of the dark layer above the metal in each experiment was the basis for this ranking. Each experiment was photographically documented. Electrolyte samples were removed at the end of most experiments and sent to Rhône-Poulenc for analysis; data in weight percent oxygen can also be found in Table III.

**Table III.** Experimental Data (Solid Oxide in Contact with Metal)

| DOE-Nd # | Composition (wt%) | $Nd_2O_3$ Added (wt%) | Stirring (Ar bubbler) | Temp. (°C) | Relative Dark Layer Formation (10=worst ↔ 0=best) | wt% O in Electrolyte Sample |
|---|---|---|---|---|---|---|
| 1-154 | 100 % LiF | 5 % | Yes | 900 | 3 | 0.0134 |
| 1-155 | 90 % LiF 10 % $NdF_3$ | 5 % | Yes | 900 | 6 | 0.0325 |
| 1-156 | 70 % LiF 30 % $NdF_3$ | 5 % | Yes | 900 | 8 | 0.0364 |
| 1-157 | 50 % LiF 50 % $NdF_3$ | 5 % | Yes | 900 | 9 | 0.0165 |
| 1-158 | 35.4 % LiF 64.6 % $NdF_3$ | 5 % | Yes | 900 | 7 | 0.0287 |
| 1-159 | 35.4 % LiF 64.6 % $NdF_3$ | 0 % | No | 900 | 4 | 0.0261 |
| 1-160 | 35.4 % LiF 64.6 % $NdF_3$ | 0 % | Yes | 900 | 5 | 0.0082 |
| 1-161 | 35.4 % LiF 64.6 % $NdF_3$ | 5 % | No | 900 | 5 | 0.0083 |
| 1-163 | 30 % LiF 70 % $NdF_3$ | 5 % | Yes | 900 | 4 | 0.0048 |
| 1-164 | 20 % LiF 80 % $NdF_3$ | 5 % | Yes | 900 | 9 | 0.0082 |
| 1-165 | 35.4 % LiF 64.6 % $NdF_3$ + 20 % $BaF_2$ | 5 % | Yes | 900 | 9 | 0.0035 |
| 1-166 | 50 % LiF 50 % $NdF_3$ + 20 % $BaF_2$ | 5 % | Yes | 900 | 8 | 0.0241 |

| DOE-Nd # | Composition (wt%) | $Nd_2O_3$ Added (wt%) | Stirring (Ar bubbler) | Temp. (°C) | Relative Dark Layer Formation (10=worst ↔ 0=best) | wt% O in Electrolyte Sample |
|---|---|---|---|---|---|---|
| 1-167 | 35.4 % LiF 64.6 % $NdF_3$ + 20 % $CaF_2$ | 5 % | Yes | 900 | 9 | 0.0075 |
| 1-168 | 50 % LiF 50 % $NdF_3$ + 20 % $CaF_2$ | 5 % | Yes | 900 | 6 | 0.0225 |
| 1-171 | 30 % LiF 70 % $NdF_3$ | 5 % | Yes | 800 | 9 | - |
| 1-172 | 30 % LiF 70 % $NdF_3$ | 5 % | Yes | 1000 | 4 | - |
| 1-173 | 20 % LiF 80 % $NdF_3$ | 5 % | Yes | 900 | 8 | - |
| 1-174 | 50 % LiF 50 % $NdF_3$ + 20 % $CaF_2$ | 5 % | Yes | 800 | 8 | - |
| 1-175 | 50 % LiF 50 % $NdF_3$ + 20 % $CaF_2$ | 5 % | Yes | 1000 | 6 | - |
| 1-176 | 30 % LiF 70 % $NdF_3$ | 5 % | Yes ($H_2O$) | 900 | 9 | - |
| 1-180 | 30 % LiF 70 % $NdF_3$ | 5 % | Yes 4 hrs 1 hr 2 % $O_2$ | 900 | 9 | - |
| 1-182 | 28.2 % LiF 54.8 % $NdF_3$ 17.0 % $CaF_2$ | 5 % | Yes | 900 | 6 | - |

Table IV lists the results of the experiments in which the solid oxide was not in contact with the metal". The experiment number, composition of electrolyte, wt% $Nd_2O_3$ added to the electrolyte, stirring, temperature and relative dark layer formation are illustrated in this table. Photographic documentation for each sectioned crucible was made.

**Table IV.** Experimental Data (Solid Oxide Not in Contact With Metal)

| DOE-Nd # | Composition (wt%) | wt% $Nd_2O_3$ Added | Stirring (Ar bubbler) | Temp. (°C) | Relative Dark Layer Formation (10=worst↔0=best) |
|---|---|---|---|---|---|
| 1-177 | 30% LiF 70% $NdF_3$ | 5% | yes | 900 | Could not Rank |
| 1-178 | 30% LiF 70% $NdF_3$ | 5% | yes | 900 | 3 |
| 1-179 | 50% LiF 50% $NdF_3$ + 20 % $CaF_2$ | 5% | Yes | 900 | 4 |
| 1-181 | 30% LiF 70% $NdF_3$ | 5% | Yes 4Hrs 1Hr 2% $O_2$ | 900 | 8 |
| 1-183 | 28.2% LiF 54.8% $NdF_3$ 17.0% $CaF_2$ | 5% | Yes | 900 | 5 |

2.2.4. Discussion of Results

Figure 21 represents data located in Table III. The correlation between degree of dark layer formation and electrolyte composition is plotted for several experiments conducted at 900 °C and 5 wt% $Nd_2O_3$, at varying ratio of $NdF_3$ to LiF. At lower and higher $NdF_3$ percentages in the electrolyte the severity of the dark layer (thickness) was less pronounced. However, around 50 wt% $NdF_3$ the dark layer occupied a large percentage of the total electrolyte. The amount of oxygen found in the electrolyte by analysis did not correlate with the severity of the dark layer.

$BaF_2$ additions to the electrolyte increased the dark layer formation. This is evident in Experiments # DOE-Nd-1-165 and 166 where the relative dark layer formations ranked at 9 and 8. $CaF_2$ showed more promise than $BaF_2$ additions. In Experiments # DOE-Nd-1-168 and 175, the relative dark layer formation ranked at a 6.

Moisture additions to the argon gas increased the dark layer formation. The entire bath volume was filled by the layer above the metal in Experiment # DOE-Nd-1-176. Oxygen gas at a level

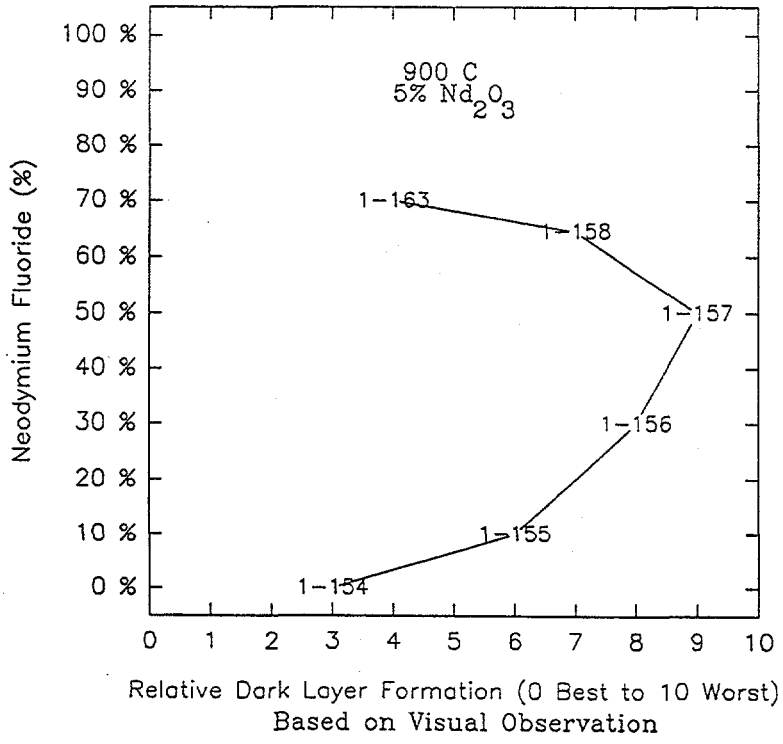


**Figure 21** Neodymium Fluoride / Lithium Fluoride vs Dark Layer Formation

of 2 wt% (2.6 mole%) in the argon was bubbled through the electrolyte in Experiment # DOE-Nd-1-180 to oxidize lower-valent species of $NdF_3$ and $Nd_2O_3$ suspected to be present in the dark layer. The severity of the layer formation appeared to be increased in this experiment, not decreased as expected.

Table IV illustrates the results from the experiments in which solid oxide was not in contact with the metal. The dark layer formation was reduced by avoiding direct contact between the oxide and the Nd-Fe alloy. Oxygen addition to the argon increased the formation of the dark layer.

The Nd-Fe alloy was cathodically polarized in Experiment # DOE-Nd-1-169. A current of 0.12 A at 3 V was applied to the metal for 6 hours under an argon purge. The dark layer was not reduced when compared to other runs with the same electrolyte (64.6 wt% $NdF_3$ / 35.4 wt% LiF) and similar experimental conditions.

The conductivity of the dark layer was determined in Experiment # DOE-Nd-1-170. Problems occurred in obtaining accurate readings with the alumina probe. A generalization, however, was established, as increasing dark layer formation led to increasing conductivity.

The observations are consistent with the theory based on earlier experimentation that the formation of the dark layer is associated with the occurrence of subvalent species whose formation is fostered by the presence of oxide in the electrolyte.

## 2.3. Selection of Cathode

Two different cathode materials were used in the electrolysis experiments: molybdenum and iron (1010 steel, a plain carbon steel with 0.1 wt% C).

Molybdenum was employed when the electrolysis temperature exceeded the melting temperature of neodymium metal. In this case, liquid neodymium was deposited. Its activity was unity and dissolution of metal into the electrolyte (or formation of subvalent species) led to metal reoxidation problems.

An iron cathode was used more often. Neodymium deposited onto iron at a temperature below the melting point of neodymium forms neodymium-iron alloys. Nd-Fe alloy of near-eutectic composition dripped off the iron cathode and was collected in a small crucible placed at the bottom of the cell. Figure 3 shows a eutectic alloy composition of 12 wt% Fe / 88 wt% Nd, with a melting point of approximately 640 °C. By forming the alloy, the activity of the deposited neodymium was reduced and the dissolution rate of metal into the electrolyte minimized. This in turn reduced the rate of metal reoxidation and is expected to lead to higher current efficiencies.

## 2.4. Anode Reactions

In the presence of sufficient amount of oxide in the electrolyte, carbon anodes were expected to participate as reactant in the anode reaction according to

$$2\ Nd_2O_3 + 3\ C \ \text{----}> \ 4\ Nd^{3+} + 3\ CO_2 + 12\ e^-\ .$$

The corresponding reaction for aluminum oxide is known to be the predominant primary reaction in the Hall-Héroult process. Almost all of the CO obtained in the off-gases, in this case, is due to secondary reduction of $CO_2$.

In our experiments we usually observed substantial quantities of CO. Weight loss data of anodes indicated that the reaction

$$Nd_2O_3 + 3\ C \ \text{----}> \ 2\ Nd^{3+} + 3\ CO + 6\ e^-$$

probably occurred at the electrode, besides the formation of $CO_2$. Due to the presence of inert gas and the lack of indications of dusting, it appears safe to rule out substantial non-electrochemical oxidation of carbon.

While anode effects accompanied by large voltage rises normally were not observed, carbon

tetrafluoride ($CF_4$) was often present in the off-gases. It appears that the electrochemical reaction at the anode changes in our case before the characteristic drastic change in the wetting characteristics of the anode surface occurs. Our data indicate that a relatively broad range of conditions exists where the reaction

$$4\ NdF_3 + 3\ C \ \text{----}> \ 4\ Nd^{3+} + 3\ CF_4 + 12\ e^-$$

occurs along with the formation of carbonaceous oxides. While we did not establish their formation by analysis, one may expect other compounds such as $COF_2$ and $C_2F_6$ to form.

As discussed later, our best electrolysis results, at least in regard to current efficiency, were achieved at conditions leading to partial formation of carbon tetrafluoride. As the emission of this compound or similar fluorine-containing compounds could not be tolerated, treatment of the off-gases would be necessary.

## 2.5. Characteristics and Treatment of Cell Off-Gases

### 2.5.1. Introduction

In analogy to the electrolysis of aluminum oxide in the Hall-Héroult process, carbon anodes are expected to react with neodymium oxide to produce primarily carbon dioxide, according to

$$2\ Nd_2O_3 + 3\ C \ \text{----}> \ 4\ Nd + 3\ CO_2\ .$$

The carbon dioxide can react with reactive metal in the electrolyte to form CO, this reaction resulting in current efficiency losses.

Our most promising results were achieved, however, in a regime where carbon tetrafluoride was evolved. $CF_4$ also forms in industrial aluminum electrolysis at low oxide contents, when the so-called anode effect occurs. In the case of neodymium oxide electrolysis, we did not observe the steep voltage increase characteristic for anode effect, although more positive electrode potentials are evidently required for the formation of $CF_4$. The analysis of gas samples usually indicated the presence of a mixture of CO, $CO_2$, and $CF_4$ (see Tables VIII and XII). Typical ratios for these gases were 1-2 : 20 : 4 for $CO_2$ : CO : $CF_4$.

It is not clear if the gas mixture is actually formed at the observed compositions at the anode. It is more likely that secondary reactions occur. Calandra [16] reports that carbon fluoride compounds react with oxide in cryolitic melts to form CO and $CO_2$.

If overriding advantages suggest the operation of the neodymium oxide electrolysis in a mode in which carbon tetrafluoride and possibly other fluorine-containing compounds, such as $COF_2$ and $C_2F_6$, are formed, cell off-gases can be treated to eliminate such undesirable components. A reaction with neodymium oxide according to

$$2\ Nd_2O_3 + 3\ CF_4 \ \text{----}> \ 3\ CO_2 + 4\ NdF_3$$

consumes neodymium oxide and the neodymium product can be fed to the electrolysis cell.

Treatment involving the use of process feed is facilitated by the fact that relatively minor amounts of the off-gas, and thus only a minor portion of the feed, needs to react.

As feeding neodymium oxide as primary process reactant is a major feature of the targeted process, and emission of $CF_4$ into the atmosphere is environmentally unsound, experimental studies of off-gas reactions were initiated.

### 2.5.2. Results of Electrolysis Experiments

Electrolysis experiments have been most successful when potentials are sufficient to electrolyze both $Nd_2O_3$ and $NdF_3$.

In a successful experiment giving 70 % cathodic current efficiency, the following composition (in mole%) was determined for a sample of the off-gas:

3.5 % $CF_4$, 0.4 % $CO_2$, 6.0 % CO ($COF_2$ not determined, rest presumed to be argon flush gas)

or for the identified electrolysis products:

35 % $CF_4$, 4 % $CO_2$, 61 % CO

It appears that about half of the Faradaic yield resulted from electrolysis of $Nd_2O_3$ producing CO and $CO_2$, and the other half from the electrolysis of $NdF_3$ producing $CF_4$.

### 2.5.3. Experimental Procedures for Study of Off-Gas Treatment

Experiments were conducted to ascertain the feasibility of reacting the $CF_4$ in the anodic gas with neodymium oxide. A weighed quantity of neodymium oxide was placed in an alumina or Inconel tube which was sealed and inserted into the heating zone of a furnace. The tube, connected to a gas recirculator, could be evacuated and backfilled with pure $CF_4$ gas. First, the $Nd_2O_3$ was exposed to a vacuum for a period of 24 hours at a temperature of 600 °C, to remove moisture from the sample. The system was backfilled with $CF_4$ and the gas recirculator activated for a period of 2 to 6 hours, depending on experimental objectives. The temperature was increased to 1000 °C for the duration of the test. A bottle placed in-line with the recirculator was used to obtain a gas sample. Gas samples were analyzed by gas chromatography at Advanced Technology Systems. Figure 22 represents the $CF_4$ recirculating apparatus.

### 2.5.4. Results of Study of Off-Gas Treatment

Several experiments were conducted in alumina and Inconel vessels connected to the recirculating apparatus. While the alumina tube system was plagued with air leakage problems, the Inconel system did prove to be vacuum-tight. Analytical results indicated that the $CF_4$ reacted almost quantitatively to form $CO_2$ (Experiment # DOE-Nd-2-10B): 0.46 mole% $CF_4$, 2.69 mole% CO, 94.23 mole% $CO_2$, 0.59 mole% $O_2$, and 2.08 mole% $N_2$.

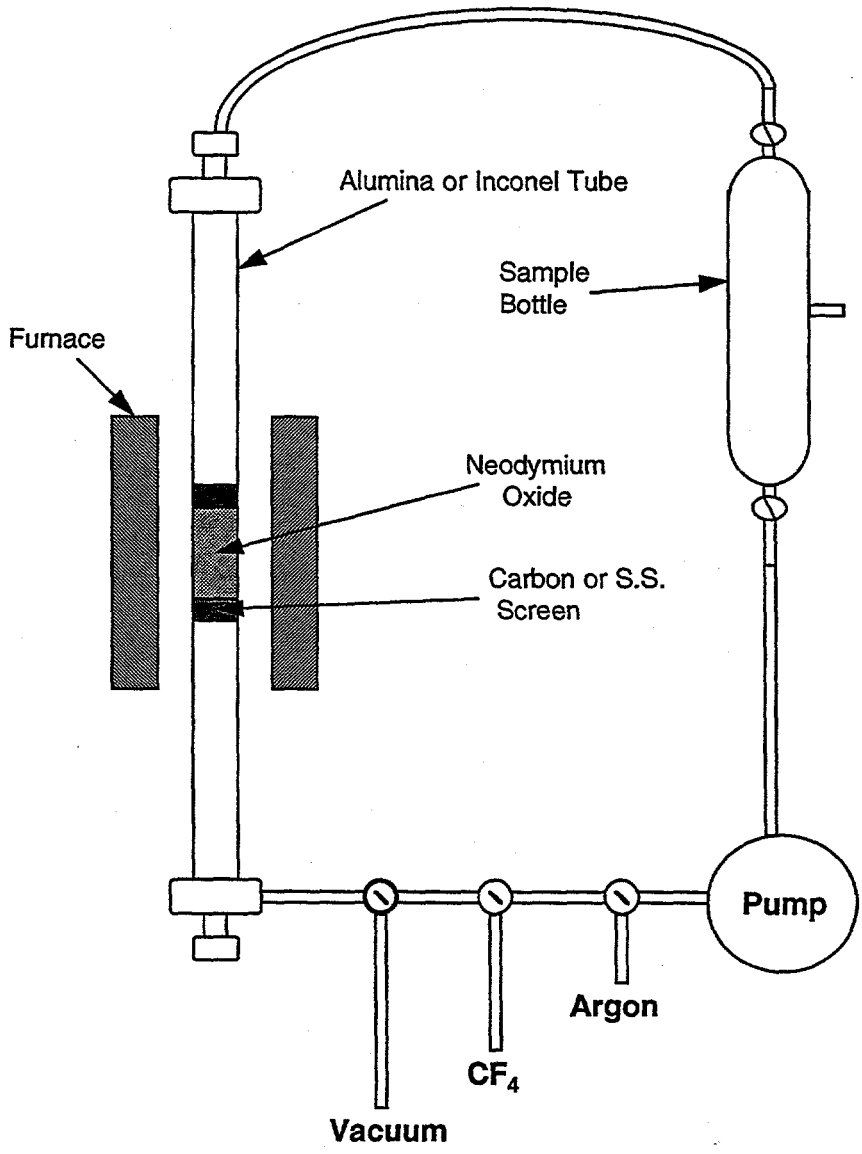


**Figure 22** $CF_4$ Reaction Apparatus with Recirculator Pump

The appearance of the neodymium oxide changed, but the solid was not analyzed. The conversion of neodymium oxide to fluoride will be verified in future work.

2.5.5. Discussion

The composition of the primary anodic product is not known; fluorocarbons can react with oxide in the electrolyte to form CO and $CO_2$ (as observed in cryolitic melts, according to Calandra et al [16]).

For an acceptable over-all electrolysis process, fluoro-carbons such as $CF_4$ and $COF_2$ must be

destroyed. The following possibilities exist:

(1) reaction with oxides in the electrolyte of the cell; possibly achievable by fully immersing electrochemically active parts of the anodes and/or designing the cell such that gases bubble through a deep layer of electrolyte;

(2) reaction with neodymium oxide feed in the dry state, in a off-gas treatment step similar to dry-scrubbing in aluminum production, but possibly conducted at elevated temperatures to promote chemical reaction;

(3) reaction with a molten salt containing neodymium oxide, either by bubbling gases through molten electrolyte in a separate vessel or through the cell, or in a molten salt scrubber system similar to one developed to scrub $SO_2$ from flue gases;

(4) reaction with other oxides such as CaO or reactive metals such as lithium.

Only a part of the off-gases are fluorine-containing compounds and needs to react. This facilitates a treatment with neodymium oxide feed.

Efforts to analyze off-gases will continue; they are to include the analysis for $COF_2$. Some preliminary bench experiments on the reactivity of fluorocarbons are presently being conducted. More extensive studies and development of an on-site analytical capability (gas chromatography) are planned for Phase II.

## 2.6. Composite Anodes

### 2.6.1. Principle of Composite Anode

To alleviate problems resulting from low oxide solubility in the electrolyte, the use of composite anodes was explored. In such consumable anodes, the oxide feed is mixed with carbon and possibly an additional conductive component. This approach was studied for the production of aluminum and found to operate with aluminum oxide even in chloride melts with low oxide solubility [17]. Evidently this is made possible by the close proximity of the oxide to the electrochemical reaction site.

In our case, neodymium oxide was mixed with the carbon that was to be electrochemically oxidized and consumed during electrolysis. The neodymium oxide then was to dissolve at an appropriate rate, as the carbon was consumed.

### 2.6.2. Preparation of Composite Anodes

Conditions to manufacture composite anodes for use during electrolysis were refined to increase strength and percent densification. Neodymium oxide and carbon powder (varying mesh sizes) were mixed for several hours in a mill which contained alumina balls for more

efficient mixing. The resulting powder was placed in a 1-inch die and pressed to pressures between 5000 and 8000 psi. After removal from the die, the green anodes were placed in an alumina crucible which was subsequently filled with carbon powder. A graphite lid was placed on top of the crucible which was then purged with argon. The anodes were heated to 400 °C at a rate of 2 °C/min, and held at that temperature for 2 hours. The temperature was then quickly increased to 1500 °C and held for 6 hours. After cooling, the anodes were drilled and tapped to accept the stainless steel anode rod.

Table V lists the composite anodes which were manufactured during this effort. The carbon powder employed, pressing pressure, theoretical density and percent densification are noted. The mixture contained 5.4 wt% carbon and 94.6 wt% neodymium oxide.

**Table V** Preparation of Composite Anodes

| Carbon Powder | Pressing Pressure (psi) | Theoretical Density ($g/cm^3$) | Percent Densification (%) |
|---|---|---|---|
| C-34 (Union Carbide) | 8000 | 6.61 | 52.5 |
| pure $Nd_2O_3$ | 8000 | 7.24 | 92.3 |
| C-34 | 8000 | 6.61 | 55.0 |
| pure $Nd_2O_3$ | 8000 | 7.24 | 89.4 |
| graphite (100×200 mesh) | 8000 | 6.61 | 62.6 |
| graphite (100×200 mesh) | 8000 | 6.61 | 64.2 |
| graphite (200×325 mesh) | 8000 | 6.61 | 62.0 |
| graphite (-400 mesh) | 8000 | 6.61 | 58.1 |
| graphite (200×325 mesh) | 5000 | 6.61 | 61.0 |
| graphite (200×325 mesh) | 12000 | 6.57 | 62.6 |
| graphite (200×325 and -325 mesh) | 8000 | 6.61 | 61.4 |

Several problems were encountered during the manufacturing of the composite anodes such as surface cracking during sintering and insufficient green strength. Surface cracking occurred due to the oxidation of carbon from the surface of the anode which permitted the $Nd_2O_3$ near the surface to sinter more easily than in the center of the anode. In order to correct this problem, the anodes were inserted into an alumina crucible, surrounded by carbon powder, and purged with argon to eliminate surface oxidation (i.e. surface cracking). The proper pressing pressure was identified and green strength improved.

Finer particle sizes of carbon generally led to decreasing percent densification. This was probably caused by the increase in the number of smaller particles at the fixed weight percentage, which in turn interfered with the sintering process. Anodes manufactured from 100×200 mesh graphite achieved the highest percent densification and strength. Pure $Nd_2O_3$ was also sintered to determine how high the densification process could be taken; approximately 90 % densification was obtained. Carbon powder from Union Carbide (C-34) provided the lowest percent densification; it was very fine and inhibited sintering of the anodes.

### 2.6.3. Testing of Composite Anodes

Electrolysis experiments with composite anodes are reported in Section 4.3.

# 3. EXPERIMENTAL TECHNIQUES

## 3.1. Materials Suitability

### 3.1.1. Objective

Stable container materials are required for both, electrolyte and cathode product. To identify suitable materials, exposure tests were conducted.

### 3.1.2. Experimental Procedure

Reactive metal or electrolyte was melted in a vessel purged with argon, which created an inert atmosphere. Dimensions of the test materials were recorded. Test materials were lowered into the reactive metal or electrolyte for a duration of 6 hours. After exposure, the samples were observed visually and dimensioned to determine if any reaction had occurred. In some cases, the reactive metal or electrolyte was analyzed for the elements contained in the test materials.

### 3.1.3. Results

Table VI presents the results of all material stability tests conducted as part of this effort. Reactive material, test material, temperature and conditions after exposure are noted.

Molybdenum and tantalum both held up to molten neodymium at temperatures of 1040 °C. However, neodymium-iron alloy attacked both molybdenum and tantalum. The analysis of the metal after exposure showed 1.0 wt% dissolved containment crucible materials (molybdenum and tantalum) in each respective neodymium/iron sample. When a nitrided crucible of titanium, niobium and tungsten, trade marked Tribocor®, was exposed to neodymium iron alloy at 900 °C, analysis indicated little or no attack of the crucible material.

Several other materials were also reacted with molten neodymium metal. Cathode block, graphite, alumina and glassy carbon were attacked by the metal, while $TiB_2$ was not.

Boron nitride was exposed to the neodymium iron alloy at a cathodic interface during electrolysis. This nonconducting material held up to the molten metal and proved to be an excellent cathodic shield during electrolysis.

$TiB_2$ and tantalum were attacked by calcium-fluoride-containing electrolytes (70 wt% $CaF_2$ / 30 wt% LiF) at 1040 °C. Molybdenum proved to be an excellent container for calcium fluoride melts at 1040 °C. Molybdenum, Tribocor® and boron nitride held up well when exposed to electrolyte containing a high concentration of neodymium fluoride (60 wt% $NdF_3$ / 20 wt% LiF / 20 wt% $CaF_2$) at various temperatures.

**Table VI** Stability of Materials

| Reactive Material | Test Material | Temperature (°C) | Condition after Exposure |
|---|---|---|---|
| 70 wt% $CaF_2$ / 30 wt% LiF | $TiB_2$ | 1040 | poor |
| Nd metal | $TiB_2$ | 1040 | excellent |
| Nd metal | cathode block | 1040 | poor |
| Nd metal | graphite | 1040 | poor |
| Nd metal | alumina | 1040 | poor |
| 70 wt% $CaF_2$ / 30 wt% LiF | tantalum | 1040 | poor ( 5 wt% Ta found in salt) |
| Nd metal | tantalum | 1040 | excellent ( < 0.5 wt% Ta in Nd) |
| Nd metal | molybdenum | 1040 | excellent ( < 0.5 wt% Mo in Nd) |
| 70 wt% $CaF_2$ / 30 wt% LiF | molybdenum | 1040 | excellent ( no Mo found in salt) |
| Nd metal | glassy carbon | 1040 | poor |
| Nd-Fe eutectic alloy | tantalum | 1040 | poor ( 1.0 wt% Ta found in Nd-Fe alloy) |
| Nd-Fe eutectic alloy | molybdenum | 1040 | poor ( 1.0 wt% Mo found in Nd-Fe alloy) |
| Nd-Fe eutectic alloy | Tribocor® * | 1015 | excellent ( <0.5 wt% Ti, <0.5 wt% Nb, <0.5 wt% W) |
| $NdF_3$/LiF/$CaF_2$ Electrolyte Mixture | Tribocor® | 900 | excellent |
| Nd-Fe | BN | 920-930 | excellent |
| $NdF_3$/LiF/$CaF_2$ Electrolyte Mixture | BN | 920-930 | excellent |

* Nitrided alloy of Ti, Nb, and W

## 3.2. Design and Operation of 10-A Electrolysis Cell

### 3.2.1: Cell Design

A single-anode, single-cathode cell to be operated at 5 to 10 A was designed, as shown in Figure 23. The round graphite anode had a diameter of 1.89 cm (3/4 inch), the cathode was a 6-mm (1/4-inch) diameter steel rod. The cell was placed in a 6-inch diameter Inconel vessel, with a lid that was designed with ports to hold the electrodes and to accommodate a vacuum line, argon purges through anode and cathode, a molybdenum bubbler, and a feeder port.

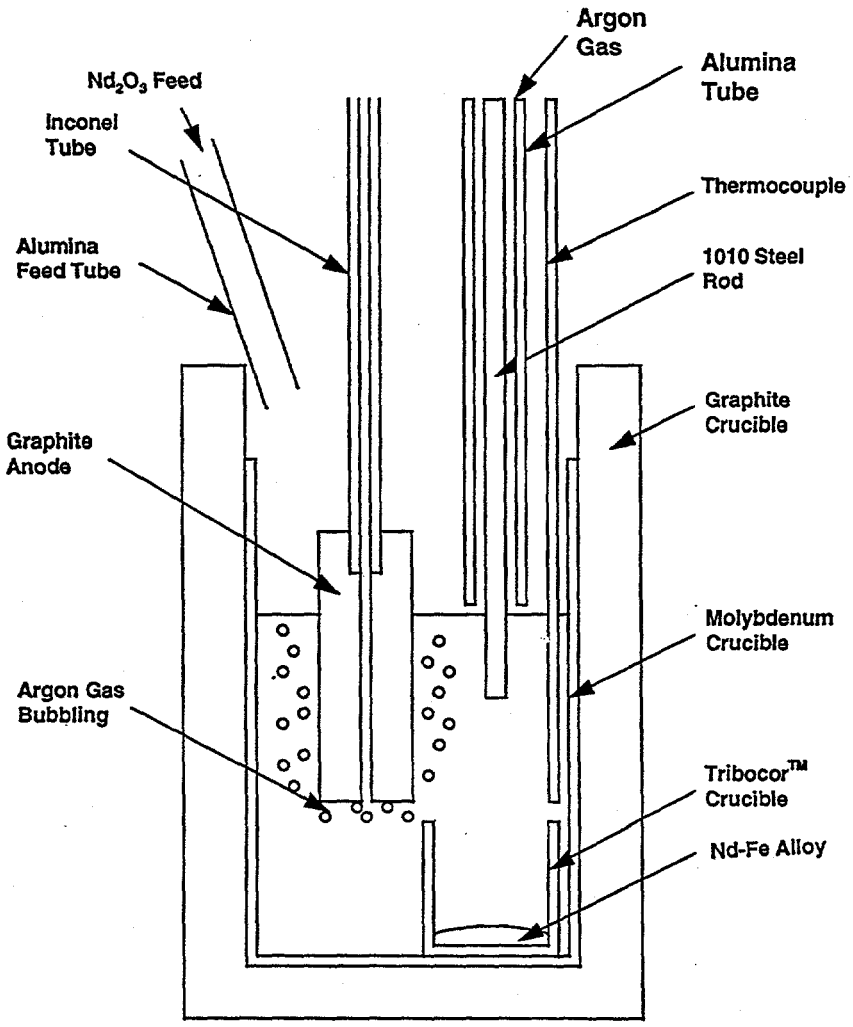


**Figure 23** 5-to-10-A Cell Design

Anode and cathode were positioned to maximize the spacing between the cell walls, graphite anode and iron cathode. A 2⅝-inch diameter by 4-inch depth molybdenum crucible contained the electrolyte. The Inconel vessel was sealed from atmospheric contamination. A feeder tube system provided semicontinuous feeding of neodymium oxide. Valves at the entrance and exit of the feeder formed an air lock to minimize air leakage into the cell. A bubbler tube of molybdenum served to agitate the electrolyte during electrolysis. A vacuum line employed to dry the electrolyte before electrolysis and a purge line used to backfill the cell with argon were also installed. The thermocouple placed above the melt could be raised and lowered to record temperatures during each experiment.

### 3.2.2. Experimental Procedure

Neodymium fluoride, lithium fluoride, and in some experiments calcium fluoride, were weighed and placed into the molybdenum crucible. Either a Tribocor® or a molybdenum crucible was placed under the cathode to collect cathode products. A graphite crucible surrounded the molybdenum crucible to contain any leaks should one occur. The lid was assembled with all the appropriate electrochemical connections. A ¾-inch diameter by 2-inch graphite anode with threaded connection was screwed on to the anode bar. The appropriate ¼-inch diameter cathode, molybdenum or iron, was inserted through the lid. There was no pretreatment of the electrolyte in experiments preceding Experiment # DOE-Nd-1-98. Vacuum drying of the electrolyte was initiated in all electrolysis experiments following and including Experiment # DOE-Nd-1-184. Vacuum drying times ranged between 4 and 12 hours at temperatures between 400 and 500 °C. The Inconel vessel was then heated to the selected temperature for cell operation. Anode and cathode were lowered into the electrolyte. Current (dc) was applied (5 to 10 A; anode current density 0.1 to 0.2 A/cm$^2$) across the anode and cathode for a targeted duration of 6 hours. Current-voltage curves were recorded at the beginning and end of several experiments. Dried neodymium oxide was fed into the cell at a theoretical feed rate of 50% for Experiments # DOE-Nd-1-184 to DOE-Nd-1-210. In preceding electrolysis experiments, DOE-Nd-1-77 to DOE-Nd-1-98, dried neodymium oxide was either fed continuously or added to the bottom of the cell during charging. Neodymium fluoride, iron oxide, and boron oxide also were fed into the cell in several experiments. Gas samples were taken during electrolysis in later experiments to determine anodic products. A boron nitride sleeve around the cathode which dipped into the electrolyte was employed in Experiment # DOE-Nd-206 to DOE-Nd-210 to shield the electrolyte-gas-cathode interface. Cathodic products dripped into the collector cup located at the bottom of the cell. If the products could be collected properly, they were weighed, along with the cathode, after the cell had cooled. The current efficiency was calculated by subtracting the cathode weight loss from the collected metal weight which was then divided by the theoretical neodymium production for each given experiment.

### 3.3. Design and Operation of 20-A Cell

#### 3.3.1. Cell Design

The 20-A cell contained three 1-inch diameter graphite anodes arranged concentrically around a ¼-inch diameter iron center cathode was designed. A larger distance between the anode and cathode than in the 5-to-10-A cell reduced shorting problems. While Figure 24 illustrates the lid design for the 20-A cell, Figure 25 presents an overall schematics.

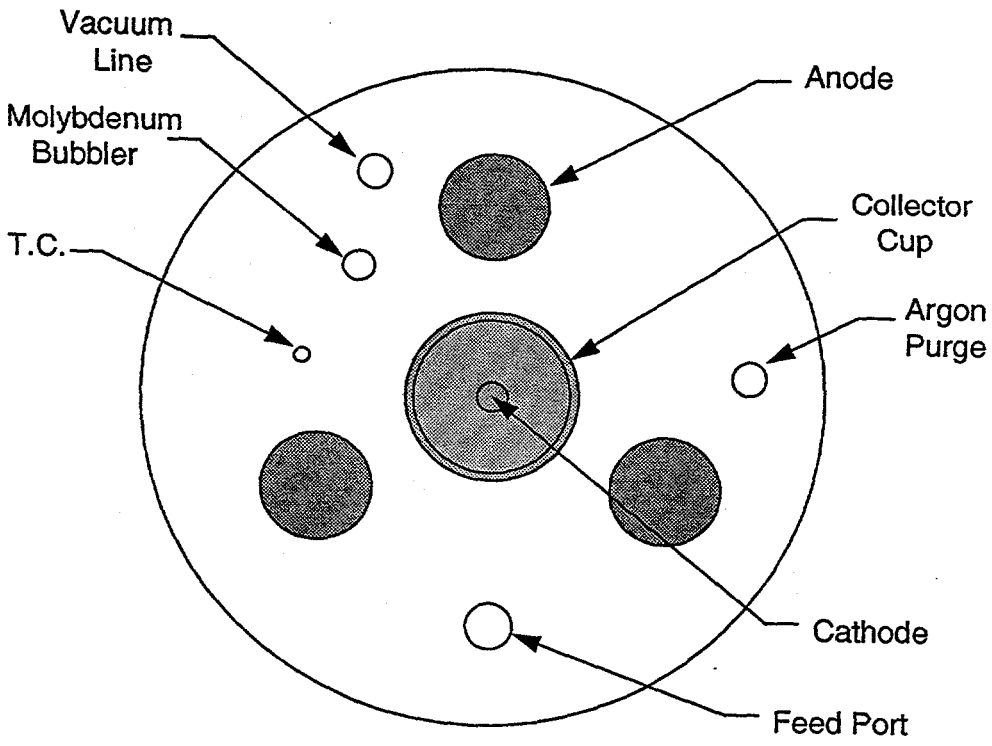


**Figure 24** 20-A Cell Lid

Three round anodes were placed around a center cathode to provide a large anode surface area. Anode current densities could be maintained at levels similar to those used in the 5-to-10-A cells. A feeder tube for semicontinuous feeding of neodymium oxide was installed next to a gas bubbler (molybdenum tube); this enhanced the dissolution of the oxide. A line for drying the electrolyte under vacuum and a line for backfilling the cell with argon were also installed through the lid.

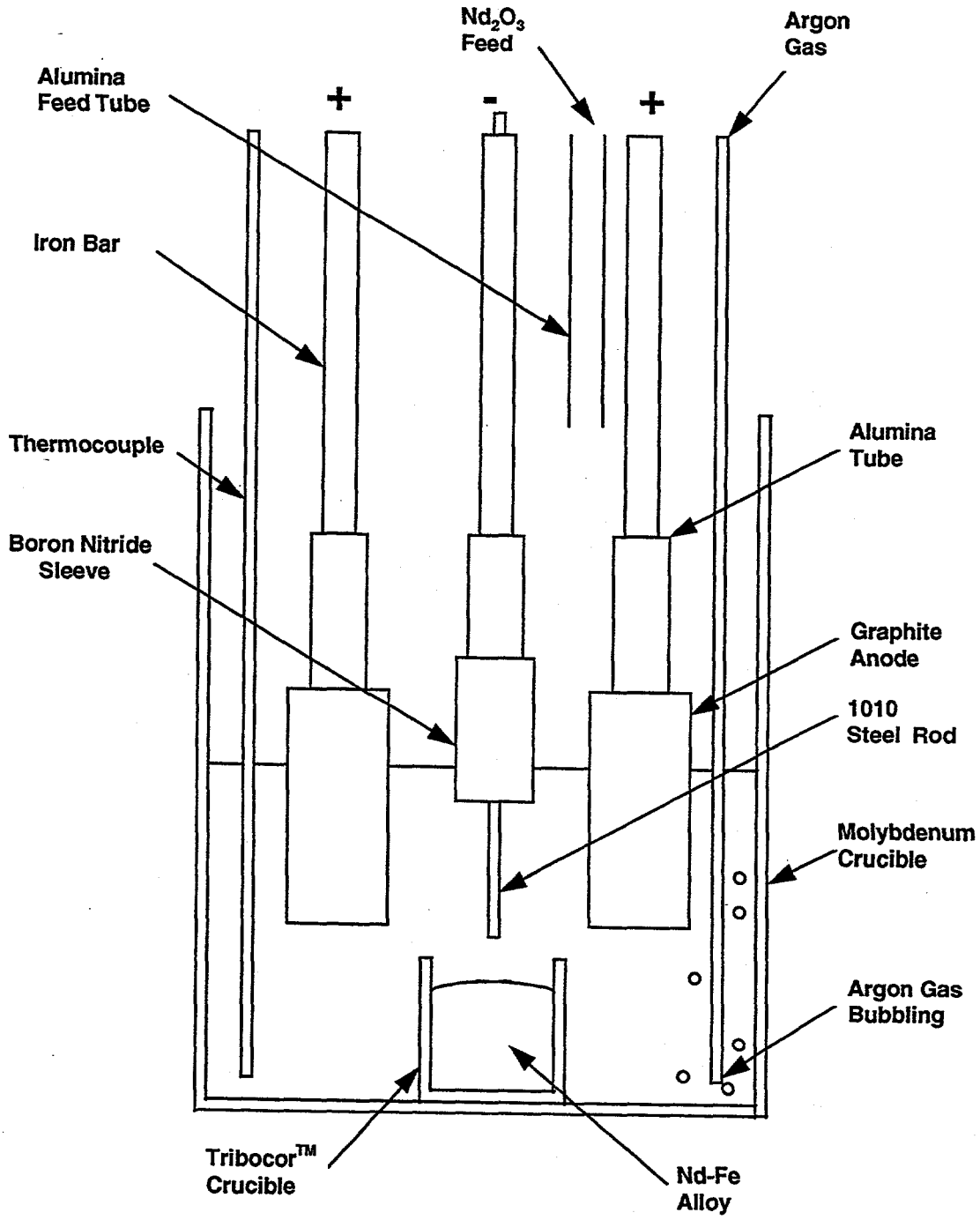


**Figure 25** Schematics of the 20-A Cell Design

### 3.3.2. Experimental Procedure

Neodymium fluoride, $NdF_3$ (60 wt%), lithium fluoride, LiF (20 wt%), and calcium fluoride, $CaF_2$ (20 wt%) were weighed and placed into a 5-inch high by 8-inch diameter molybdenum crucible. The crucible contained a centering plate to hold the collector cup (molybdenum or Tribocor®) stationary during electrolysis. The lid was assembled with all the appropriate electrochemical connections. Three graphite anodes, 3-inch high by 1-inch diameter, were attached to three stainless steel bars by threaded connections. A ¼-inch diameter iron rod (1010 steel) with a boron nitride protective sleeve was inserted through the lid. The charged cell was placed into the Inconel vessel and the lid installed. Vacuum drying of the electrolyte was initiated for a period of between 12 and 24 hours at temperatures between 500 and 600 °C. After drying, the cell was backfilled with argon and heated to 900 to 920 °C. The anodes were lowered 1⅝ inches into the electrolyte, and a surface area of 39 $cm^2$ for each anode was exposed to the electrolyte. Based on this surface area, a nominal current densities of 0.17 $A/cm^2$ was maintained during electrolysis. The cathode was lowered until the boron nitride sleeve was immersed ¼ inch; this suppressed reactions at the cathode-gas-electrolyte interface. Neodymium oxide was vacuum-dried at 500 to 600 °C for 24 hours, then to the electrolyte 30 minutes before electrolysis to give a concentration of 1.5 wt% $Nd_2O_3$. DC power was applied for a targeted duration of 6 hours. Neodymium oxide was fed into the cell at a theoretical feed rate of 50 % utilization (3.49 g / 10 min). Gas samples were taken during electrolysis to determine anodic products. Neodymium-iron alloy dripped off the cathode into the collector cup located at the bottom of the cell. The iron cathode was lowered into the electrolyte as it was consumed. The current efficiency was calculated from the cathode weight loss and total alloy recovered. Several metal samples were analyzed to determine iron and neodymium concentrations.

## 4. ELECTROLYSIS EXPERIMENTS

### 4.1. Electrolysis in $CaF_2$-LiF-CaO-$Nd_2O_3$ System

Three experiments were completed in the 10-A cell, utilizing a molybdenum crucible as the cathode. Agglomerated metal was neither visually observed nor recovered. Hydrogen evolution experiments on the electrolyte after solidification indicated the presence of metal in the vicinity adjacent to the molybdenum crucible; only small volumes of gas were evolved. No metal was recovered from this experiment.

Two experiments were conducted utilizing a ¼-inch diameter iron bar as the cathode. In both experiments, no metal was visually observed in the electrolyte. The cathode maintained its geometry throughout the run. Substantial metal accumulation at the cathode was indicated by hydrogen evolution experiments.

No metal was recovered from any of these experiments. While the presence of reactive metal in the electrolyte was indicated by hydrogen evolution analysis, it could not be established whether calcium, lithium, neodymium, or a combination of the three was present in the bath after electrolysis. Experiments in which an iron cathode was employed resulted in no consumption of the cathode, and no agglomerated cathodic metal was found in the solidified bath material after electrolysis. If neodymium metal had been produced, it would have attacked the iron cathode. One has to conclude, therefore, that no neodymium metal was deposited. Calcium and lithium do not attack iron and were the most likely metals produced in the 70 wt% $CaF_2$, 30 wt% LiF runs. With a high solubility of reactive metals such as calcium and lithium in the electrolyte, reoxidation resulted in a poor current efficiency.

### 4.2. Electrolysis in $NdF_3$-LiF-$Nd_2O_3$ and $NdF_3$-LiF-$CaF_2$- $Nd_2O_3$ Systems

#### 4.2.1. Electrolysis in 10-A Cell

Conditions and Current Efficiencies. Table VII lists the results obtained with the 10-A cell. Experiment number, electrolyte composition, temperature, cathode material, feed, duration, and current efficiency are presented. Compositions listed in Table VII are:

1 68 wt% $NdF_3$ / 32 wt% LiF

2 64.6 wt% $NdF_3$ / 35.4 wt% LiF

3 41.7 wt% $NdF_3$ / 41.7 wt% LiF / 16.6 wt% $CaF_2$

4 60 wt% $NdF_3$ / 20 wt% LiF / 20 wt% $CaF_2$

**Table VII** Experimentation in 10-A Cell

| Exp. # DOE-Nd- | Elec. Comp. | Temp. (°C) | Cathode Material | Feed | Duration Hr:Min | Current Eff. % *** |
|---|---|---|---|---|---|---|
| 1-77 | 1 | 1030-1040 | Mo | $NdF_3$ | 4:48 | ** |
| 1-78 | 1 | 925 | Fe | $NdF_3$ | 6:00 | 16.0 |
| 1-80 | 1 | 925 | Fe | $NdF_3$, $Nd_2O_3$ | 6:56 | 26.2 |
| 1-81 | 1 | 1030 | Mo | $NdF_3$ | 2:00 | ** |
| 1-82 | 1 | 922-945 | Fe | $NdF_3$ | 6:00 | 20.9 |
| 1-83 | 1 | 920-930 | Fe | $Nd_2O_3$ | 6:00 | 9.7 |
| 1-84 | 1 | 930-945 | Fe | $Nd_2O_3$ | 6:30 | 18.0 |
| 1-85 | 1 | 925-940 | Fe | $Nd_2O_3$ | 14:00 | 9.7 |
| 1-87 | 2 | 807-814 | Fe | $Nd_2O_3$ | 6:30 | 17.5 |
| 1-88 | 2 | 800-805 | Fe | $Nd_2O_3$ | 6:30 | 43.8 |
| 1-89 | 2 | 754-780 | Fe | $Nd_2O_3$ | 6:05 | 30.3 |
| 1-90 | 2 | 798-802 | Fe | $Nd_2O_3$ | 6:05 | 14.6 |
| 1-91 | 2 | 806-809 | Fe | $Nd_2O_3$ | 6:00 | 53.8 |
| 1-92 | 2 | 804-809 | Fe | $Nd_2O_3$ | 6:00 | 26.0 |
| 1-93 | 2 | 805-810 | Fe | $Nd_2O_3$ | 6:24 | 26.4 |
| 1-94 | 2 | 800-813 | Fe | $Nd_2O_3$ | 6:00 | 52.0 |
| 1-95 | 2 | 800-810 | Fe | $Nd_2O_3$ | 6:00 | ** |
| 1-97 | 2 | 809-813 | Fe | $Nd_2O_3$, $B_2O_3$ | 6:00 | 6.4 |
| 1-98 | 2 | 809-812 | Fe | $Nd_2O_3$, $Fe_2O_3$ | 6:00 | 34.6 |
| 1-184 | 3 | 900-925 | Fe | $Nd_2O_3$ | 5:00 | 67.2 |
| 1-185 | 3 | 900-905 | Fe | $Nd_2O_3$ | 6:00 | 51.4 |

| Exp. # DOE-Nd- | Elec. Comp. | Temp. (°C) | Cathode Material | Feed | Duration Hr:Min | Current Eff. % *** |
|---|---|---|---|---|---|---|
| 1-186 | 3 | 900-905 | Fe | $Nd_2O_3$ | 6:00 | 6.8 |
| 1-187 | 3 | 890-900 | Fe | $Nd_2O_3$ | 6:00 | 48.1 |
| 1-188 | 3 | 900-905 | Fe | $Nd_2O_3$ | 6:00 | 17.4 |
| 1-189 | 3 | 900-910 | Fe | $Nd_2O_3$ | 6:00 | 29.8 |
| 1-190 | 3 | 900-910 | Fe | $Nd_2O_3$ | 3:00 | * |
| 1-191 | 3 | 910-925 | Fe | $Nd_2O_3$ | 3:40 | 14.2 |
| 1-192 | 3 | 910-920 | Fe | $Nd_2O_3$ | 1:00 | * |
| 1-193 | 3 | 910-920 | Fe | $Nd_2O_3$ | 4:10 | * |
| 1-194 | 3 | 900-920 | Fe | - | 5:25 | 36.0 |
| 1-195 | 3 | 900-1000 | Fe | $Nd_2O_3$ | 2:30 | * |
| 1-196 | 3 | 940-950 | Fe | $Nd_2O_3$ | 2:35 | 16.7 |
| 1-197 | 3 | 930-940 | Fe | $Nd_2O_3$ | 3:10 | 40.0 |
| 1-198 | 3 | 930-940 | Fe | $Nd_2O_3$ | 6:00 | 52.0 |
| 1-199 | 3 | 940-950 | Fe | $Nd_2O_3$ | 3:30 | * |
| 1-200 | 3 | 910-920 | Fe | $Nd_2O_3$ | 6:00 | 45.6 |
| 1-206 | 3 | 910-920 | Fe | $Nd_2O_3$ | 6:00 | 44.6 |
| 1-207 | 4 | 910-920 | Fe | $Nd_2O_3$ | 3:20 | 74.5 |
| 1-208 | 4 | 910-920 | Fe | $Nd_2O_3$ | 5:10 | * |
| 1-209 | 4 | 900-910 | Fe | $Nd_2O_3$ | 6:00 | * |
| 1-210 | 4 | 910-920 | Fe | $Nd_2O_3$ | 6:00 | 32.2 |

* Could not be determined

** No visible metal recovered

*** Current efficiency based on metal recovered and cathode loss

Current-Voltage Characteristics. An example of a current-voltage curve is shown in Figure 26. In this figure, the cell voltage is plotted versus the electrolysis current. To obtain this plot, the DC current was increased linearly while both the voltage and current were recorded on a strip chart instrument. In Experiment # DOE-Nd-1-206 (Figure 26), curves were recorded at the beginning and end of the experiment, to show variations caused by the dissolved neodymium oxide content.

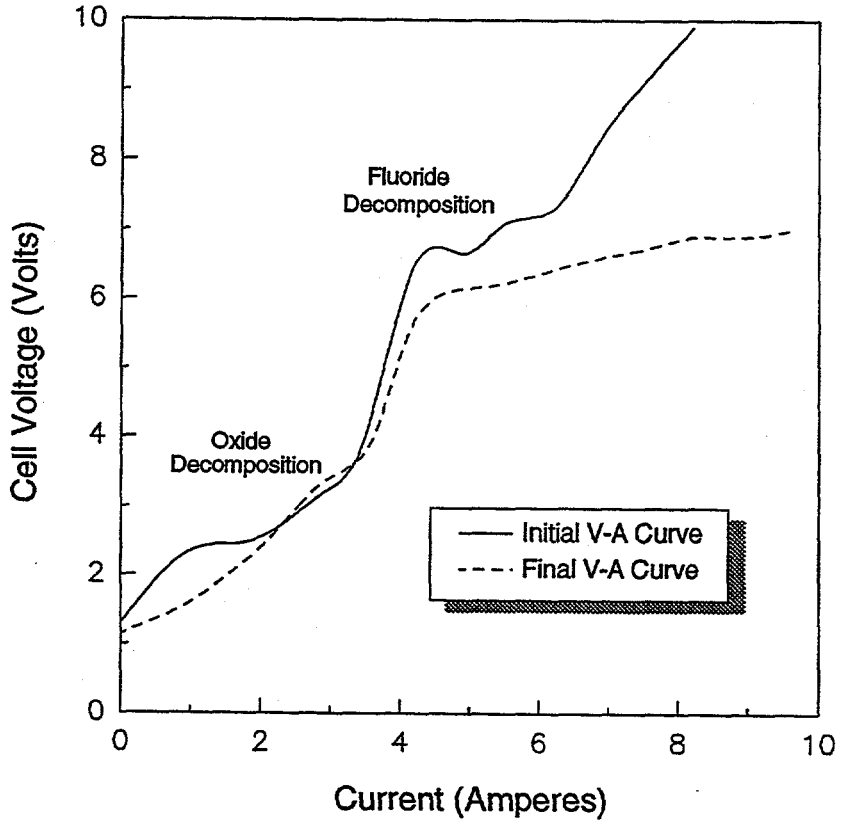


**Figure 26** Current-Voltage Characteristics (Experiment # DOE-Nd-1-206)

Analysis of Feed and Anode Gases. Moisture in the feed and electrolyte was determined to be critical to smooth operation of the electrolytic cell. Moisture content before drying for $Nd_2O_3$, $NdF_3$, LiF, and $CaF_2$ were determined at Rhône-Poulenc by TGA analysis. $NdF_3$ contained only 0.4 wt% $H_2O$ at a temperature up to 800 °C while both LiF and $CaF_2$ contained about 1.0 wt% $H_2O$ at a temperature up to 1000 °C. Neodymium oxide contained approximately 2.0 wt% $H_2O$ in the as received condition. Gas samples collected at the end of several electrolysis experiments were analyzed at Advanced Technology Systems by gas chromatography. Experiment #, mole% $CF_4$, mole%, CO, and mole% $CO_2$ are listed in Table VIII. The balance of the gas was argon, which was employed to stir the electrolyte during electrolysis.

**Table VIII** Analysis of Cell Gases from Experiments in 10-A Cell

| Experiment # DOE-Nd-1- | Mole % $CF_4$ | Mole % CO | Mole % $CO_2$ |
|---|---|---|---|
| 189 | 3.6 | 19.2 | 1.0 |
| 200 | 0.9 | 2.4 | 0.1 |
| 206 | 0.4 | 1.7 | 0.2 |

In Experiments # DOE-Nd-1-188 through DOE-Nd-1-196, the calcium fluoride containing a relatively high concentration of magnesium fluoride impurity, unknown at the time. The problem was discovered when metal from Experiment # DOE-Nd-1-194 was analyzed and found to contain 26.3 wt% magnesium. Electrolyte components were then analyzed to determine where the magnesium originated. It was found that the calcium fluoride contained 2.7 wt% magnesium, while other components contained <30 ppm magnesium. The remaining calcium fluoride was discarded, and new pure calcium fluoride (Mg <30 ppm) was procured.

Analysis of Cathode Deposits and Dust in Electrolyte. Formation of black dust in the electrolyte and buildup of solid deposits on the iron cathode were evident in most of the electrolytic experiments. Samples were collected after solidification of the electrolyte and analyzed by the Pittsburgh Applied Research Corporation for neodymium, iron, calcium, lithium and carbon content. The results are given in Table IX.

**Table IX** Analysis of Cathode Deposits and Dust in Electrolyte

| Exp. # DOE-Nd- | Dust or Cathode Buildup | wt% Nd | wt% Ca | wt% Li | wt% C | wt% Fe |
|---|---|---|---|---|---|---|
| 1-194 | dust | 20.5 | 8.1 | 6.8 | 8.1 | 1.3 |
| 1-197 | buildup | 47.0 | 5.7 | 7.0 | 2.7 | - |
| 1-206 | dust | 32.5 | 3.8 | 8.9 | 3.0 | 0.12 |

4.2.2. Discussion of Results in 10-A Cell

The following conclusions were drawn from the experiments listed in Table VII (5-10-A Cell Runs).

- Lower current efficiencies were observed in Experiments # DOE-Nd-1-77 through DOE-Nd-1-90 where the electrolyte was not vacuum-dried before electrolysis.

- No neodymium metal was recovered in experiments where molybdenum was used as a cathode. The activity of the neodymium was not reduced when deposited on the molybdenum, hence it dissolved into the electrolyte. Where iron was employed as a cathode, the reduced activity of neodymium allowed metal production.

- Higher current efficiencies were observed in Experiments # DOE-Nd-1-91 and DOE-Nd-1-94. In this case, neodymium oxide was added with the electrolyte and not fed continuously during electrolysis. The undissolved oxide in these two experiments did not contact the metal pool at the bottom of the cell. This resulted in less back reaction of the deposited Nd-Fe alloy.

- Drying of the electrolyte in Experiments # DOE-Nd-1-184 through DOE-Nd-1-210 generally produced higher current efficiencies than when drying was not employed.

- Calcium fluoride, used in Experiments # DOE-Nd-1-188 to DOE-Nd-1-196, containing relatively high concentrations of magnesium fluoride, led to poor current efficiencies. During electrolysis brittle metal high in magnesium was deposited.

- Boron nitride shielding of the iron cathode in Experiment # DOE-Nd-1-207 resulted in the highest current efficiency. The use of boron nitride as a shield eliminated the black build-up on the iron cathode.

- Calcium fluoride additions to the electrolyte improved metal coalescence resulting in higher current efficiencies. This increased coalescence reduces the neodymium alloy surface area exposed to the electrolyte and thus reduces its back reaction into the electrolyte.

Figure 26 represents a typical current-voltage curve. An initial oxide decomposition potential of approximately 2.2 to 2.4 volts can be observed along with an initial fluoride decomposition potential at 6.5 to 6.7 volts. The final decomposition curve illustrates a less pronounced oxide decomposition potential and a slightly lower fluoride decomposition potential. This may have resulted from anode surface alterations and anode geometrical changes that occurred during electrolysis.

Table VIII illustrates the anodic gas produced during electrolysis. If the ratio of moles of fluorine to moles of oxygen are taken into account for each experiment, the number of electrons reacting with oxide ranged between 41.9 % and 59.6 % (Experiment # DOE-Nd-1-200 and DOE-Nd-1-189 respectively). Higher oxygen ratios can be expected with increasing oxide concentrations and lower anode current densities.

The black dust observed on the surface of the electrolyte during and after electrolysis first was thought to be particles that spalled off the anode during electrolysis. Table IX representing two analyses conducted on samples of black dust shows the low percentage of carbon actually present. The following reaction was theorized as the origin of the black dust:

$$Nd_{\text{dissolved in electrolyte}} + CO_2 \text{ or } CF_{4\ \text{anodic products}} \rightarrow Nd_2O_3 \text{ or } NdF_3 + C$$

Reducing metal solubility was observed to minimize black dusting and give higher current efficiencies.

Cathode buildup problems were eliminated by the use of a boron nitride protection sleeve. Electrochemical reduction of anodic gases at the cathode-electrolyte-gas interface resulted in carbon deposition onto the cathode when no shield was present. Analysis of the deposits are shown in Table IX (black dust and cathode buildup), illustrating the carbon present in the buildup. A strong carbide smell also was noted.

### 4.2.3 Electrolysis with 20-A Cell

Table X lists the results from the 20-A electrolytic experiments. Experiment number, electrolyte composition, temperature, cathode type, feed, duration, and current efficiency are shown.

Examples of current-voltage curves recorded during two experiments are shown in Figures 27 & 28. The plot was obtained using the same experimental technique described in the 5-10-A cell experiments. Cell voltage vs DC current is plotted in these figures. Curves were recorded at start-up and toward the end of the experiments. The temperature was varied in the second experiment.

Metal analysis were performed on several samples to verify reduction components. Samples were drilled and the filings were collected. Analysis of the filings by atomic absorption were conducted by the Pittsburgh Applied Research Corporation. Table XI illustrates analytical results from 20-A electrolytic experiments.

Gas samples collected at the end of several 20-A electrolytic experiments are listed in Table XII. The same procedure described for 5-to-10-A cell runs was used to collect gas samples. Experiment number, mole% $CF_4$, mole% CO, and mole% $CO_2$ are given. The balance of the gas can be assumed to be argon.

**Table X** Results of Experiments with 20-A Cell

| Exp. # DOE-Nd- | Elect. Comp. | Temp. (°C) | Cathode | Feed | Duration Hr:Min | Current Eff. % |
|---|---|---|---|---|---|---|
| 1-211 | 4 | 910-920 | Fe | $Nd_2O_3$ | 6:00 | 66.3 |
| 1-212 | 4 | 900-920 | Fe | $Nd_2O_3$ | 6:00 | 70.0 |
| 1-213 | 4 | 900-920 | Fe | $Nd_2O_3$ | 6:00 | 40.4 |
| 1-214 | 4 | 900-920 | Fe | $Nd_2O_3$ | 6:00 | 60.2 |
| 1-215 | 4 | 900-920 | Fe | $Nd_2O_3$ | 6:00 | * |
| 1-216 | 4 | 900-920 | Fe | $Nd_2O_3$ | 6:00 | 48.8 |
| 1-217 | 4 | 900-920 | Fe | $Nd_2O_3$ | 6:00 | 45.3 |
| 1-218 | 4 | 900-920 | Fe | $Nd_2O_3$ | 6:00 | 87.0 |
| 1-219 | 4 | 900-920 | Fe | $Nd_2O_3$ | 3:20 | 57.8 |
| 1-220 | 4 | 900-920 | Fe | $Nd_2O_3$ | 6:00 | 53.0 |
| 1-221 | 4 | 900-920 | Fe | $Nd_2O_3$ | 6:00 | 62.3 |
| 1-222 | 4 | 900-920 | Fe | $Nd_2O_3$ | 6:00 | 45.0 |

* Could not be obtained

**Table XI** Analysis of Metal from Electrolysis Experiments with 20-A Cell

| Exp. # DOE-Nd- | wt% Nd | wt% Fe | wt% Li | wt% Ca | wt% Pr |
|---|---|---|---|---|---|
| 1-211 | 80.8 | 14.5 | 0.02 | 0.07 | 1.1 |
| 1-212 | 77.1 | 15.9 | <0.02 | 0.05 | 1.2 |

**Table XII** Analysis of Cell Gases from Experiments with 20-A Cell

| Exp. # DOE-Nd- | Mole % $CF_4$ | Mole % CO | Mole % $CO_2$ |
|---|---|---|---|
| 1-211 | 7.63 | 6.59 | 2.07 |
| 1-212 | 3.55 | 5.95 | 0.37 |
| 1-218 | 17.94 | 7.04 | 1.43 |

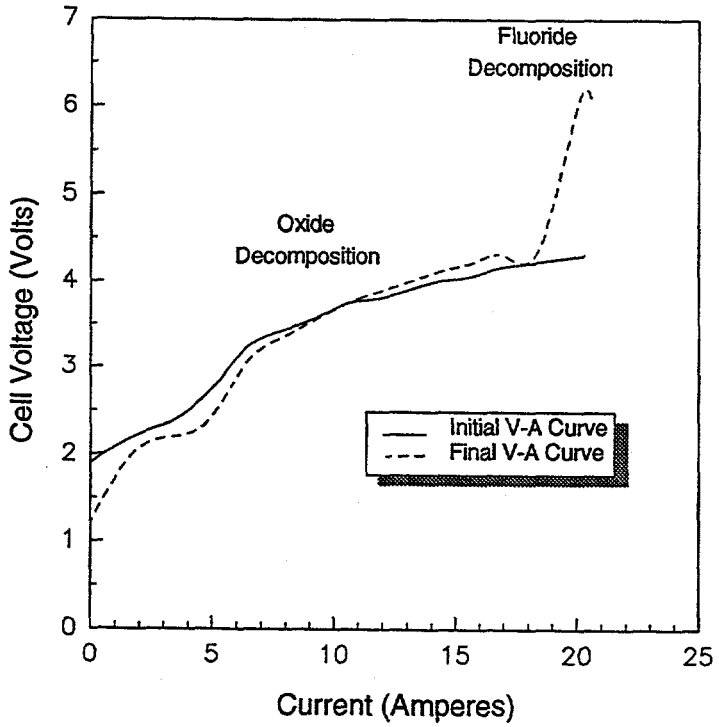


**Figure 27** Current-Voltage Characteristics
(Experiment # DOE-Nd-1-216)

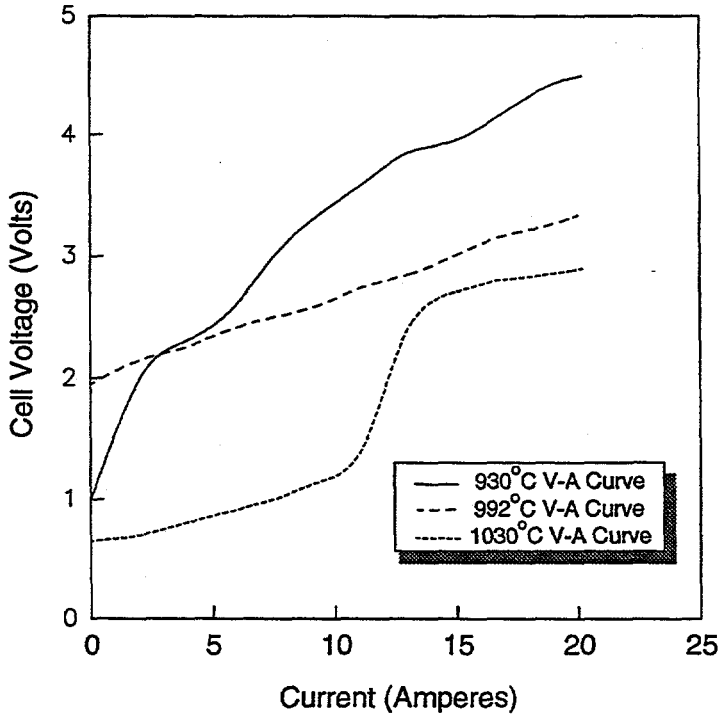


**Figure 28** Current-Voltage Characteristics
(Experiment # DOE-Nd-1-224)

4.2.4. Discussion of Results Obtained with 20-A Cell

The following conclusions were drawn from the experiments listed in Table X (20-A cell).

- Larger cell size (i.e. greater distance between anode and cathode) reduced cell shorting problems that occurred in the 5-to-10-A cell runs.

- Improved current efficiency over the 5-to-10-A cell runs can be attributed to the following:
  (1) Vacuum drying of feed and electrolyte which reduced the tendency to form subvalent species of neodymium;
  (2) larger cell size (reduced shorting); and
  (3) installation of the boron nitride as shield around the cathode which eliminated cathode buildup by preventing electrolytic reduction of anodic gas at the cathode-gas-electrolyte interface.

- Current efficiencies as high as 87 % were obtained with a total average of 58% for all experiments.

- Higher current efficiency runs were associated with reduced dusting in the cell and less neodymium metal dissolved in the electrolyte, and there was less back reaction with anodic gas.

Figure 27 shows a current-voltage characteristics (Experiment # DOE-Nd-1-216) taken during electrolysis of neodymium oxide in the 20-A cell. Initial and final decomposition potentials between 2.1 and 2.3 volts can be observed in this plot. Fluoride decomposition could not be obtained at currents up to 20 A initially. However, at the end of the experiment (final current-voltage curve), fluoride decomposition potentials were obtained at 20 A. The difference between the two curves was attributed to anode surface changes (anode becoming smoother with less surface area) and slow dissolution rates of oxide.

In Experiment # DOE-Nd-1-224, variation of temperature changed the current-voltage characteristics. These changes are too difficult to interpret at this time. They may be associated with changes in surface compounds forming at the electrode.

Analysis of several metal samples are shown in Table XI. Samples from Experiments # DOE-Nd-1-211 (CE = 66.3 %) and DOE-Nd-1-212 (CE = 70 %) were analyzed to contain 80.8 wt% and 77.1 wt% neodymium, respectively. Iron concentrations determined between 14.5 and 15.9 wt% lead to liquidus temperatures between 750 and 800 °C, respectively, as seen in the Nd-Fe phase diagram of Figure 3. Praseodymium metal concentration of approximately 1.0 wt% came from impurities in the neodymium oxide and neodymium fluoride. Praseodymium is the major impurity contained in neodymium compounds. Lithium and calcium in

very low concentrations were also found in the Nd-Fe alloy. These two elements came from the lithium and calcium fluoride electrolyte components.

Gas analysis for the three highest current efficiency experiments are listed in Table XII. The highest current efficiency of 87 %, obtained in Experiment # DOE-Nd-1-218, is associated with the highest $CF_4$ content in the anodic product. In this experiment, 78.4% of the total electrons produced $CF_4$ while 21.6% of the electrons produced CO and $CO_2$. For Experiment # DOE-Nd-1-212, a much more favorable percentage of oxygen to fluorine was obtained; 48.5 % of the electrons reacted with oxide while only 51.5 % went into producing fluorine-containing compounds.

## 4.3. Electrolysis with Composite Anodes

### 4.3.1. Experimental Procedure

Five tests were made with composite anodes. Electrolyte containing 64.6 wt% $NdF_3$ / 35.4 wt% LiF was melted in the inert atmosphere electrolyte cell. A prefabricated composite anode and a ¼-inch diameter iron cathode were immersed into the electrolyte once the cell temperature reached 900 °C. Anode current densities between 0.33 A/cm$^2$ and 1.2 A/cm$^2$ (at 5 A maximum current) were maintained for the duration of the experiments.

### 4.3.2. Results

The composite anode in each test failed after 15 and 20 minutes of electrolysis. Reasons for anode failure were:

- Anode fell into the electrolyte because the threaded connection weakened.
- Anode became non-conducting due to the breakdown of carbon-carbon contacts inside the anode.

Neodymium metal production was verified in Experiment # DOE-Nd-1-138 leading to a current efficiency of 30.4 %.

### 4.3.3. Discussion of Results

Five preliminary electrolytic experiments with composite anodes were enough to identify several problems which could occur during electrolysis. Problems with anode strength resulted in the anodes falling into the melt causing premature failure of the test. These difficulties were minimized by increasing the strength of the anode (i.e. by densification) in later experiments. Anode conductivity problems were not solved. Possible solutions to this problem are listed below:

- Increase the percent carbon contained in the anode so more carbon-carbon bonds are present.
- Add a conducting metal such as iron or boron to the anode to enhance conductivity.
- Increase the percent densification in the anode by longer sintering and slightly higher sintering temperatures.

# DISCUSSION

## MAIN FACTORS AFFECTING ELECTROLYSIS

### Anode Effect

The term "anode effect" is used in molten salt electrolysis to describe a phenomenon associated with a substantial rise in electrode potential. When the oxide concentration in aluminum electrolysis, for example, is not sufficient to maintain a normal oxidation of the carbon to carbon dioxide, carbon fluorides form on the electrode surface, whose wetting characteristics change to cause decreased wetting by electrolyte. A gas film forms on the surface and potentials of 20 to 30 V are necessary to conduct the direct current through this film. A similar phenomenon can be observed in the electrolysis of neodymium oxide.

Current-voltage characteristics and analysis of cell gases indicate that with $NdF_3$-LiF electrolytes there exists a potential region between the oxidation of oxide and the anode effect in which $CF_4$ is evolved electrochemically, without ohmic blocking of the current. Extended operation in this region is possible and may be advantageous.

### Scum Formation

Neodymium metal interacting with electrolyte was observed to form scum. This scum formation was increased by increasing oxide content in the bath and was particularly pronounced in the presence of moisture.

Solidified scum was found to contain neodymium metal. It is possible that this metal forms on cooling by disproportionation of a subvalent neodymium species.

Sludge formation observed during the reduction of tantalum [18] has been ascribed to the disproportionation of lower-valent complexes that formed when fluoride had been added to the chloride electrolytes and a tantalum anode was used. A suspension of metallic tantalum contributed both to the formation of sludge and the formation of metal dendrites growing out from the electrodes at the surface of the electrolyte.

### Cathode Deposits

Neodymium metal tends to dissolve into the electrolyte. Deposition of solid, dendritic or dispersed neodymium with a high surface area is to be avoided. Such deposits can form on any cathode substrate, but are expected to be particularly numerous when reduced incoherent impurity deposits become reduction sites for neodymium.

Solid carbonaceous deposits can form by reduction of anode gases at the cathode. A particularly sensitive area is the vicinity of the three-phase boundary of solid cathode, electrolyte and cell gas above the electrolyte. Significant operational improvement has been achieved by shielding the cathode in this area with an electrically non-conductive material such as boron nitride.

## PATH TO HIGH CURRENT EFFICIENCIES

Current efficiency losses occur when neodymium metal dissolves into the electrolyte and then is reoxidized at the anode or, more likely, by anode products. The true mechanism may involve the formation of subvalent species rather than a physical dissolution of reactive metal, and the oxidation of such species.

Scum formation and metal dissolution or formation of subvalent species are suspected to be related. At low oxide content, less scum formation has been observed. High current efficiencies were obtained, but high concentrations of fluorocarbon compounds were found in the off-gases.

Current efficiency losses are less if no pure neodymium is exposed to the electrolyte. Neodymium in neodymium-iron alloy has a reduced activity and, thus, a reduced tendency to dissolve into the electrolyte.

To achieve high current efficiency, the deposition of neodymium to form an iron-neodymium alloy at potentials permitting the formation of fluorocarbon anode products is tentatively recommended. This means that the anode gases need to be reacted with neodymium oxide to form neodymium fluoride and carbon oxides. This may occur, at least partially, in the electrolyte; a similar reaction has been reported for cryolitic melts [16]. The $CF_4$ in cell off-gases, furthermore, may be reacted externally with $Nd_2O_3$ to form neodymium fluoride.

# CONCLUSIONS AND RECOMMENDATIONS

The electrolysis of neodymium oxide continues to show promise for implementation as a low-cost process to produce high-quality neodymium or neodymium-iron alloy.

Optimum process design and operation remains to be established. While current efficiencies up to 87 percent were demonstrated, factors essential to achieving consistent results have not been fully identified. Scale-up from a 5-to-10-A cell size to a 20-A laboratory unit removed some of the operational difficulties. Further scale-up and extension of electrolysis duration are expected to alleviate negative effects associated with cell start-up.

It is recommended that boundaries of acceptable operation will be further explored with a 20-A laboratory cell, including extension to 30 hours of electrolysis. A 100-A cell then should be designed and operated. Experimentation with this cell will provide data necessary to plan a pilot cell operation.

The analysis of economic aspects clearly showed the merits of a neodymium oxide electrolysis in comparison to present manufacturing of neodymium. Broad implementation of advanced electric motor technology employing neodymium-containing permanent magnets would lead to substantial energy savings.

# References


[1] R. A. Sharma, "Neodymium Production Processes", Journal of Metals, February 1987, pp. 33-37.

[2] W. G. Moffatt, Binary Phase Diagram Handbook, General Electric Company (1976).

[3] M. F. Chambers and J. E. Murphy, "Electrolytic Production of Neodymium Metal from a Molten Chloride Electrolyte", Bureau of Mines Report of Investigations, RI 9391 (1991).

[4] E. S. Shedd, J. D. Marchant, and T. A. Henrie, "Electrowinning and Tapping of Lanthanum Metal", Bureu of Mines Report of Investigations, RI 6882 (1966).

[5] E. Morrice and T. A. Henrie, "Electrowinning High-Purity Neodymium, Praseodymium, and Didymium Metals from their Oxides", Bureau of Mines Report of Investigations, RI 6957 (1967).

[6] E. Morrice, E. S. Shedd, and T. A. Henrie, "Direct Electrolysis of Rare-Earth Oxides to Metals and Alloys in Fluoride Melts", Bureau of Mines Report of Investigations, RI 7146 (1968).

[7] E. Morrice, E. S. Shedd, M. M. Wong, and T. A. Henrie, "Preparation of Cobalt-Rare-Earth Alloys by Electrolysis", Journal of Metals, January 1969, pp. 34-37.

[8] J. E. Murphy, Technical Discussion at Bureau of Mines, Reno, Nevada, 12 July 1993.

[9] Z. Zhihong, W. Diwu, J. Shizhou, L. Wenhuai, and C. Anhong, "The Preparation of Nd-Fe Alloy by Electrowinning from Neodymium Oxide", Proceedings 12th Int. Workshop on RE Magnets and their Applications, Canberra, Australia (1992).

[10] EMEC Consultants, "Dry Extraction of Silicon and Aluminum from Lunar Ores", Final Report, Contract NAS 9-17811, submitted to NASA Johnson Space Center, September 1989.

[11] Handbook of Chemistry and Physics, 45th edition, The Chemical Rubber Company (1964).

[12] Reynolds Metals Company, "Alumina Concentration Meter", U.S. Patent No. 3,471,390 (1969).

[13] T. J. Johnston and N. E. Richrads, "Laboratory and Field Studies with an Improved Direct-Reading Alumina Concentration Meter", Light Metals 1974, Vol. 1, p.94.

[14] A. T. Tabereaux and N. E. Richards, "An Improved Alumina Concentration Meter", Light Metals 1983, pp. 495-506.

[15] A. S. Dworkin and M. A. Bredig, "Miscibility of Liquid metals with Salts. X. Various Studies in Alkaline Earth Metal-Metal Fluoride and Rare Earth Metal-Metal Difluoride and Trifluoride Systems" J. Phys. Chem., **75**, 2340-2344 (1971).

[16] A. J. Calandra, "The Reaction Occurring Between Gaseous $CF_4$ and Oxides Dissolved in Different Molten Fluorides. Some Practical Aspects", J. Appl. Electrochemistry, **12**, 411-416 (1982).

[17] J. C. Withers and G. V. Upperman, "Composite Anode for the Electrolytic Deposition of Aluminum", U. S. P. 4,342,637 (1982).

[18] L. P. Polyakova, E. G. Ploykov, A. I. Sorokin, and P. T. Stangrit, "Secondary processes during tantalum electrodeposition in molten salts", J. Applied Electrochemistry, **22**, 628-637 (1992).

# APPENDIX I

## ECONOMIC / BENEFIT ANALYSIS

### Electrolysis vs. Calciothermic Reduction -- Economic Comparison

**Contributed by Dr. Charles O. Bounds**

Dr. Bounds is Director of R & D, Rare Earths and Gallium, Rhône-Poulenc Basic Chemicals Co., Cranbury, New Jersey.

Rhône-Poulenc participated in this project as partner and subcontractor whose contribution constitute in-kind cost-sharing.

The importance of the cost and quality of the neodymium raw material (either pure Nd metal or Nd/Fe eutectic) to the production of a typical NdFeB magnet alloy is easily seen by examining the Alloy Specification shown in Table I. Note that the specification shown defines an alloy for a sintered magnet. Since neodymium accounts for approximately one-third of the alloy's weight, the financial importance is obvious. For quality, the specification indicates that two issues are of potential importance: first, minor elements can be a "poison" to the performance of the alloy (e.g., Ca, Mg, Si, C) indicating that refractory selection is critical, and second, the very tight control required for the alloy composition indicates that, if a Nd/Fe eutectic is produced, very accurate TRE (total rare earth content) control and/or analysis is required, as well as the production of either raw material with very low levels of dissolved gases (e.g., O and N). The quality aspects must be very carefully monitored as the cell is scaled-up.

Despite the early studies of Nd electrolysis by the U. S. Bureau of Mines, no Nd metal or Nd/Fe eutectic is being produced by the electrolytic process in the western world. Five American and European companies have been reported as producing or having recently produced neodymium via some form of calciothermic production: Rhône-Poulenc; Treibacher; Neomet; Rare Earth Products; and General Motors (Magnaquench). It is reported that Nd/Fe eutectic is being produced electrolytically in Japan by Santoku, Shin Etsu, Sumitomo Light Metals, and Showa Denko. In the Peoples Republic of China, there are reports of literally dozens of producers utilizing both electrolytic and calciothermic techniques.

## INTRODUCTION

A variety of metallothermic production variations have been reported in the literature; all of these can be considered enhancements of the pioneering work by the Ames Laboratories. The enhancements involve the use of fluxes and/or the production of the eutectic to simplify how the process deals with the control of Ca, N, O, etc. in the final product. It is beyond the scope of this report to consider these variations, which are not believed to make a major impact on the economic assessment. Thus, in this report, we will compare the classical two-step Ames calciothermic production process with the electrolytic production of Nd/Fe eutectic as described in Figure 1. The unit costs and factors used to calculate the requirements for the various raw materials, reagents and utilities are summarized in Table II.

### Calciothermic Reduction

Since the electrolytic process is described fully elsewhere in this report, this process will not be more fully described in this section. A brief description of the calciothermic process is included, however, to provide sufficient background to understand the cost issues.

The calciothermic process is inherently a batch process that is typically conducted in a vacuum-induction-melt (VIM) furnace. The reduction is effected by the addition of calcium metal to neodymium fluoride per the following reaction:

$$3\ Ca + 2\ NdF_3 \text{ ----> } 3\ CaF_2 + 2\ Nd\ .$$

The fluoride raw material has been chosen, rather than the chloride, because it is relatively nonhygroscopic. The raw material and reductant are selected or preprocessed to minimize the introduction of dissolved gases. A sufficient excess of the calcium reductant is added to insure a high recovery of neodymium.

The raw materials are blended and charged into a tantalum crucible. After the VIM furnace has been evacuated and sometimes backfilled with argon, the reaction mass is heated by induction to the selected reaction temperature, typically 1400 °C. The mixture is maintained at temperature long enough to insure complete reduction has occurred. The entire molten mass is then poured into a suitable mold, wherein the slag separates cleanly from the solidifying metal. After cooling to room temperature, the salt layer, being quite brittle, is removed from the metal. The metal product at this point is impure, with calcium being the chief impurity; calcium levels greater than 1 % by weight are frequently encountered. This calcium is removed by reheating the impure ingot in vacuum at about 1100 °C.

This process is characterized as having a relatively low capital intensity, even if two VIM furnaces are utilized. The process is quite flexible, easily accommodating relatively wide demand swings. The process drawbacks are:

- The requirement that relatively expensive $NdF_3$ be used as the only viable raw material;

- the use of a very expensive reductant, Ca metal, and the demand that only Ca with a low gas content be used;

- the requirement that a very stable crucible, normally Ta, be utilized; and

- the relatively high labor intensity inherent with a batch process, that can unlikely be operated continuously.

## CALCIOTHERMIC PROCESS OPERATING COST

We have somewhat arbitrarily decided to estimate the costs of the calciothermic process at two plant capacities: 235 MT and 1175 MT annually. Utilizing the unit costs and the consumption factors shown in Table II, the direct operating costs are computed to be $ 27.26 and $ 25.75 per kg of product metal at 235 MT and 1175 MT, respectively. These costs exclude the costs of local taxes, depreciation, interest on borrowed money and/or working capital, analytical laboratory expenses, etc. As noted above, the operating costs are dominated by the raw material cost (70 %), the Ca-reductant cost (13 %), and the labor cost (7 %). Since the raw material and reductant costs are so high and are completely variable, there is only a 5 % decrease in the unit cost of production even with a five-fold increase in the production rate.

## ELECTROLYTIC PROCESS COST

The direct operating costs of the electrolytic process are presented in Table IV for the same two capacities of 235 MT and 1175 MT annually. The estimated costs are $ 18.50 and $ 17.49 per kg at 235 MT and 1175 MT, respectively. The raw material cost for $Nd_2O_3$ totally dominates, exceeding 80 % of the direct operating expense. Again, only a very minor cost reduction is projected for a throughput increase from 235 MT to 1175 MT per year. The major difference between the calciothermic and electrolytic process costs, at 235 MT/year are:

| | Calciothermic | Electrolytic | Difference |
|---|---|---|---|
| Raw Materials | $ 18.77 | $ 15.34 | $ 3.43 |
| Reductants | 3.93 | - | 3.93 |
| Labor | 1.90 | 1.46 | 0.44 |
| Maintenance & Crucibles | 1.76 | 0.22 | 1.54 |
| Electricity | 0.08 | 0.21 | (0.13) |

As expected, the potential savings in raw materials and reductants dominate. The total operating cost reduction is estimated to exceed 30 percent.

### Capital Costs

A very preliminary capital cost estimate for the electrolytic process is compared in Table V to a more reliable estimate for the calciothermic process. It is realistic to anticipate that the capital cost estimate for the electrolytic process will escalate as the process is more fully defined. This preliminary analysis, however, suggests that the electrolytic process will not be substantially more costly to build than the calciothermic process. The operating cost dominates the comparison and the projected 30+ % savings justifies the development expense for electrolysis.

## DISCUSSION AND SUMMARY

This economic analysis confirms the potential of the electrolytic process. The critical factors on which the success of the electrolytic process rests are:

- The use of $Nd_2O_3$, and not $NdF_3$, as the primary source of Nd;
- a reasonably high yield of Nd (>90 % utilization efficiency) must be realized;
- a pure Nd product (low oxygen and calcium contents) must be generated without post-electrolysis refining.

This analysis suggests that a high electrolytic Faraday yield, anode consumption rate and cell campaign life (electrolyte make-up rate) are not critical.

Appendix I

**Table I.** Typical NdFeB Alloy Specification

| Element | Weight |
|---|---|
| TRE | 30.5 ± 0.3% |
| Nd (TRE-Dy) | 98% |
| Dy | 2.50 ± 0.05% |
| Nb, V, Mo | 0.65 to 2.0 ± 0.03% |
| Al, Cu | 0.05 to 0.30 ± 0.02% |
| Ca | 500 ppm max. |
| Mg | 500 ppm max. |
| Si | 2000 ppm max. |
| C | 500 ppm max. |
| O | 750 ppm max. |

**Table II.** Unit Costs and Factors

| Calciothermic Process & Electrolytic Process | |
|---|---|
| | |
| Nd Raw Material (Ca-thermic) | $NdF_3$ |
| Nd Content of $NdF_3$ | 71.7% (by weight) |
| Nd Yield to Purified Product | 93% (Ca-thermic) |
| $NdF_3$ Premium vs. $Nd_2O_3$ | 15% |
| Price for $NdF_3$ | $13.75 per kg NdF3 |
| Stoichiometric Excess of Ca | 3% |
| Ca-metal Price | $8.50 per kg |
| Direct Labor Rate | $15.00 per mhr |
| Electricity Rate | $0.035 per KWH |
| Argon Gas | |
| | |
| Nd Raw Material (Electrolytic) | $Nd_2O_3$ |
| Nd Content of $Nd_2O_3$ | 85.7% (by weight) |
| Price for $Nd_2O_3$ | |
| Carbon For Electrodes | $3.50 per kg |
| Iron for Cathodes | $1.50 per kg |
| Electrolyte Make-up KRate | 5% |
| Nd Yield to Eutectic | 99% (Electrolytic) |

**Table III.** Calciothermic Process -- Direct Cost Breakdown *

| | at 235MT | at 1175MT |
|---|---|---|
| ■ $NdF_3$ Raw Material (@ 93% yield and $12.50/kg) | 18.77 | 18.77 |
| ■ Calcium Metal (@ 3% excess and $10.00/kg refined) | 3.93 | 3.93 |
| ■ Miscellaneous Other Materials | 0.10 | 0.10 |
| ■ Labor and Supervision (@ $15.00/hr. for labor and 30% for fringes) | 1.90 | 1.02 |
| ■ Electricity (@ 3.5 cents/kWH) | 0.08 | 0.08 |
| ■ Crucibles (Ta) | .92 | 0.74 |
| ■ Maintenance | 0.84 | 0.57 |
| ■ Miscellaneous | 0.72 | 0.54 |
| **Total** | **$27.26** | **$25.75** |

* Cost is exclusive of taxes, depreciation, interest, analytical, etc.

**Table IV.** Electrolytic Process -- Direct Cost Breakdown *

| | 235MT | 1175MT |
|---|---|---|
| ■ $Nd_2O_3$ Raw Material (@ 98% Yield and $13.00/kg) | $15.34 | $15.34 |
| ■ Carbon Anodes | 0.30 | 0.30 |
| ■ Iron Cathodes (30,000 kg/yr @ $1.30/kg) | 0.17 | 0.17 |
| ■ Electrolyte Make-Up (5%) | 0.02 | 0.02 |
| ■ Argon ($15,000 per yr.) | 0.06 | 0.06 |
| ■ Electricity (6 kWH/kg @ 3.5 cents/kWH) | 0.21 | 0.21 |
| ■ Labor (2 direct + support + supervision + fringes @ $15.00/hr.) | 1.46 | 0.45 |
| ■ Maintenance | 0.22 | 0.22 |
| ■ Miscellaneous | 0.72 | 0.72 |
| **Total** | **$18.50** | **$17.49** |

* Cost is exclusive of taxes, depreciation, interest, analytical, etc.

**Table V.** Capital Costs *

**Calciothermic:**

Estimates based on actual cost of equipment circa 1987 and then extrapolated to targeted capacity and to 1994 construction

| | | |
|---|---|---|
| 235 MT/Annum | - | $1,018,000 |
| 1175 MT/Annum | - | $3,560,000 |

**Electrolytic:**

Estimate based on EMEC breakdown of Cell Cost Components and assumption that installation cost will equal 50% of equipment cost

| | | |
|---|---|---|
| 235 MT/Annum | - | $ 774,000 |
| 1175 MT/Annum | - | $2,610,000 |

* Order of magnitude estimates - not based on engineering analysis

Calciothermic

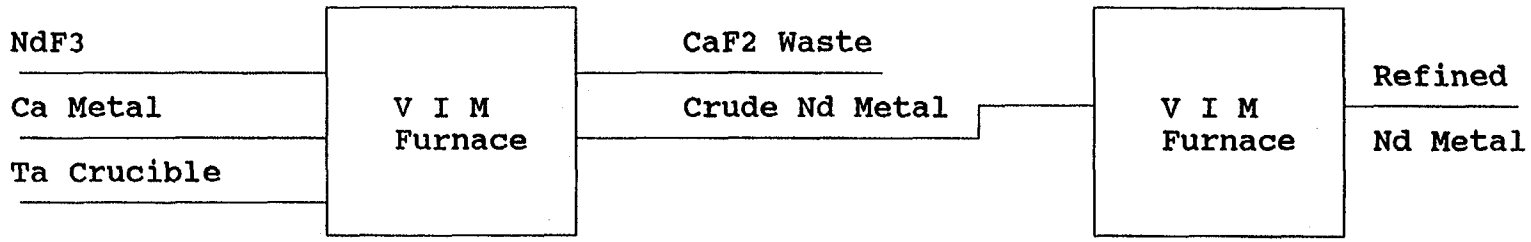


Electrolysis

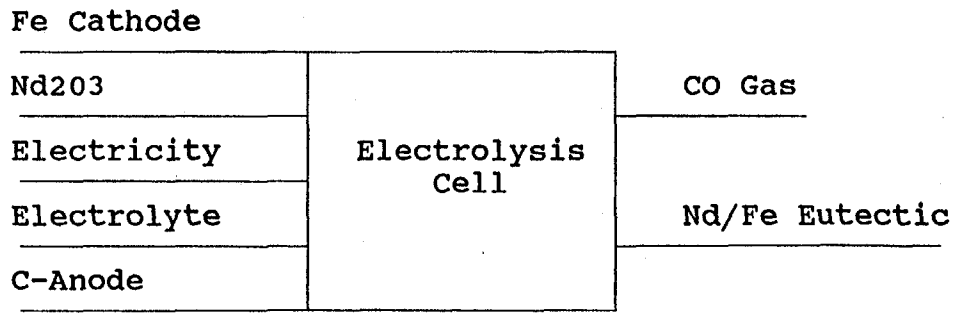


**Figure 1.** Processes to Produce Nd-Metal and Nd/Fe Eutectic

# APPENDIX II

## ECONOMIC / BENEFIT ANALYSIS

### Projected Cost and Energy Savings with Neodymium Alloy Magnet Motors

**Contributed by Mr. C. Norman Cochran**

Mr. Cochran is a Consulting Scientific Associate of EMEC Consultants. He prepared this contribution as independent contractor.

Mr. Cochran spent a career with the Aluminum Company of America, conducting process-related physico-chemical R & D, serving as Division Manager, and engaging in systematic technology forecasting.

TABLE OF CONTENTS

# PROJECTED COST AND ENERGY SAVINGS WITH NEODYMIUM ALLOY MAGNET MOTORS

## OVERVIEW

The potential annual reduction in U.S electrical energy use with neodymium (Nd) alloy magnets motors in the place of existing electrical motors is estimated to be 124 x $10^{12}$ watt-hours, about 4.4% of the electricity generated in 1990 or 1.30-quadrillion BTU's, as summarized in Table 1. This is based on the 1988 U.S. electric motor population mix not including electric motors in motor vehicles and commercial aircraft. The potential fuel savings for Nd-alloy magnet motors in 1989 U.S. motor vehicles and commercial aircraft are approximated at 0.23-quadrillion BTU's for increased efficiencies and 0.16-quadrillion BTU's for lighter weight. This brings the potential total annual reduction in U.S. energy use with Nd-alloy magnet motors to about 1.7-quadrillion BTU's for the 1988-1989 base or about 2.1% of the nation's total energy consumption for these years, as in Table 1. Satisfactory resolution of corrosion and thermal stability issues with Nd-alloy magnets is assumed.

These projections are based upon published literature for six motors, designed to use sintered Nd-alloy magnets and cover a range of motor types and horsepower ratings. Only two of the six motors were actually built and tested, one

with samarium-cobalt magnets.

There are potential cost savings in both producing and using Nd-alloy magnet motors. At a 5% discount rate, the present values of lifetime electricity savings for average use, other than in motor vehicles and commercial aircraft, increase from $260/Kg Nd-alloy magnet in 1/4-horsepower motors to $1400-$2000/Kg Nd-alloy magnet for motors in the 5 to 200-horsepower range. These savings are compared to the nominal $100/Kg cost of Nd-alloy magnets as simple tests of economic justification. For motor vehicles the approximate discounted lifetime fuel savings per kilogram of Nd-alloy magnet are $65 for increased operating efficiency plus $40 for lower motor weight. For commercial aircraft, the discounted lifetime fuel savings per kilogram of Nd-alloy magnets are about $460 for increased energy efficiency plus $44,000 for lower motor weight. The high values for aircraft explain why this application is moving forward. Lighter electric motors enable the $44,000 saving by increasing the payload that can be transported per unit of fuel used.

Neodymium-alloy magnet motors could cost less to mass produce than conventional motors because the motor weight can be cut in half, possibly more than offsetting added costs for Nd-alloy magnets. This is important because the saving in finished copper and steel would accrue immediately to the motor producer. This is in addition to the saving to the

user over time from electricity or transportation fuel. The potential to reduce motor production costs could accelerate implementation of this energy-saving technology; market forces alone, without the coercion of government regulations, would suffice. Reduced production costs could enable still more energy to be conserved by making Nd-alloy magnet motors more affordable for applications in which electrical energy or fuel savings alone, while significant, are insufficient to justify paying premiums for an energy-efficient motor.

Producers of electric motors for large markets such as cars and household appliances will probably be the first to mass produce Nd-alloy magnet motors. This will require a tremendous increase in the supply of Nd-alloy magnets since present production is only a little over 5% of the estimated requirements for total conversion of new motor production, world-wide, to Nd-alloy magnet motors, leaving out use in motor vehicles and commercial aircraft. Also, only a small portion of present magnet production goes into motors covered by this analysis. Increasing the production of Nd-alloy magnet motors at a rapid pace could cause a surge in magnet prices that jeopardizes the potential reduction in production costs. Long term prospects are good for real price reductions for Nd-alloy magnets, based on the abundance of Nd-bearing ores and strong possibilities for learning curve advances and breakthroughs to production processes that are continuous and amenable to economies of scale.

TABLE 1

PROJECTED COST AND ENERGY SAVINGS WITH NEODYMIUM

ALLOY MAGNET MOTORS

Quadrillion, (Q), Btu's Energy Savings - Annual U.S. Savings for Electrical Energy (@ 10,500 Btu's/kWh) and Transportation Fuels (@ 125,000 Btu's/gallon of gasoline and 135,000 Btu's/gallon of jet fuel)

$ Cost Savings - Savings in Finished Copper and Steel and Present Values of Lifetime Cost Savings For Electrical Energy and Fuel, per Kilogram of Nd-Alloy Magnet to Compare With the Nominal $100/kg Cost of Magnets

| Attributes of Nd-Alloy Magnet Motors | Electrical Energy Savings Other Than In Transportation Applications | Potential Savings of Finished Copper and Steel in Mass Production of Motors | Fuel Savings in Transportation Applications | |
|---|---|---|---|---|
| | | | Motor Vehicles | Commercial Aircraft |
| Increased Electrical Efficiency | 1.30 Q's $260 to $2000 | | 0.20 Q's $65 | 0.03 Q's $460 |
| Lower Weight | | up to $900 | 0.14 Q's $40 | 0.02 Q's $44,000 |

# PROJECTED ENERGY AND COST SAVINGS WITH NEODYMIUM ALLOY MAGNET MOTORS

## INTRODUCTION

The technical literature contains many references to the higher energy efficiency of neodymium (Nd)-alloy magnet motors. However, no comprehensive account has been found of the potential for these motors to reduce national energy needs and electric motor operating costs. Such reductions in operating costs could encourage energy conservation with these motors. The potential energy savings include not only electricity savings but fuel savings from reduced weight and higher operating efficiencies in transportation applications.

Also, there may be cost saving in production of Nd-alloy magnet motors in the place of conventional motors. The reduced need for copper and steel in Nd-alloy (Nd-Fe-B) magnet motors could lower costs in mass production unless offset by the costs of Nd-alloy magnets. With possibilities for cost savings in both motor production and use, lifetime savings need to be assessed. This also means the rate at which this technology is adopted could be strongly influenced by whether motor producer, motor user or both are motivated to save, and whether saving occurs immediately, as with the motor producer, or over an extended period of time, as for the motor user.

Accordingly, this analysis was undertaken to broadly assess savings in energy and costs, and resulting motivations, in replacing conventional electric motors with Nd-alloy magnet motors.

## DEVELOPING AN APPROACH FOR PROJECTIONS

The specifications reported in the literature for specific Nd-alloy magnet motors were gathered, correlated, and melded into a data base that underpins the energy and cost projections. This analysis is described in detail to assist any future efforts to improve the projections as better information becomes available. A road map is described here for the calculations of the ensuing pages to help the reader trace the development and flow of information from the literature references on through to the final projections.

Specifications for six Nd-alloy magnet motors, covering a range of sizes and types, were located in the technical literature and listed in Table 2. This included total weights, magnet weights, horse-power, efficiencies, design criteria, revolutions per minute, and full load power factors. The efficiencies for these motors are compared to those for conventional motors and high efficiency motors of the same horsepower in Table 3 and Figure 1. A merit factor for power demand reductions with Nd-alloy magnets is devised for plotting in Figure 2. Calculations follow in Table 3 for

the potential U.S. electrical energy savings with conversion of the entire 1988 U.S. electric motor population, including high efficiency motors, to Nd-alloy magnet motors, and the total Nd-alloy magnet requirements for this. The discounted lifetime savings in electrical energy costs for individual Nd-alloy magnet motors of different sizes are developed in Table 4 for comparison with the cost of the magnets. Potential production cost changes from reduced needs for finished copper and steel in mass producing Nd-alloy magnet motors are developed in Table 6 for comparison, again, with the cost of the magnets. All of these energy and cost changes and their sources are summarized in Table 1 of the Overview.

Only rudimentary analyses of production cost changes and electrical energy or fuel savings are possible from the literature data. All cost changes are expressed relative to conventional motors of the same horsepower ratings. Production cost changes are compared with electrical energy or fuel savings to see if lifetime costs of production and operation increase or decrease. It is assumed that the profit, marketing expense, overhead, etc., remain the same for the mass-produced Nd-alloy magnet motor as for the conventional motor. The goal of this analysis is to approximate the savings of Table 1 well enough to understand which saving or which combinations of savings in different applications might be sufficiently large to promote the

production and use of Nd-alloy magnet motors. The cost changes are expressed in dollars per kilogram of Nd-alloy magnet employed. This permits direct comparison of cost changes with the cost of magnets also expressed in dollars per kilogram of Nd-alloy magnet:

(lifetime cost change) = (cost change in producing the Nd magnet motor) - (present value of lifetime electrical energy and fuel savings)

The cost change in producing the Nd-alloy magnet motor is taken to be the cost of the finished and assembled magnets minus the cost saving in finished and assembled copper and steel motor components:

(lifetime cost change) = (cost of finished and assembled magnets) - (cost saving in finished and assembled copper and steel) - (present value of lifetime electrical energy and fuel savings)

The cost saving in finished and assembled copper and steel motor components is established by estimating the reduction in motor weight. There is a lifetime cost saving, and the application is cost justified, if electrical energy or fuel cost savings equal or exceed any increase in the cost to produce the motor. A lifetime cost saving is obtained any time motor production costs are decreased with Nd-alloy magnets. Often, the electrical energy and fuel savings greatly exceed any cost increase in motor production. This should lessen concern about technical uncertainties in the analysis and the simple treatment given costs and the cost/price relationship.

ANALYZING MOTOR SPECIFICATIONS

Specifications for six Nd-alloy magnet motors in Table 2 are from literature references.[1,2,3] The motors, ranging in horsepower from 0.29 to 770, include dc or 3-phase ac synchronous and variable speed versions with the magnets either in the stator or in the rotor. All of the motor designs were developed by computer design optimization programs in which either energy efficiency was maximized (0.29 and 0.80-horsepower motors) or lifetime costs of production and operation were minimized on a present value basis (7.7-, 77-, 253-, and 770-horsepower motors). Only the smallest two of the six motors were actually built and tested, the larger of the two using a samarium-cobalt magnet. It appears that essentially all of the designs were based on the properties of sintered rather than bonded Nd-alloy magnets.

Efficiencies for comparable horsepower induction motors are also listed in Table 2, as are the full-load power factors that are used in determining electrical energy charges. Efficiencies for the Nd-alloy magnet motors, and comparable standard efficiency and high efficiency motors are all plotted side-by-side in Figure 1. The weights of the Nd magnets are divided by the reduced input power requirements to calculate a merit factor, (kg Nd-alloy)/(kW power demand reduction), for each motor. When plotted against horsepower,

Figure 2, the values of this merit factor vary systematically between 0.3 and 2.3, passing through a pronounced minimum between 10 and 20 horsepower and increasing at horsepowers higher or lower than this. This minimum implies that Nd-alloy magnets are much more effective in improving the efficiency of conventional electric motors in the 10 to 20-horsepower range than in motors of other horsepowers. It is uncertain whether the shape of this curve and its minimum are valid or are the consequence of using values for three types of Nd-magnet motors, each type having different horsepower ratings. Since this relationship critically affects the projected savings it should be reviewed for reasonableness and accuracy in any further work.

## REDUCING NATIONAL ENERGY NEEDS WITH Nd-ALLOY MAGNET MOTORS

Data from Table 2 are combined with data on the U.S. 1988 electric motor population for different horsepower ranges and the estimated average hours annual use in each range[4] in Table 3. Actual usage of individual motors can vary significantly from these averages to change the given cost savings. For comparison, data are also included for electrical energy savings with existing high-efficiency motors.[4,5] The potential additional watt-hour savings with Nd-alloy magnet motors in each horsepower range are calculated in Table 3. For high efficiency motors the additional savings are about half of those for Nd-alloy

magnet motors across the whole size range. The total with Nd-alloy magnet motors for all of the ranges is 124 x $10^{12}$-watt-hours or 4.8% of the U.S. electrical energy usage of 2578 x $10^{12}$-watt-hours in 1988.(6) Over 40% of the total potential savings are in the 1/6- to 1-horsepower range. The remaining potential savings are distributed across the other five ranges with the least saved in the 5- to 20-horsepower range. Even though Nd-alloy magnets are most effective in improving efficiency in the 10-to 20-horsepower range in Figure 2 this is more than offset by the low average hours of use for 5- to 20-horsepower motors in Table 3.

## PREDICTING U.S. Nd-ALLOY MAGNET NEEDS

The total Nd-alloy market for complete conversion of the 1988 U.S. electric motor population (Table 3) is 188 x $10^6$-kg. With a 15-year average life(4) for electric motors and one billion U.S. motor population,(4) the need for Nd-alloy magnets for converting all new electric motors (omitting those in motor vehicles and commercial aircraft) is about 13 x $10^6$-kg per year, from this analysis. The potential world market for Nd-alloy magnets in electric motors is projected to be 35,000-tons, or 32 x $10^6$-kg.(7) In 1991 the total world market for sintered Nd-alloy magnets was about 1820-tons(8) or 1.6 x $10^6$-kg, about 5% of the potential world market for new electric motors, omitting electric motors in motor vehicles and commercial aircraft. Only a small portion

of the Nd-alloy magnets produced today is used in fractional and larger horsepower motors.

## REDUCING MOTOR LIFETIME ENERGY COSTS

The lifetime (15-year) energy cost savings with Nd-alloy motors in different horsepower size ranges and average use are given in Table 4, as calculated from the data of Table 3. The average 1990 U.S. cost of $0.066/kWh[9] (including any power factor and demand charges) is used with discount rates of 5, 10, and 20%. The discounted values of lifetime electrical energy cost savings are greater than the cost of the Nd-alloy magnets projected from the listed magnet weights using a nominal cost of $100/kg.[3] This is true for all horsepower ranges in Table 4, even at the highest discount rate. The discounted energy cost savings per kilogram of Nd-alloy magnets are listed and ranged from $260 for the smallest motor to the $2000 range for the larger motors. Average 1990 U.S. electrical energy costs, including power factor and demand charges, are $0.078/kWh for residential customers, $0.073/kWh for commercial customers, and $0.047/kWh for industrial customers.[9] There are considerable regional variations from these average values among individual power companies. The exact savings for particular cases depend on customer classifications, the power companies involved, and the exact hours of use.

Since the electrical energy rates are not inflated with time in this analysis, 5% is probably the most reasonable discount rate to use. The historically proven time value of money with little or no inflation or risk is only a little over 3%. Present value factors for different numbers of years and other discount rates are listed in Table 5.(10)

LOWERING PRODUCTION COST BY REDUCING MOTOR WEIGHT

The weights shown in Table 6 for the Nd-alloy magnet motors of Table 2, are either given or estimated from data in the references. For comparison, typical weights are also listed in Table 6 for induction motors of similar horsepower ratings from commercial catalogs.(11) The Nd-alloy magnet motors reduce motor weight nearly 50% in motors of less than 10 horsepower but increase weight for the 77-, 253-, and 770-horsepower examples for reasons that are not understood. Since neodymium represents less than 1% of the weight in the larger motors, the weight increases may be from using much more copper and steel than in conventional motors of these horsepower ratings. The 7.7-, 77-, 253-, and 770-horsepower motors were designed with a computer program in which the sums of the production costs and the lifetime electrical energy costs were minimized.(3) Weights and production costs were linked in this program: $5 per kg of finished and assembled copper and steel and $100 per kg of finished and assembled Nd-alloy magnet. These costs, if correct, apply

only for production lines and would not be obtained with one-of-a-kind or even limited-production motors. With these costs for finished Nd-alloy magnets, copper, and steel the production cost saving for the 7.7-horsepower motor is $212, or $884/kg Nd-alloy magnets in Table 6. Expressed on this basis, the saving in production costs can be compared with the cost of the Nd-alloy magnets as with the saving in operating costs. The minimum percent weight reductions for production cost savings with these costs for finished motor materials are listed in Table 6 for the motors of Table 2.

Minimization of lifetime costs in the computer program may skew the design toward high efficiency (for lower electrical energy costs) at the expense of higher production costs from increased weight. This could occur because lifetime energy costs are always much greater than production costs. With efficiencies already exceeding 90% for conventional electric motors in the high horsepower range, achieving still higher efficiency may be accomplished about as easily and economically with more copper and steel as with larger Nd-alloy magnets. Lower motor weights might be obtained if the computer optimization program gave more importance to minimization of production costs. This would increase the short-term economic incentive that could motivate motor manufacturers to switch to producing Nd-alloy motors. This could also encourage motor users to change to Nd-motors assuming lower production costs would be reflected,

eventually, in lower prices. The high-efficiency motors already on the market are not chosen, in many cases, because of premium costs, even though the pay back time from energy saving is only a few years.[4,5] Thus, the total amount of saving may not be as important as to whom and when the saving occur. This may determine how fast the move to Nd-alloy magnet motors takes place.

## SAVING FUEL WITH Nd-ALLOY MAGNET MOTORS IN TRANSPORTATION VEHICLES

### Saving Fuel By Raising Efficiency

The high-energy efficiency of Nd-alloy magnet motors and alternators can save fuel in automobiles and trucks, apart from the fuel saved because of their lighter weight. Sovran[12] analyzed fuel consumption in the EPA city/highway driving schedule and estimated that GM cars from the early 80s used 9.6% of fuel to power the alternator, radiator fan, and power steering pump. If Nd-alloy magnet motors could reduce the energy consumption of the alternator and the fan motor by 20%, and if these motors consume 6% out of the 9.6% fuel share, fuel consumption would decrease by 6% of the 20%, or 1.2%. In 128,000-miles of driving in 12.5-years[13] at an average fuel economy of 23.4-miles per gallon[14], 128,000 x 0.012/23.4 = 66-gallons would be saved. At $1.10/gallon this is worth $73, which has a value of $53 when discounted at

5%/year for 12.5-years. If the alternator is a 100-A model (1.6-equivalent horsepower) and the fan motor is 1/4-horsepower the respective estimated amounts of Nd-alloy required for the efficiency gain are estimated to be 0.60-kg + 0.21-kg = 0.81-kg (Fig. 2). The Nd-alloy saves $53/0.81-kg = $65/kg Nd-alloy on this basis. This is below the nominal $100/kg price of finished Nd-alloy magnets but does not include the savings from weight reduction to be discussed subsequently.

The fuel saving for improved alternator and fan motor efficiency in automobiles is also used to estimate the fuel saving for improved electric motor efficiency in commercial aircraft by compensating for the longer life of commercial aircraft (24-years [15] compared to 12.5-years for cars), the longer use per day (6.13-hours compared to an estimated 0.75-hours for cars)[15], the lower cost of jet fuel ($0.64/gallon[15] compared to about $1.10/gallon for cars), and a larger present value discount for the longer life. The resulting cost saving of $460/kg Nd-alloy magnet[16] exceeds the nominal $100/kg cost of the magnets. This cost saving alone justifies the use of Nd-alloy magnet motors in commercial aircraft and together with the still larger saving from weight reduction discussed subsequently, explains why this application is moving forward rapidly.

Applying this conservative 1.2% reduction in fuel consumption

for increased efficiency of Nd-alloy magnet motors and alternators to all motor vehicles would conserve 0.012 x 132 x$10^{9}$[17] = 1.6-billion gallons of gasoline or about 0.2-quadrillion BTU's[6] annually in the U.S. Further, if this 1.2% value is also applied to the fuel consumption of U.S. commercial aircraft as a first approximation, an additional 0.012 x 16 x $10^{9}$[17] = 0.2-billion gallons of jet fuel and 0.03-quadrillion BTU's[6] would be conserved annually in the U.S. with Nd-alloy magnet motors and generators.

Saving Fuel By Lowering Weight

The lower weight of Nd-alloy magnet motors and generators can also save fuel in various means for transportation. There can be additional weight saving and associated fuel saving because structural and mechanical components supporting the lighter Nd-alloy magnet motors and generators can also be lighter. For automobiles, this compounding of weight reduction to supporting components was as high as 50%[18] in the 1970s but a conservative value of 25%, more appropriate to todays weight-conscious designs, is used in this analysis.

If the supporting components are not downsized, only the primary weight reductions can be realized, not the compounded weight saving. The vehicle will have increased acceleration but save only 60%[12] as much fuel as a car with the drive train downsized to just maintain base-line performance.

Except for passenger automobiles, vehicle weight reduction has its greatest economic value and saves the most energy when used to carry more cargo or passengers per trip up to the vehicle capacity limit. In this case, the saving is in the amount of fuel/ton of cargo or passengers transported. A significant exception to this occurs for trucks, trailers, and freight cars in transporting low bulk density cargos that fill the cargo area before reaching the vehicle weight limit. The fuel saved per ton of cargo transported is less for this case. Other considerations for trucks include a higher number of miles driven per year and a slightly longer life compared to cars. This is partially offset both by decreased gallons per ton-mile with the lower performance of trucks and by a higher percentage of more efficient diesel engines in trucks.

The lifetime value of weight reduction differs significantly with different kinds of vehicles. With drive trains downsized to keep performance the same as before weight reduction in trucks and cars, and weight reduction in commercial aircraft used for carrying additional passengers or cargo per trip, the approximate values discounted at 5%/year for 24-years for commercial aircraft and 12.5-years for trucks and cars are as follows:

Commercial Aircraft $2800/kg. (19)

Motor Vehicles $2.54/kg. (20)

A significant variable, accounting for part of the

differences in values for commercial aircraft and motor vehicles, is the much greater distances travelled in the lifetime of commercial aircraft (22,000,000-miles in the average 24-year life[15] compared to 128,000 miles in 12.5 years for cars.[13]

A weight reduction of 12.75-kg is estimated for the Nd-alloy magnet alternator and fan motor discussed previously by assuming they weigh 10-kg and 2.75-kg, respectively, half the weight of the conventional equipment they replace. The weight saving is enabled by the use of 0.81-kg of Nd-alloy magnets. At $2.54/kg of weight saved, the discounted lifetime fuel cost saving is

$$\frac{\text{12.75-kg X \$2.54/kg}}{\text{0.81-kg Nd-alloy}} = \$40/\text{kg Nd-alloy magnet.}$$

For commercial aircraft, the use of the weights for the automobile alternator and fan motor increase the discounted fuel cost saving to

$$\frac{\text{12.75-kg. X \$2800/kg}}{\text{0.81-kg Nd-alloy}} = \$44{,}000/\text{kg Nd-alloy magnet.}$$

With these assumptions, the fuel cost saving in commercial aircraft applications for either higher efficiency or lighter weight greatly exceeds the nominal $100/kg for the magnets.

By assuming 50% weight reduction with Nd-alloy magnet motors compared to conventional motors, and costs of $100/kg Nd-alloy magnets and $5/kg finished copper and steel in mass

production of motors, the maximum weight of Nd-alloy magnets for cost saving can be calculated for different cases. For motor vehicles, the lifetime motor costs including production and operation increase if the weight of Nd-magnets in the motors exceed 13.5% of motor weight. For the alternator and fan motor example, the magnets were 6.0% of the alternator weight and 7.6% of the fan motor weight. For other than transportation applications, the cost of mass production is reduced if the magnet weight is less than 5.3% of motor weight for the listed assumptions.

The 12.75-Kg weight reduction in the fan motor and alternator example is about 0.8% of an average car's inertia weight. This 0.8% factor is used as a first approximation of the potential for fuel conservation with Nd-alloy magnet motors in all motor vehicles and in commercial aircraft by multiplying the total U.S. fuel consumption in these sectors by 0.8%. For motor vehicles this is 0.8% of 132-billion gallons[17] or 1.1-billion gallons which is 0.14-quadrillion BTU's.[6] For commercial aircraft the saving would be 0.8% of 16-billion gallons[15] or 0.13-billion gallons which is 0.017-quadrillion BTU's.[6]

REDUCING MOTOR VOLUME

The volume saved with Nd-alloy magnet motors is valuable in appliances and transportation vehicles, particularly in

aerospace applications. In all types of applications, development of additional power per unit volume should enable many new application for motors. The small volume and high power capability of these motors may qualify them for powering pumps and compressors currently driven by belts from other power sources. This could improve energy efficiency by eliminating the friction of drive belts, particularly when the belts are idling. A side benefit for the environment could be elimination of the present leakage of refrigerants through shaft seals on belt-driven condensers for air conditioning and refrigeration.

## COMMERCIALIZING Nd-ALLOY MAGNET MOTORS

The potential energy saving in implementing this technology could be obtained sooner and without energy regulations if the projected cost saving of reduced material usage can be attained in mass production. This poses the classic chicken and egg conundrum of "which comes first." Any production cost saving from less material usage cannot be realized until the market is large enough for mass production, but the market may not be large enough until the price of motors drops because of cost saving in mass production from lower material usage. This conundrum will probably be resolved by producers of electric motors for mass market products such as cars or household appliances.

Otherwise, the near-term market growth for Nd-magnet motors will be in applications for which energy saving, rather than potentially lower production cost, justifies implementation. As economies of scale are eventually realized in production in this case, and as competition ultimately causes motor prices to reflect these potentially lower costs, use will finally spread to products in which the energy saving is presently insufficient to justify use at todays prices for high efficiency motors.

The present capacity for producing Nd-alloy magnets for its present applications is well below that required for substantial implementation of Nd-alloy magnet technology in new electric motor production. A sudden surge in demand for Nd-alloy magnets for new motor production might increase Nd-alloy magnet prices and jeopardize the potential production cost saving for a time.

Cost reductions may come from processes for production of neodymium and the alloy magnets that are continuous, scalable, and lower in capital requirements. Even incremental cost decreases for neodymium magnets can tip the balance toward cost saving in motor production which could accelerate the development of markets in which the energy saving may be marginal. As shown in the supply/demand/price histories of other materials, real price decreases are inevitable in the long term for materials, such as neodymium,

which are based on plentiful resources.[21] These price decreases occur from learning curve advances and technology developments, economies of scale, and management moves to lower cost resources and manufacturing methods. The long-term downward pressure on real prices is from competition, whether from other producers of the same product or from producers of other products vying for the same markets.

## DISCUSSION

Most of the early applications for Nd-alloy magnets were based on performing critical and valuable functions not easily accomplished by any other means. Neodymium-alloy magnets are now starting to penetrate electric motor markets in which cost saving must be shown against conventional motors. The potential cost saving occurs not only because of higher operating efficiencies but because of lighter weight and smaller volumes. To motor producers these advantages could accelerate motor replacement, reduce costs, and increase motor market growth and market share for Nd-alloy magnet motors. For motor users and the nation these motors should reduce costs, reduce energy needs and any emissions in producing the energy, and enable products that are lighter, more compact, faster, or more powerful than ones they replace.

REFERENCES

1. T.Renyuan, G.Lianfa, and C.Yicheng, "The Development and Design of the Nd-Fe-B Permanent Magnet Motor," Proceedings of the International Conference on Rare Earth Development and Applications, Beijing, The People's Republic of China, September 10-14, 1985, pp.1029-1034.

2. G.Wakui, K.Kurihara, and T.Kubota,"Hybrid Permanent-Magnet Synchronous Motor," T.IEE Japan, 110-D, 7, 1990 pp.841-847.

3. G.R.Slemon and X.Liu, "Modeling and Design Optimization of Permanent Magnet Motors," Electric Machines and Power Systems, 20, 2, 1992, pp.71-92.

4. S.Nadel, et al. Energy Efficient Motor Systems : A Handbook on Technology, Program and Policy Opportunities, American Council for an Energy-Efficient Economy, Washington D.C. and Berkeley, California, 1991

5. G.A.McCoy, T.Litman, and J.G.Douglass, Energy-Efficient Electric Motor Selection Handbook, Revision 2, Bonneville Power Administration, United States Department of Energy, Revision 2, 1992.

6. Monthly Energy Review, September 1991, Energy Information Administration, Office of Energy Markets and End Use,

U.S. Department of Energy, Washington, D.C. 20585.

7. Port Wheeler, "Reassessing the Business Opportunities, Markets, and Technology for Neodymium-Iron-Boron Permanent Magnets," Gorham Advanced Materials Conference, February 16-18, 1992, Orlando, Florida.

8. Robert E. Wolf, "Reassessing the Business Opportunities, Markets, and Technology for Neodymium-Iron-Boron Permanent Magnets," Gorham Advanced Materials Conference, February 16-18, 1992, Orlando, Florida.

9. Electric Sales and Revenue 1990, Energy Information Administration, Office of Coal, Nuclear, Electric and Alternate Fuels, U.S. Department of Energy, Washington, DC 20585

10. T.M.Carroll, Microeconomic Theory, Concepts and Applications St.Martin's Press, New York, 1983.

11. G.E. Supply National Catalog, 1991, also Grainger Industrial and Commercial Equipment and Supplies, General Catalog, Fall 1992, No. 382, 120 Beta Drive, Pittsburgh, PA 15238.

12. G.Sovran, "Tractive-Energy-Based Formulae for the Impact of Aerodynamics on Fuel Economy over the EPA Driving

Schedules," SAE Paper No. 830304, Society of Automotive Engineers, Inc. Warrendale, PA 15906, 1983.

13. The 1988 U.S. average miles traveled per household vehicle was 10,246-miles in Household Vehicles Energy Consumption 1988, DOE/EIA-0464(88), Energy Information Administration, Office of Energy Markets and End Use, U.S. Department of Energy, Washington, DC 20585, 1988. U.S. car registrations are listed for the 13 most recent registration years for each model year in MVMA Motor Vehicle Facts and Figures '91, Motor Vehicle Manufacturers Association of the United States, Inc., 7430 Second Avenue, Suite 300, Detroit, MI 48202, 1991. Half of the 1977 models originally registered were not being registered after 12.34 years. For 1978 models, half were not being registered after 12.48-years. The indications from the early registration years for more recent model years is that median car life may be increasing beyond 12.5-years. Mean car ages tabulated back to 1941 in this same reference have always been greater than the median age, usually by a year or less. Thus the median life is probably slightly less than the mean life. Combining the average miles driven per year with the median car life gives a conservative estimate for the mean car lifetime mileage of 10,246-miles/year x 12.5-years = 128,000-miles.

14. R.M.Heavenrich, J.D.Murrell, and K.H.Hellman, "Light-Duty

Automotive Technology and Fuel Economy Trends Through 1990", PB 91-206342, May 1991, Environmental Protection Agency, Ann Arbor, MI 48105. Also Gas Mileage Guide, EPA Fuel Economy Estimates, U.S. Dept of Energy, DOE/CE-0019/8, Oct.19,1989, available at car dealers.

15. Calculated from data in Statistical Abstract of the United States 1991, Tables 1071, 1072 & 1073, U.S. Department of Commerce, Washington, DC

16.

$$\frac{\text{65-gal.X 24-yr.X 6.13-hr.X \$0.64/gal.X 0.5685}}{\text{12.5-yr. X .75-hr. X 0.81-kg Nd-alloy}} = \frac{\$460}{\text{kg Nd-alloy}}$$

17. MVMA Motor Vehicle Facts and Figures '91, Motor Vehicle Manufacturers Association of the United States, Inc. 7430 Second Avenue, Suite 300, Detroit, MI 48202

18. K.D.Marshall, "The Economics of Automotive Weight Reduction," SAE Paper No. 700174, Society of Automotive Engineers, Inc. Warrendale, PA 15906 1970.

19.
$$\frac{\text{24-yrs X \$10,025,000,000-fuel/yr X 0.5685 discount factor}}{\text{4477-planes X [8184-kg (passengers+bags) + 2636-kg freight]}}$$

Values calculated from data in Tables 1071, 1072, and 1073 of Statistical Abstract of the United States, U.S. Department of Commerce, Average aircraft life taken as twice

the mean age.

20. 3.18-gal/kg X $1.10/gal X 0.72587 discount factor, 3.18-gal/kg was calculated for "On-Road" EPA city/highway driving cycle from 1991 EPA average weights and fuel economies for U.S. car sales,[14] 128,000-mile car lifetime,[13] 25% compounding of weight changes into supporting components, and powertrain downsized for reduced weight to maintain baseline performance.

21. C.N.Cochran, "Long-term Substitution Dynamics of Basic Materials in Manufacture," Materials and Society, Vol.12, No.2, pp.125-150, 1988.

TABLE 2

PERFORMANCE SPECIFICATIONS FOR Nd-ALLOY MAGNET MOTORS AND COMPARABLE HORSEPOWER STANDARD EFFICIENCY MOTORS

| OUTPUT KILOWATTS | | 0.22 | 0.60 | 5.75 | 57.5 | 189 | 575 |
|---|---|---|---|---|---|---|---|
| HORSEPOWER | | 0.29 | 0.80 | 7.7 | 77 | 253 | 770 |
| VOLTS | | 50 | 180 | - | - | - | - |
| POWER | | DC | 3 PHS | 3 PHS | 3 PHS | 3 PHS | 3 PHS |
| MOTOR TYPE | | BRUSH | SYNC | --4 POLE,2 SLOTS/POLE-- | | | |
| LOCATION OF MAGNETS | | STATOR | ----------ROTOR---------- | | | | |
| RPM | | 2150 | 1500 | ----VARIABLE SPEED----- | | | |
| EFFICIENCY % | | 72.7 | 83 | 94 | 96.9[a] | 97.5 | 98.2[a] |
| EFFICIENCY OF COMPARABLE INDUCTION MOTOR | % | 55.0 | 73.3 | 85[a] | 91.6[a] | 94.5[a] | 96.5[a] |
| FULL LOAD POWER FACTOR | % | - | 97 | 100 | 100 | 100 | 100 |
| FULL LOAD POWER FACTOR OF COMPARABLE INDUCTION MOTOR, | % | 57[b] | 68.8 | 72[c] | 83[c] | 90[c] | >90[c] |
| Nd-ALLOY WEIGHT, kg | | 0.19 | 0.158 | 0.24 | 2.2 | 8.2[d] | 24 |
| RESIDUAL FLUX DENSITY OF Nd | Tesla | - | 1.2 | 1.1 | 1.1 | 1.1 | 1.1 |
| MOTOR DESIGN AND PERFORMANCE REFERENCE | | e | f | g | g | g | g |
| DESIGN OPTIMIZATION CRITERIA | | MAXIMUM EFFICIENCY | | MINIMUM PRESENT VALUE OF LIFETIME COSTS | | | |
| MOTOR BUILT AND TESTED | | YES | SmCo ONLY | NO | NO | NO | NO |
| kg Nd-ALLOY/kW REDUCTION | | 1.95 | 1.65 | 0.37 | 0.67 | 1.34 | 2.32 |

a Estimated from Figure 1, this report
b Nadel et al, page 40
c McCoy et al, Figure 12
d Interpolated
e Renyuan et al
f Wakui et al
g Slemon et al

TABLE 3
POTENTIAL ENERGY SAVINGS WITH Nd-ALLOY MAGNET AND HIGH EFFICIENCY MOTORS IN THE 1988 U.S. ELECTRIC MOTOR POPULATION

| Horsepower Size Range | 1/6-1 | 1-5 | 5-20 | 20-50 | 50-125 | >125 | |
|---|---|---|---|---|---|---|---|
| Average HP[a] | 0.25 | 2.1 | 11.9 | 32.5 | 86.7 | 212 | |
| AVG. EFFIC,%[b] | | | | | | | |
| Std. Motor | 55 | 79 | 86 | 89 | 92 | 94 | |
| Hi.Effic.Motor | 64 | 85 | 91 | 93 | 95 | 96 | |
| Nd-Alloy Motor | 71 | 90 | 95 | 96 | 97 | 97.5 | |
| AVG.kW[c] | | | | | | | |
| Std. Motor | 0.34 | 1.98 | 10.3 | 27.3 | 70.3 | 168 | |
| Hi.Effic.Motor | 0.29 | 1.84 | 9.8 | 26.2 | 68.0 | 165 | |
| Nd-Alloy Motor | 0.26 | 1.74 | 9.3 | 25.3 | 66.7 | 162 | |
| Avg.Hours Per Year[d] | 732 | 1080 | 600 | 1200 | 1600 | 2900 | |
| Number of U.S. Motors[e] x $10^{-6}$ | 900 | 75 | 15 | 5 | 3 | 1.2 | |
| Number of U.S. High Effic. Motors[f] x $10^{-6}$ | 10 | 6 | 2 | 1 | 0.6 | 0.24 | |
| kg Nd-Alloy Per kW Reduction[g] | 2.0 | 1.0 | 0.3 | 0.4 | 0.7 | 1.2 | |
| POTENTIAL ADDED Wh/YR SAVINGS[h] X $10^{-12}$ | | | | | | | TOTALS |
| 100% Hi.Effic. | 33 | 10 | 4 | 5 | 9 | 8 | 69 |
| 100% Nd-Alloy | 52 | 19 | 8 | 11 | 15 | 19 | 124 |
| Required Kg. Nd-Alloy[i] x $10^{-6}$ | 144 | 18 | 5 | 4 | 8 | 9 | 188 |

**a** Table 7-1, Nadel et al. **b** Best fit in Fig.1 using data from Renyuan et al, Slemon et al, Wakui et al, Fig.6-1 and Table 7-1 of Nadel et al and Fig.3 of McCoy et al. **c** kW = (horsepower/1.34) x (efficiency). **d** Back calculated from Fig.6-1, Nadel et al (with correction of the probable typo for the population of the 1988 >125 horsepower motors), using the kilowatt values listed above. **e** Fig.6-1, Nadel et al, with correction of probable typo (see reference 4.). **f** Tables 6-5 and 7-1, and Fig 6-1, Nadel et al. **g** Fig. 2. **h** (Delta kW) x (no. of motors) x (hours operation) - (savings with present high efficiency motors). **i** (kg Nd-Alloy/kW) x (no. of motors) x (Delta kW) - (savings with present high efficiency motors).

TABLE 4

FIFTEEN YEAR LIFETIME ENERGY COST SAVINGS IN REPLACING CONVENTIONAL MOTORS WITH Nd-ALLOY MAGNET MOTORS

| Horsepower Range | | 1/6-1 | 1-5 | 5-20 | 20-50 | 50-125 | >125 |
|---|---|---|---|---|---|---|---|
| Weighted Average HP | | 0.25 | 2.1 | 11.9 | 32.5 | 86.7 | 212 |
| Average Hours/Year | | 732 | 1080 | 600 | 1200 | 1600 | 2900 |
| Kilograms Nd-Alloy per Motor | | 0.16 | 0.24 | 0.3 | 0.8 | 2.5 | 7.2 |
| Power Saving, kW | | 0.08 | 0.24 | 1.0 | 2.0 | 3.6 | 6.0 |
| 15 Year Energy Cost Saving @ $0.066/kWh | $ | 60 | 260 | 590 | 2400 | 5700 | 17000 |
| 15 Year Energy Cost Saving Discounted at 5% Per Year | $ | 41 | 180 | 410 | 1600 | 3900 | 12000 |
| 15 Year Energy Cost Saving Discounted at 10% Per Year | $ | 29 | 130 | 290 | 1200 | 2800 | 8500 |
| 15 Year Energy Cost Saving Discounted at 15% Per Year | $ | 17 | 75 | 170 | 670 | 1600 | 4900 |
| 15 Year Energy Cost Saving Discounted at 5%/year per Kg Nd-Alloy Magnet | | 260 | 750 | 1400 | 2000 | 1600 | 1700 |

TABLE 5

PRESENT VALUE FACTORS FOR DIFFERENT DISCOUNT RATES AND TIMES

Monthly Compounding

| | Discount Rates | | |
|---|---|---|---|
| Years | 5% | 10% | 20% |
| 1 | 0.95133 | 0.90521 | 0.81941 |
| 2 | 0.92817 | 0.86231 | 0.74631 |
| 5 | 0.86312 | 0.74910 | 0.57347 |
| 10 | 0.76784 | 0.60221 | 0.39310 |
| 12 1/2 | 0.72587 | 0.54426 | 0.33426 |
| 15 | 0.68658 | 0.49372 | 0.28836 |
| 20 | 0.61702 | 0.41234 | 0.22731 |
| 24 | 0.56850 | 0.36145 | 0.19141 |

TABLE 6

WEIGHT REDUCTIONS NEEDED FOR COST SAVINGS IN MASS PRODUCTION OF Nd-ALLOY MAGNET MOTORS IN THE PLACE OF CONVENTIONAL ELECTRIC MOTORS

ASSUMPTIONS
($/kg finished magnets) = 20 ($/kg finished copper + steel)

| Horsepower | 0.29 | 0.80 | 7.7 | 77 | 253 | 770 |
|---|---|---|---|---|---|---|
| Approx. Motor Wt. Estimated From Original Reference kg. | 2.8 | -- | 45 | 430 | 950 | 3300 |
| Nd-Alloy Magnet Weight kg. | 0.19 | 0.158 | 0.24 | 2.2 | 8.2 | 24 |
| Percent of Motor Weight that is Nd-alloy Magnet | 6.8 | -- | 0.53 | 0.51 | 0.86 | 0.73 |
| Minimum Percent Weight Reduction for Production Cost Saving * | 56 | -- | 9 | 9 | 14 | 12 |
| Approximate Average Conventional Motor Weight kg. | 5.5 | 10 | 92 | 395 | 940 | 2000 |
| Actual Percent Weight Reduction | 49 | -- | 51 | ----- weight increase ----- | | |
| $ Production Cost Saving Per kg Nd-Alloy | none | -- | 884 | ------- none ------- | | |

* Minimum percent weight reductions for cost saving in production are based on Nd-alloy magnet motor weighing half as much conventional motor.

# ELECTROLYSIS OF NEODYMIUM OXIDE

**Final Report**
**for the Period 1 April 1994 - 28 February 1997**
**(Phase II)**

Rudolf Keller
Kirk T. Larimer

24 March 1997

EMEC Consultants
4221 Roundtop Road
Export, PA 15632

Work Performed Under Cooperative Agreement No. DE-FC07-91ID13104

Prepared for
the U.S. Department of Energy
Office of Industrial Technologies

# FOREWORD

This Final Report was submitted by EMEC Consultants to the Department of Energy according to the reporting requirements of Cooperative Agreement No. DE-FC07-91ID13104. It describes and discusses the project activities during the period 1 April 1994 to 28 February 1997.

The following members of EMEC Consultants' staff contributed to this report: D. L. Anthony, W. C. Cochran, D. G. Gatty, D. M. Hydock, R. Keller, K. T. Larimer, and D. B. Stofesky. In addition, C. N. Cochran and W. E. Haupin participated as consultants, and H. E. Smith as a laboratory assistant on temporary assignment. The experimental work was performed in EMEC Consultants' laboratory in New Kensington, Pennsylvania.

The effort benefitted from the cooperation with Rhône-Poulenc Basic Chemicals Company which provided the cost share. Dr. Charles O. Bounds, Director of R&D, Rare Earths and Gallium, Cranbury, New Jersey, made the interactions particularly productive and enjoyable.

Mr. J. Donald Talbot, Consultant, provided appreciated support in estimating costs.

We gratefully acknowledge the support of the DOE Idaho Operations Office, with Mr. D. W. Robertson and Mr. J. Yankeelov serving as Project Managers. We thank Mr. J. V. Anderson and Dr. Charles Mohr, Idaho National Engineering and Environmental Laboratory, who served as Technical Monitors, for their interest and advice, also Mr. J. O. Lee, Ms. K. Stallman, Ms. L. A. Hallum, and Ms. C. L. Bruns for negotiating and administering the agreement. We also owe thanks, in particular, to Mr. M. J. McMonigle, DOE Office of Industrial Technologies, Washington, D.C., for his interest, support, and stimulating discussions, as well as his successors, Dr. Larry Boxall and Dr. Sarah Dillich.

This report was prepared as an account of work sponsored by an agency of the United States Government. Neither EMEC Consultants, its owner, nor any of its employees or consultants makes any warranty, expressed or implied, or assumes any legal liability or responsibility for the accuracy, completeness, or usefulness of any information, apparatus, product, or process disclosed, or represents that its use would not infringe privately owned rights. Reference herein to any specific commercial product, process or service by trade name, trademark, manufacturer, or otherwise, does not necessarily constitute or imply its endorsement, recommendation, or favoring by EMEC Consultants, by the United States Government, or by any agency thereof.

# SUMMARY

## USE AND PRODUCTION OF NEODYMIUM

Neodymium is one of the dominant rare earth elements, typically occurring in rare earth ores at concentrations of about 10 to 15 wt%. Correspondingly, it is a major component of misch metal (a mixture of lanthanide or rare-earth metals). Recently, neodymium has found increased use as constituent in advanced permanent magnets; with the composition $Nd_2Fe_{14}B$ as a basis, extremely high field strengths have been demonstrated. Neodymium also is receiving attention as a component in alloys for metal hydride battery electrodes.

The application of primary interest in this effort is the use in magnets for high-efficiency electric motors. Based on an analysis of cost benefits and potential energy savings presented in the Phase I Final Report, it has been projected that annual energy savings of 1.7 quadrillion Btu could result from implementation of new technology involving neodymium-containing permanent magnets; part of the savings are to be achieved by higher efficiency of electric motors, a smaller fraction by weight reductions in the transportation sector.

Neodymium presently is mainly produced by calciothermic reduction in a batch process [1]. Electrolysis would have the advantage of continuous operation and actually has been implemented with neodymium halides as feed material [2] [3]. These halides are manufactured from the oxide or from solutions. A direct electrolysis of $Nd_2O_3$, essentially the chemical form occurring naturally, would be more cost-effective. The total reduction of operating costs in the production of neodymium by substituting an efficient neodymium oxide electrolysis for the calciothermic production is estimated to exceed 30 percent (see analysis in Phase I Final Report part).

## NEODYMIUM OXIDE ELECTROLYSIS

Neodymium oxide is the neodymium compound most readily available for the production of neodymium metal or alloys. The oxide, $Nd_2O_3$, can be electrolyzed to obtain the metal:

$$2\ Nd_2O_3 + 3\ C \longrightarrow 4\ Nd + 3\ CO_2\ .$$

This process is analogous to the electrolysis of aluminum oxide in Hall-Héroult cells and is also conducted in fluoride-based molten salt electrolyte with carbon anodes. Investigations by the Bureau of Mines have shown promising possibilities for the production of neodymium by such an electrolytic process. It is the main objective of the present work to refine the

approach, identify and overcome obstacles, and to develop a commercially attractive process to the pilot stage.

## EXPERIMENTAL INVESTIGATIONS

Phase II investigations focused on

- -- achieving consistently good results at the 10-20-A level
- -- validating a modified concept assuring the absence of perfluorinated carbon compounds (PFCs) in the off-gases
- -- scaling-up to the 100-A cell level
- -- identifying critical parameters to be considered for large-scale cell design
- -- operating a 100-A cell consistently for an extended time period of 96 hours

While electrolysis experiments to produce appreciable amounts of neodymium-iron alloy at high quality and with acceptable current efficiency and utilization efficiency for the oxide occupied center stage, supporting research yielded increased knowledge on metal solubility, oxide dissolution, anode effect occurrence, electrolyte flow conditions, and materials preparation.

## ACHIEVEMENTS

Operating with a current of 20 A, conditions were identified at which operation proceeded smoothly and yielded good results. No anode effects interrupted the production, but the off-gases contained significant amounts of perfluorinated carbon compounds ($CF_4$ and $C_2F_6$). It was discovered that under certain conditions an electrolysis regime exists at relatively high voltage, in which high currents can be maintained with only partial occurrence of an oxide-related anode effect that manifests itself, however, by the anodic formation of PFCs. Subsequent efforts focusing on an electrolysis in a low-voltage regime, where no undesirable perfluorinated carbon compounds are emitted, were successful. Experiments were carried into the 100-A scale where good-quality alloy was produced in 96-hour experiments at current efficiencies exceeding 60 percent; only CO and $CO_2$ were present in the off-gases.

Details to be considered in cell construction and operation were discovered. It is important that the oxide concentration of electrolyte contacting metal product and cathodes is as low as possible. Reoxidation of neodymium, furthermore, can be minimized by reducing mass transport rates in the cathode region, also by eliminating opportunities for corrosive action

provided by the contact of metal product with other metallic components of the cell.

Preliminary plans for a pilot cell were made. As Phase II goals were met, a logical continuation will involve the construction and operation of a pilot or prototype cell.

## ENVIRONMENTAL IMPLICATIONS

Other sources have patented or are practicing a neodymium oxide electrolysis [1] [4]. There are indications that in all cases the electrolysis is conducted in a high-voltage regime in which substantial amounts of perfluorinated carbon compounds are emitted. Based on our results, we estimate that an annual production of 2,000 t of neodymium potentially may produce as much or more of the undesirable greenhouse gases as the entire domestic aluminum industry. A costly treatment of the cell off-gases to remove the chemically unreactive compounds $CF_4$ and $C_2F_6$ seems inevitable; avoiding their formation is clearly more attractive.

## RECOMMENDATIONS

The essential goals of Phase II were met. A concept for a cost-effective, energy-efficient and environmentally acceptable process was established, based on experimental results on the scale of up to 100 A. A continuation into pilot cell experimentation in the planned Phase III was recommended to the Department of Energy, but refocussing of the program at the Office of Industrial Technologies eliminated any funding for such a continuation.

An opportunity may have been lost. An aggressive progression into a pilot scale campaign may have led to establishing a technology in the United States that would have given the domestic industry a competitive advantage. With lower-risk technological alternatives and foreign sources for neodymium available, it appears likely that the technology successfully developed by this program will not be utilized. On the other hand, global restrictions in the emission of greenhouse gases re-establish interest in our technology.

Aside from neodymium for magnetic materials, misch metal is a related rare earth product that is rapidly gaining importance. It is recommended that the prospects of cost-reduction by adapting our concept to the production of misch metal be examined.

# CONTENTS

## LIST OF FIGURES

## LIST OF TABLES

# INTRODUCTION

## USE AND PRODUCTION OF NEODYMIUM

Neodymium is a rare earth metal. In ores it is usually associated with the more dominant cerium and lanthanum. The metal has a bright silvery metallic luster. Neodymium is a reactive metal and tarnishes in air, forming an adherent or non-adherent, protective or non-protective oxide.

Neodymium oxide ($Nd_2O_3$) is used in specialty glasses and as a colorant for enamels. The metal, in conjunction with iron and boron, has been found to yield permanent magnets with very high field strength. Recently it is also receiving attention as a component in high performance alloys for metal hydride battery electrodes.

The application of primary interest in this effort is the use in magnets for high-efficiency electric motors. With the composition $Nd_2Fe_{14}B$ as a basis, field strengths (normally referred to as energy product) typically vary from 30 up to 54 MGOe. Such material is being used in small compact electric motors for special applications. A broader use in high-efficiency motors could lead to substantial energy savings.

Neodymium can be produced by reducing its halides such as neodymium fluoride with a reactive metal such as calcium. An alternative approach is electrolysis. In an approach developed at General Motors, the electrolysis of sodium has been combined with the subsequent reduction of neodymium. This "NEOCHEM" process and other major processes have been reviewed by Sharma [4].

At the present time, most commercial neodymium is produced in the western world by reduction of its fluoride with calcium or sodium by the following (or equivalent) reaction:

$$3\ Ca + 2\ NdF_3 \longrightarrow 3\ CaF_2 + 2\ Nd\ .$$

This is a somewhat cumbersome batch process, produces considerable amounts of waste materials, and requires the preparation of calcium metal by electrolysis of calcium chloride.

Rare earth metals can be produced, as is presently being done in China, by the electrolysis of their anhydrous chlorides. The electrolyte consists of the rare earth chloride and alkali or alkaline-earth chlorides. Typical temperatures are 800 to 900 °C. These temperatures are below the melting point of neodymium (1020 to 1050 °C). Generally it is difficult in molten salt electrolysis to deposit and collect a solid metal, i.e. a metal deposited at a temperature below its melting point. If an iron-neodymium (Fe-Nd) alloy is the required product, it is possible to recover the neodymium as component of a liquid alloy. According to the iron-neodymium phase diagram [5] (also in the Phase I Final Report part), this permits one to operate at lower temperatures.

Using neodymium oxide as the raw material for an electrolysis is an attractive alternative, as treatment of the process feed is minimized.

## ELECTROLYSIS OF NEODYMIUM OXIDE

Neodymium oxide is the most readily available compound for the production of neodymium metal or alloys. The oxide, $Nd_2O_3$, can be electrolyzed to obtain the metal:

$$2\ Nd_2O_3 + 3\ C \ \text{----}> \ 4\ Nd + 3\ CO_2\ ,$$

by the following electrochemical reactions:
at the cathode:

$$Nd_2O_3 + 6\ e^- \ \text{----}> \ 2\ Nd + 3\ O^{2-}$$

and at the anode:

$$Nd_2O_3 + 3\ C \ \text{----}> \ 2\ Nd^{3+} + 3\ CO_2 + 6\ e^-\ .$$

These equations represent overall reactions and do not reflect details of the reaction mechanism.

The approach is similar to the Hall-Héroult process to produce primary aluminum. Carbon anodes are employed and minimal metallic contaminants are introduced by the anode.

It is conceivable to conduct the electrolysis with oxygen-evolving anodes:

$$2\ Nd_2O_3 \ \text{----}> \ 4\ Nd + 3\ O_2\ .$$

Very likely, however, the use of such anodes would lead to undesirable impurities in the electrolyte and, consequently, in the metal. An iron-oxide based anode could be an exception, if iron-containing neodymium alloys are produced.

An electrolysis process is expected to yield a pure metal whose quality is essentially governed by the purity of the feed materials (including carbon anodes). If the deposited neodymium forms an alloy with the cathode substrate, such alloys with a lower melting point than neodymium may be collected as the cathodic product. It is, furthermore, possible to co-deposit alloy components.

Electrolysis of neodymium oxide was studied by the Bureau of Mines. While the electrolysis of neodymium chloride received some attention [6], several reports were published dealing with the electrolysis of rare earth oxides. An effort to produce lanthanum metal [7] preceded the electrolysis work on neodymium. This electrolysis was conducted with an electrolyte composed of 70 wt% $LaF_3$ / 20 wt% $BaF_2$ / 10 wt% LiF, which separated into two phases. The $La_2O_3$ solubility in the electrolyte was about 2 wt% at an operating temperature of 975 °C. Three bath compositions were employed in studies to produce neodymium [8]:

90 wt% $NdF_3$ / 10 wt% LiF
80 wt% $NdF_3$ / 20 wt% LiF
74 wt% $NdF_3$ / 26 wt% LiF

The solubility of $Nd_2O_3$ in these baths was determined to be about 2 wt%. The electrolysis produced a current efficiency of 78 %, an oxide utilization of about 60 %, and an atmosphere in the cell chamber of 7 mole% CO, 3 mole% $CO_2$, and 0.5 mole% $CF_4$, in helium. To achieve high current efficiency (CE), a thermal gradient cell was used, collecting the metal product at a lower temperature (740 °C) than the average electrolyte temperature (1198 °C). This work was extended to electrowinning of liquid rare-earth ferroalloys [9]. A samarium-iron alloy was of particular interest. Later, rare-earth-cobalt alloys were studied because of their

potential use as permanent magnet materials [10]. Cobalt-neodymium alloy was prepared with a CE of 73 %. More recent work was published by the Bureau of Mines in Reno [11], and was discussed with the authors before its publication [12].

The electrolysis of neodymium oxide and/or neodymium fluoride and or related rare earth oxides has been covered by a number of patents [13] [14] [15] [16] [17] [18] [19] [20] [21]. In none of these patents, nor in any other published literature, could we find a statement that the off-gases were free of perfluorinated carbon compounds. We suspect that in all cases either a mixed oxide-fluoride electrolysis or even a pure fluoride electrolysis occurred and may actually be practiced industrially at this date. The Pechiney patent [15] acknowledges the presence of substantial amounts of $CF_4$ and suggests a treatment of the off-gases by liquefaction and distillation.

## GOALS OF THE PRESENT EFFORT

The present effort aimed at the development of a cost-effective neodymium oxide electrolysis process, yielding a high-quality product. The main goal was to achieve a consistent electrolysis on the pre-pilot-scale over extended periods of time. The approach built on the examination of critical aspects in Phase I. Electrolysis experiments at the 20-A level were started, then modified to be operated with a current of 10 A. When consistent cell operation over a period of 30 hours with current efficiencies exceeding 50 % and without emission of perfluorinated carbon compounds was achieved, a larger cell was constructed. Details were modified in the course of 100-A tests, to finally reach the goal of uninterrupted 96-hour operation with acceptable current efficiency, high oxide utilization, and no C-F compounds in the off-gases.

Phase II goals have been met; progression into the next phase consisting of pilot cell experimentation is justified.

# EXPERIMENTAL RESULTS

## OVERVIEW

Electrolysis experiments were the main part of the experimentation. The following sequence evolved during the course of this phase:

(1) 20-A experiments resulting in mixed oxide-fluoride electrolysis

(2) 10-A experiments resulting in an all-oxide electrolysis, without emission of perfluorinated carbon compounds

(3) electrolysis with 100-A cell, with results reaching the goals set for Phase II: 96-hour duration; current efficiency >50 %; good-quality, tappable metal; high feed utilization

In addition, the following supporting research was conducted:

(1) metal solubility studies

(2) oxide dissolution studies

(3) investigation of off-gas treatment to remove $CF_4$

(4) anode effect studies

(5) room temperature flow modeling

(6) preparation of new materials compatible with purity requirements of system

A 10,000-A pilot cell was designed and costs estimated. With an annual production of about 100 t neodymium, such a cell, in order of magnitude, is actually of an industrially viable size. We can envision an operation consisting of five 20,000-A cells and producing 1,000 t of neodymium annually.

## ELECTROLYSIS IN 10-A AND 20-A CELL

### 1.1 6-Hour Experiments (Mixed Fluoride-Oxide Electrolysis)

#### 1.1.1 Cell Design

The 20-A cell contained three 1-inch diameter graphite anodes arranged concentrically around a center cathode which was made of 1010 steel. The cell itself was a 5-inch diameter molybdenum crucible 8" in height. A small collector cup made out of molybdenum or iron was placed under the cathode for collection of Nd-Fe alloy produced during electrolysis. The cell was placed inside an Inconel 600 vessel of 6 inch diameter with water-cooled lid. Ports for the three anodes, center cathode, argon bubbler (for electrolyte agitation), thermocouple, vacuum line, argon backfill purge, and feeding were installed through the lid. A schematic of the top view of the cell is shown in Figure 1, a side view, representing the cell in operation, in Figure 2.

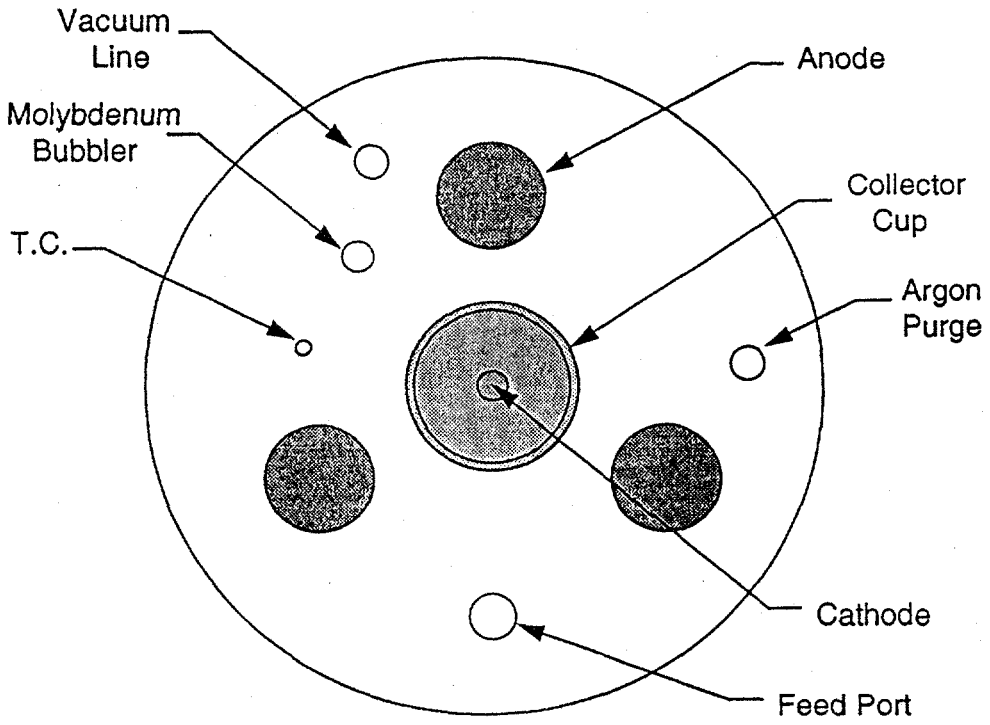


**Figure 1** 20-A cell schematic (top view)

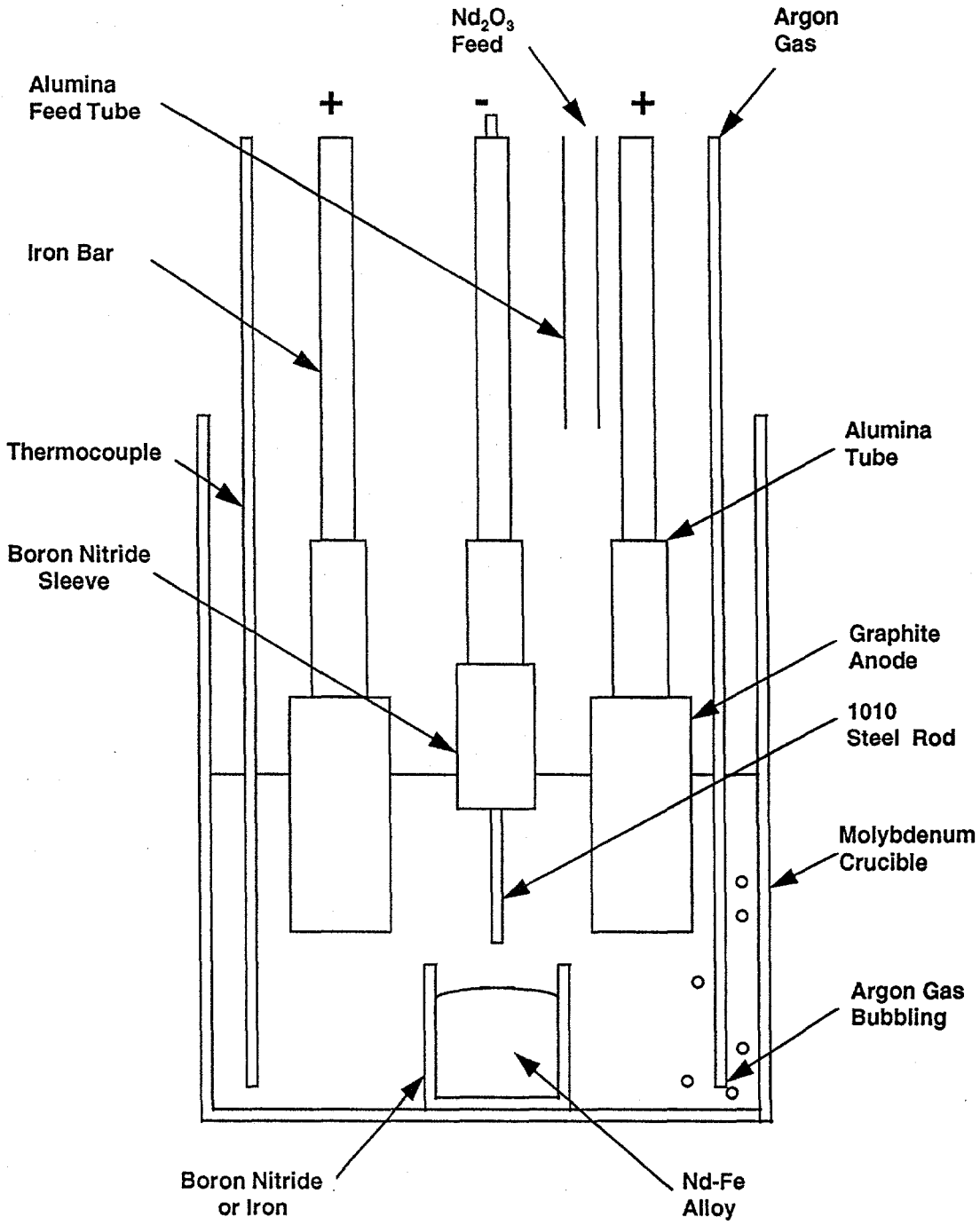


**Figure 2** 20-A cell schematic (side view)

### 1.1.2 Experimental Procedure

Neodymium fluoride, $NdF_3$ (60 to 70 wt%), lithium fluoride, LiF (10 to 20 wt%), and calcium fluoride, $CaF_2$ (20 to 25 wt%), were weighed and placed into a 5-inch diameter by 8-inch high molybdenum crucible. The water-cooled lid was assembled with all the appropriate electrochemical and physical connections. Three graphite anodes, 3-inch high and with 1-inch diameter, were attached to three stainless steel solid bars with threaded connections. A ¼"- to ½"-diameter 1010 steel rod with boron nitride protective sleeve, to be purged with argon, was inserted through the lid. The charged cell was placed into the Inconel vessel with a vacuum tight lid installed. The electrolyte was vacuum-dried for 24 hours at a temperature of 500 °C, to insure excellent starting conditions. After drying, the cell was heated to 910 to 925 °C. The anodes were lowered and immersed 1⅝" into the electrolyte. A surface area of 39 $cm^2$ for each anode was exposed to the electrolyte. A nominal anode current density of 0.17 $A/cm^2$ was maintained with an applied current of 20 A. The cell voltage was between 5 and 7 V. The cathode which was ¼ inch in diameter was lowered until the boron nitride sleeve was immersed ¼ inch. The boron nitride sleeve was purged with argon to suppress reactions at the cathode - gas - electrolyte interface. Neodymium oxide which had been vacuum-dried at 500 °C for 24 hours was added to the cell as needed. Typically, neodymium oxide was fed into the cell at a rate corresponding to a theoretical consumption at 50 % current efficiency at 20 A (3.49 g / 10 min).

Gas samples were collected from the off-gas port and injected into the gas chromatograph which was capable of analyzing for Ar, CO, $CO_2$, $C_2F_6$, $CF_4$ and $N_2$. Neodymium alloy dripped off the cathode into the collector cup located in the center at the bottom of the cell. The iron cathode was lowered into the cell as it was consumed. Current efficiencies were calculated based on the iron loss and total weight of the alloy recovered.

### 1.1.3 Results from 20-A Electrolysis Cell

Table I lists the results obtained in Experiments # DOE-Nd-3-1 through DOE-Nd-3-23 in the 20-A cell. Experiment number, electrolyte composition, temperature, current efficiencies, collector cup type, feed type, and remarks about cell conditions are presented in this table.

#### Current - Voltage Characteristics

Current - voltage curves were completed at the beginning and the end of each experiment to obtain data on oxide, fluoride and mixed oxide-fluoride decomposition potentials. To obtain this plot, the DC current was increased linearly with the use of a function generator driving a DC power supply, while both the voltage and current were recorded with a strip chart recorder. A current - voltage curve typical of the curves recorded in Experiments # DOE-Nd-3-1 to 3-23 is shown in Figure 3. This figure illustrates Experiment # DOE-Nd-3-20; variations caused by dissolved oxide present in the electrolyte can be observed.

**Table I.** Results from 6-hour Experiments # DOE-Nd-3-1 to DOE-Nd-3-23

| Exp # | Bath Comp. (wt%) $NdF_3/CaF_2/LiF$ | Temp. (°C) | CE (%) | Collector Cup | Feed | Remarks |
|---|---|---|---|---|---|---|
| 3-1 | 60/20/20 | 920 | 52.7 | Mo | $Nd_2O_3$ | BN collector cup cathodically protected |
| 3-2 | 60/20/20 | 910 | 24.8 | Mo | $Nd_2O_3$ | low cell voltage (2.5-3.0) |
| 3-3 | 60/20/20 | 925 | 51.3 | Mo | $Nd_2O_3$ | short between cathode and metal sump, increased CCD |
| 3-4 | 60/20/20 | 925 | 51.9 | Mo | $Nd_2O_3$ | buildup on BN sleeve, furnace left off |
| 3-5 | 60/20/20 | 925 | 45.8 | Mo | $Nd_2O_3$ | metal deposit on Mo bubbler tube |
| 3-6 | 60/20/20 | 920 | 72.4 | Mo | $Nd_2O_3$ | bubbler and lid isolated |
| 3-7 | 60/20/20 | 920 | 58.2 | Mo | $Nd_2O_3$ | repeat of 3-6 |
| 3-8 | 60/20/20 | 920 | 63.2 | Mo | $Nd_2O_3$ | repeat of 3-6, cathode-lowering device installed |
| 3-9 | 60/20/20 | 920 | 71.2 | Mo | $Nd_2O_3$ | repeat of 3-6 |
| 3-10 | 60/25/15 | 920 | 87.3 | Mo | $Nd_2O_3$ | increased CE observed with different bath composition |
| 3-11 | 60/20/20 | 920 | 48.7 | Mo | $Nd_2O_3$ | Mo collector cup isolated with BN sleeve |
| 3-13 | 65/20/15 | 1015 | ND | Mo | $Nd_2O_3$ | metal intermixed with electrolyte |
| 3-16 | 60/20/20 | 1015 | ND | Mo | $Nd_2O_3$ | A.E. occurred, test discontinued early |
| 3-17 | 70/20/10 | 1015 | 60.7 | Mo | $Nd_2O_3$ | A.E. occurred, test discontinued early |
| 3-18 | 60/20/20 | 850 (875) | 47.5 | Mo | $Nd_2O_3$ | A.E. occurred at 850 °C, temp increased to 875 °C |

| Exp # | Bath Comp. (wt%) $NdF_3/CaF_2/LiF$ | Temp. (°C) | CE (%) | Collector Cup | Feed | Remarks |
|---|---|---|---|---|---|---|
| 3-19 | 60/20/20 | 920 | 69.4 | Fe | $Nd_2O_3$ | iron collector cup employed |
| 3-20 | 60/20/20 | 920 | 60.2 | Fe | $Nd_2O_3$ | repeat of 3-19 |
| 3-21 | 60/20/20 | 920 | ND | Fe | $Nd_2O_3$ | gas composition vs. cell voltage obtained |
| 3-22 | 60/20/20 | 915 | 14.6 | Fe | $Nd_2O_3$ | fixed cell voltage at 3.5 V, current dropped to 3.5 A |
| 3-23 | 60/20/20 | 915 | ND | Fe | $Nd_2O_3$ | gas composition vs. cell voltage obtained |

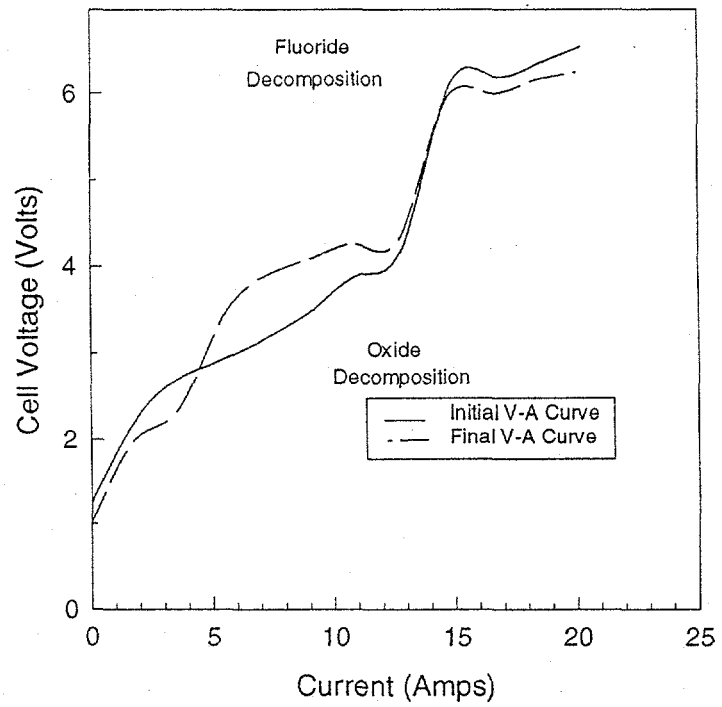


**Figure 3** Current-voltage characteristics (Experiment # DOE-Nd-3-20)

Anode Off-Gas Composition as a Function of Cell Voltage

A gas chromatograph for determining carbon oxides, CO and $CO_2$, and the perfluorinated carbon compounds $CF_4$ and $C_2F_6$ was employed to obtain data on off-gas composition in relation to applied voltage. A special anode arrangement, shown in Figure 4, was used to collect off-gas samples during electrolysis. It minimized the gas volume for quick turn around times during analysis at varied voltages. Argon gas was passed down the center tube, to entrain anode gases during electrolysis. The gas was swept up the outside tube and sampled for analysis. Relative gas composition values were determined in this manner. This arrangement was installed on all three anodes.

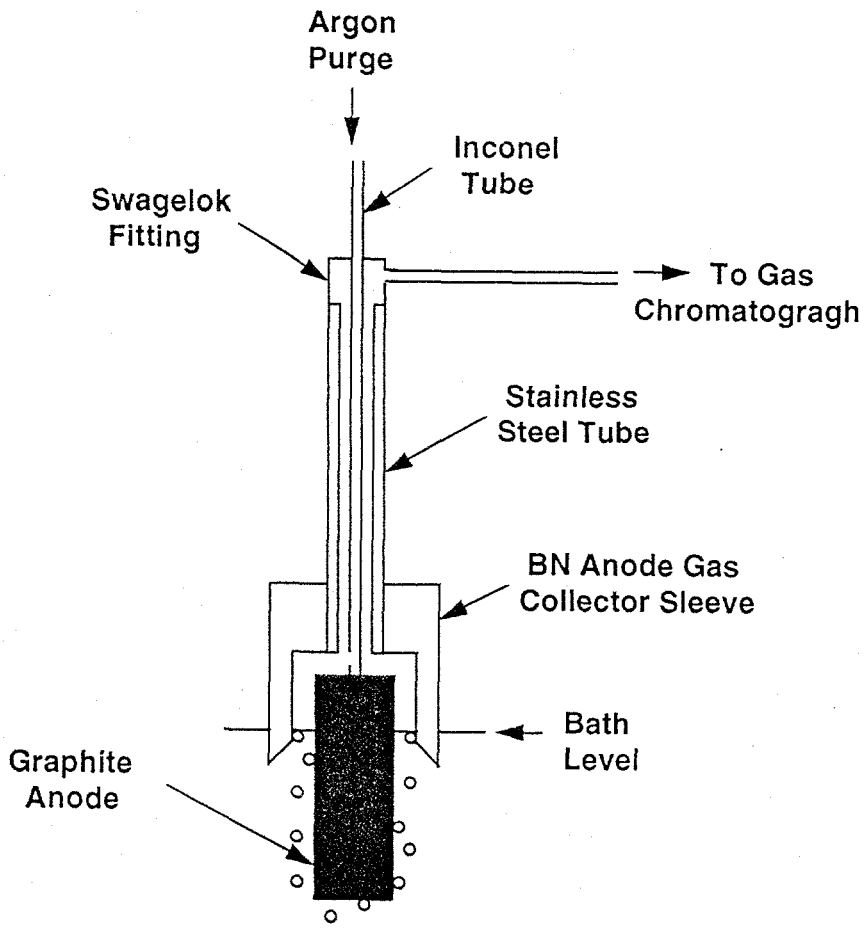


**Figure 4** Anode off-gas collection device

Figure 5 illustrates one graph obtained during Experiment # DOE-Nd-3-23 where the relative composition of the anode off-gas, in weight percent, was plotted versus the cell voltage. The electrolyte (for composition see Table I) contained 1 wt% added $Nd_2O_3$.

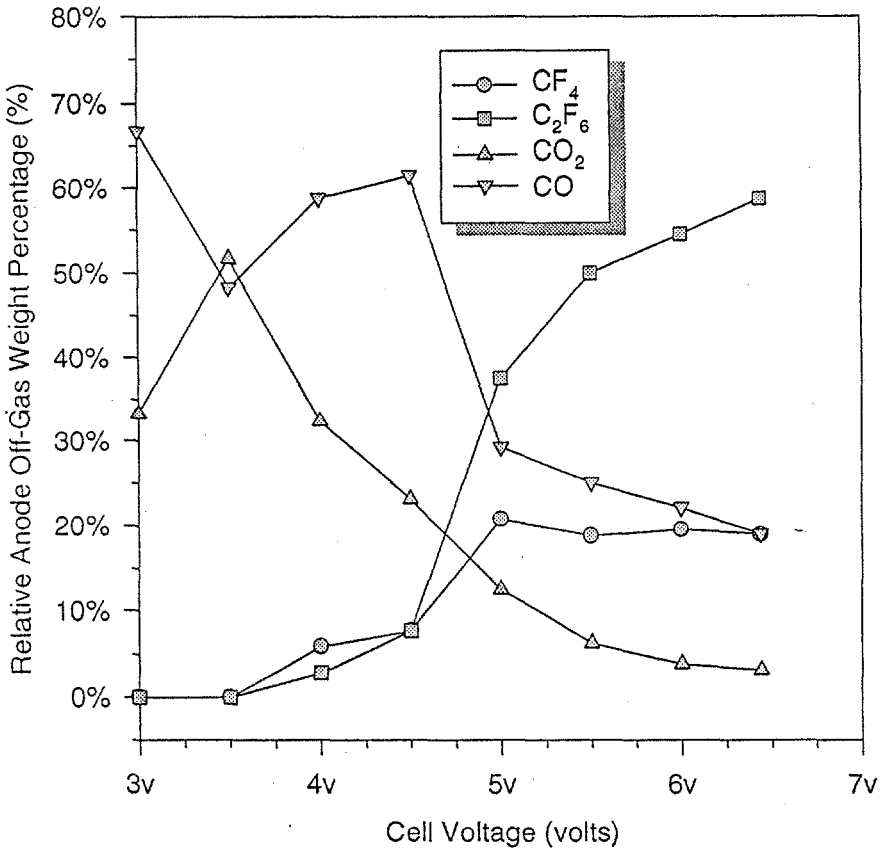


**Figure 5** Relative concentration of anode off-gas constituents as a function of cell voltage (Experiment # DOE-Nd-3-23)

Gas Composition Versus Time

Another interesting plot of data taken during electrolysis is the anode off-gas composition versus time. In Figure 6, $CF_4$, $C_2F_6$, $CO_2$ and CO contents, taken over the duration of a 6-hour experiment (Experiment # DOE-Nd-3-20), are plotted versus time.

### 1.2 6-Hour Experiments (All-Oxide Electrolysis)

#### 1.2.1 Cell Design

The 10-A cell design is identical to the 20-A design shown in Figure 1 (top view) and Figure 2 (side view). However, in later experiments, completed under all-oxide electrolysis conditions, a modified anode configuration was employed. A circular anode was designed to minimize surface area, and also to set up conditions at which a high concentration of oxide would be

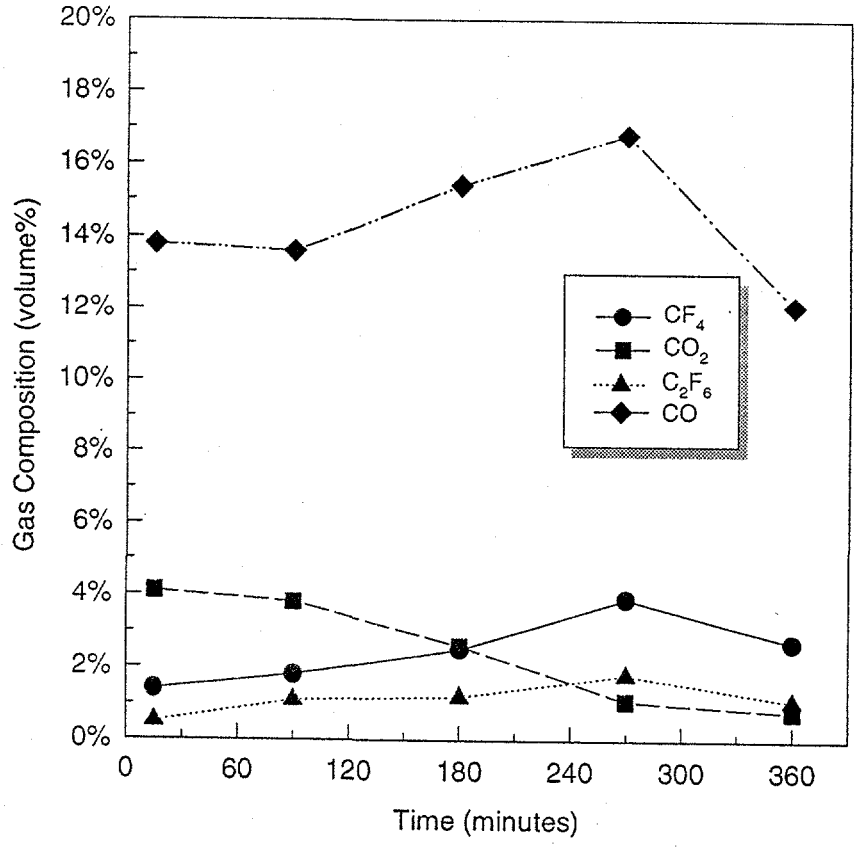


**Figure 6** Gas composition as a function of time (Experiment # DOE-Nd-3-20)

present on the outside of the anode, while a lower concentration of oxide would be present on the inside of the anode. This concept is referred to as the high-low oxide concentration cell. With this cell, one could feed oxide on the outside of the anode while the oxide concentration on the inside of the anode was depleted. It was expected that lower concentrations of oxide on the inside of the anode, near the cathode, would minimize cathodic deposition problems. Figure 7 represents this modified 10-A electrolytic cell.

### 1.2.2 Experimental Procedure

Neodymium fluoride, $NdF_3$ (50 to 65 wt%), lithium fluoride, LiF (20 to 35 wt%), and calcium fluoride, $CaF_2$ (0 to 30 wt%), were weighed and placed into a 5-inch diameter by 8-inch high iron crucible. The crucible contained a centering plate to hold the collector cup, made out of iron in initial tests and boron nitride in later tests. The water-cooled lid was assembled with all the appropriate electrochemical and physical connections. Three graphite anodes, 3-inch high by 1-inch diameter, were attached to three stainless steel solid bars with threaded

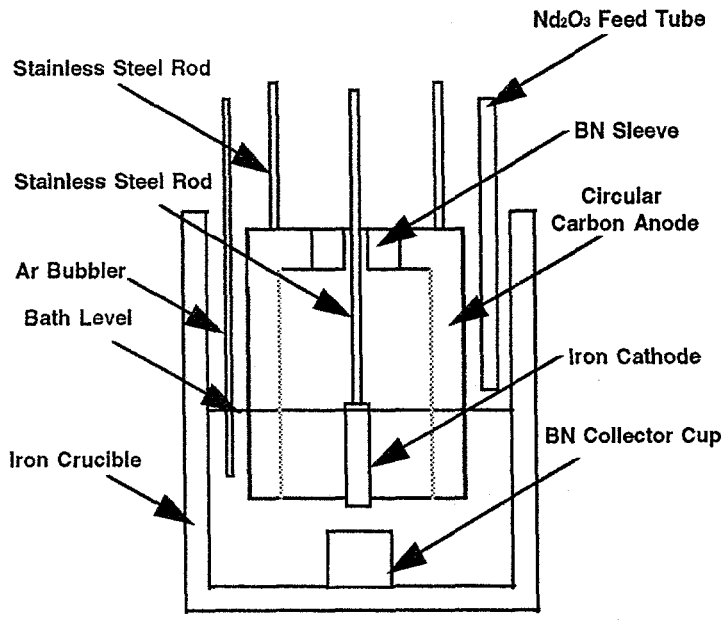


**Figure 7** Modified 10-A cell with circular anode (side view)

connections. In later experiments, the cylindrical carbon anode was employed (Experiment # DOE-Nd-3-51 to DOE-Nd-3-59). A ¼"- to ½-diameter 1010 steel rod with boron nitride protective sleeve, which was purged with argon, was inserted through the lid. The charged cell was placed into the Inconel vessel with a vacuum-tight lid installed. The electrolyte was vacuum-dried for 24 hours at a temperature of 500 °C. After drying, the cell was heated to 1030 to 1040 °C. The anodes were immersed by 1⅝", and a surface area of 39 $cm^2$ for each anode was exposed to the electrolyte. A nominal anode current density of 0.08 $A/cm^2$ was maintained with an applied current of 10 A. With the cylindrical anode, a current density of 0.03 $A/cm^2$ was maintained at this current. The corresponding cell voltage was between 3 and 4 V. The cathode, which was ¼ inch to ½ inch in diameter, was lowered until the boron nitride sleeve was immersed ¼ inch. The boron nitride sleeve was purged with argon to suppress reactions at the interface of electrolyte and cathode gas. Neodymium carbonate [$Nd_2(CO_3)_3$] or partially decomposed neodymium carbonate [$Nd_2O_2CO_3$] was vacuum-dried at 500 °C under an argon atmosphere for 24 hours and was added to the cell as needed. Typically, neodymium compounds were fed into the cell at a feed rate which allowed the cell to operate at 3.5 V and 10 A. Gas samples were collected from the off-gas port and injected into the gas chromatograph which was capable of analyzing for Ar, CO, $CO_2$, $C_2F_6$, $CF_4$ and $N_2$. Neodymium alloy dripped off the cathode into the collector cup centrally located at the bottom of the cell. The iron cathode was lowered into the cell as it was consumed. Current efficiencies were calculated based on the iron loss and the total weight of the alloy recovered.

### 1.2.3 Results from 10-A Electrolysis Cell (6-hr Experiments)

Table II lists the results obtain in Experiments # DOE-Nd-3-24 to DOE-Nd-3-54 in the 10-A all-oxide electrolysis cell. Experiment number, electrolyte composition, temperature, current efficiencies, collector cup type, feed type, and other remarks about cell conditions are presented in this table.

**Table II.** Results from 6-hr Experiments # DOE-Nd-3-24 to DOE-Nd-3-59

| Exp # | Bath comp (wt%) $NdF_3/CaF_2/LiF$ | Temp (°C) | CE (%) | Collector Cup | Feed | Remarks |
|---|---|---|---|---|---|---|
| 3-24 | 60/20/20 | 915 | 53.8 | Fe | $Nd_2(CO_3)_3$ | Fed $Nd_2(CO_3)_3$ |
| 3-27 | 60/20/20 | 915 | ND | Fe | $Nd_2O_2CO_3$ | No fluoride compounds found in off-gas, fixed cell voltage at 3.5 V |
| 3-28 | 60/20/20 | 920 | 48.3 | Fe | $Nd_2O_2CO_3$ | ⅛" cathode employed |
| 3-29 | 60/20/20 | 920 | 49.1 | Fe | $Nd_2O_2CO_3$ | ¼" cathode employed, current dropped to 6 A |
| 3-30 | 60/20/20 | 1025 | 49.6 | Fe | $Nd_2O_2CO_3$ | Fe cell employed, current maintained at 10 A |
| 3-31 | 60/20/20 | 1025 | ND | Mo | $Nd_2O_2CO_3$ | Metal intermixed with electrolyte, Mo cell employed |
| 3-32 | 60/20/20 | 1025 | ND | Fe | $Nd_2O_2CO_3$ | Metal intermixed with electrolyte, back to Fe cell |
| 3-33 | 65/0/35 | 1025 | ND | Fe | $Nd_2O_2CO_3$ | Metal intermixed with electrolyte |
| 3-34 | 50/30/20 | 1030 | 13.0 | Fe | $Nd_2O_2CO_3$ | Metal layered with electrolyte |
| 3-35 | 60/20$BaF_2$/20 | 1030 | ND | Fe | $Nd_2O_2CO_3$ | $BaF_2$ promoted metal-salt intermixing |
| 3-36 | 50/30/20 | 1030 | 48.1 | BN | $Nd_2O_2CO_3$ | BN collector cup promoted metal coalescence |

| Exp # | Bath comp (wt%) $NdF_3/CaF_2/LiF$ | Temp (°C) | CE (%) | Collector Cup | Feed | Remarks |
|---|---|---|---|---|---|---|
| 3-37 | 50/30/20 | 1030 | 17.0 | BN | $Nd_2O_2CO_3$ | Increased CCD, decreased CE |
| 3-38 | 50/30/20 | 1030 | 0 | BN | $Nd_2O_2CO_3$ | Cathode bent and shorted cell |
| 3-39 | 50/30/20 | 1030 | 62.5 | BN | $Nd_2O_2CO_3$ | Lower CCD improved current efficiency |
| 3-40 | 50/30/20 | 1025 | 41.2 | BN | $Nd_2O_2CO_3$ | Dark layer formed at top of cathode |
| 3-41 | 50/30/20 | 1030 | 23.3 | BN | $Nd_2O_2CO_3$ | Rotation of cathode enhanced dark layer formation at cathode |
| 3-42 | 50/30/20 | 1030 | 38.1 | BN | $Nd_2O_2CO_3$ | Lower CCD did not improve CE |
| 3-43 | 50/30/20 | 1030 | 40.7 | BN | $Nd_2O_2CO_3$ | Maintained temp above the M.P. of Nd still resulted in dark layer |
| 3-44 | 50/30/20 | 1030 + | ND | BN | $Nd_2O_2CO_3$ | Three cathodes all coated with dark layer |
| 3-45 | 50/30/20 | 1030 + | ND | BN | $Nd_2O_2CO_3$ | Rhone-Poulenc Fe cathode employed, coated with dark layer |
| 3-46 | 50/30/20 | 1040 + | 21.4 | BN | $Nd_2O_2CO_3$ | Precoating cathode with Nd did not eliminate dark layer formation |
| 3-47 | 20/60/20 | 1030 | 0 | BN | $Nd_2O_2CO_3$ | Different electrolyte with high $CaF_2$ resulted in poor CE |
| 3-48 | 50/30/20 | 1030 | 0 | BN | $Nd_2O_2CO_3$ | Reversing current during electrolyte did not reduce dark layer |
| 3-49 | 50/30/20 | 1025 | ND | BN | $Nd_2O_2CO_3$ | No coating forms on cathode during preheat |
| 3-50 | 50/30/20 | 1030 | 9.4 | BN | $Nd_2O_2CO_3$ | Reversing current for 2 min/hr did not eliminate dark layer formation |

| Exp # | Bath comp (wt%) $NdF_3/CaF_2/LiF$ | Temp (°C) | CE (%) | Collector Cup | Feed | Remarks |
|---|---|---|---|---|---|---|
| 3-51 | 50/30/20 | 1030 | 70.0 | BN | $Nd_2O_2CO_3$ | Circular anode with high-low oxide concentration cell employed |
| 3-52 | 50/30/20 | 1030 | 55.9 | BN | $Nd_2O_2CO_3$ | No BN sleeve used on cathode in preparation for 30 hr run |
| 3-53 | 50/30/20 | 1030 | 54.3 | BN | $Nd_2O_2CO_3$ | BN sleeve in contact with cathode employed in preparation for 30 hr run |
| 3-54 | 50/30/20 | 1030 | 50.4 | BN | $Nd_2O_2CO_3$ | $Al_2O_3$ sleeve in contact with cathode employed in preparation for 30 hr run |
| 3-57 | 50/30/20 | 1030 | 49.7 | BN | $Nd_2O_2CO_3$ | Finger circular anode used to see if high-low cell is established |
| 3-58 | 50/30/20 | 1030 | 0 | BN | $Nd_2O_2CO_3$ | Repeat of 3-51, short between anode and cathode developed |
| 3-59 | 50/30/20 | 1030 | 42.0 | BN | $Nd_2O_2CO_3$ | Repeat of 3-51 |

## 1.3 30-Hour Experiments, 20-A Cell (Mixed Fluoride-Oxide Electrolysis)

### 1.3.1 Cell Design

The same cell design as shown in Figures 1 and 2 was employed for the three 30-hour experiments that were completed. The only difference was that a large collector cup was used to retain increased amounts of Nd-Fe alloy product.

### 1.3.2 Experimental Procedure

The same experimental procedures were followed as described in section 1.1.2. The duration of the run was extended to 30 hours and several cathode changes were needed at 6-hour intervals due to the extended duration of the experiment. The feed added to the cell was modified and included $NdF_3$, taking into account true off-gas composition.

### 1.3.3 Experimental Conditions and Current Efficiencies

Table III lists the results obtained during three 30-hour attempts in the 20-A cell operated with mixed fluoride-oxide electrolysis. Experiment number, bath composition, temperature, current efficiencies (not determinable due to intermixing of electrolyte and metal), duration, feed, and experimental remarks are listed in this table.

**Table III.** Results from 30-hr experiments (mixed fluoride-oxide electrolysis)

| Exp # | Bath comp (wt%) $NdF_3/CaF_2/LiF$ | Temp (°C) | C.E. (%) | Duration (Hr:Min) | Feed | Remarks |
|---|---|---|---|---|---|---|
| 3-12 | 65/20/15 | 925 | ND | 30:00 | $Nd_2O_3$/ $NdF_3$ | Fed $Nd_2O_3$ at 20% C.E. and $NdF_3$ at 50% C.E. |
| 3-14 | 60/20/20 | 925 | ND | 30:00 | $Nd_2O_3$/ $NdF_3$ | Fed $NdF_3$ at 70% C.E. no product recovered |
| 3-15 | 65/20/15 | 925 | ND | 30:00 | $Nd_2O_3$/ $NdF_3$ | Fed $Nd_2O_3$ at 20% C.E. and $NdF_3$ at 50% C.E. |

## 1.4 30-Hour Experiments, 10-A Cell (All-Oxide Electrolysis)

### 1.4.1 Cell Design

The cell design used during the 30-hour all-oxide electrolysis employed the circular anode concept. Figure 7, shown previously, shows the modified 10-A cell with circular anode. The collector cup size was increased to collect larger quantities of alloy produced during four extended runs.

### 1.4.2 Experimental Procedure.

Section 1.2.2 experimental procedures were followed for the 30-hour runs with the cylindrical anode. The duration of the experiments was extended from 6 to 30 hours. Cathode changes were needed at about 6-hour intervals as the cathodes were consumed. $Nd_2O_2CO_3$ feed was added to the cell to maintain a voltage of 3.5 V.

### 1.4.3 Experimental Conditions and Current Efficiencies

Table IV lists the results obtained during four 30-hour attempts in the 10-A all-oxide electrolysis cell. Experiment number, bath composition, temperature, current efficiencies, duration, feed, and experimental remarks are listed in this table.

**Table IV.** Results from 30-hour experiments (all-oxide electrolysis)

| Exp # | Bath comp (wt%) $NdF_3/CaF_2/LiF$ | Temp (°C) | C.E. (%) | Duration (Hr:Min) | Feed | Remarks |
|---|---|---|---|---|---|---|
| 3-25 | 60/20/20 | 915 - 940 | 11.7 | 30:00 | $Nd_2(CO_3)_3$ | Current maintained at 10-A at 3.5 V; no C-F compounds |
| 3-26 | 60/20/20 | 920 - 930 | ND | 15:00 | $Nd_2O_3$ | Current dropped to 2.5 A with circular anode arrangement at 3.5 V; no C-F compounds |
| 3-55 | 50/30/20 | 1030 - 1040 | 56.3 | 30:00 | $Nd_2O_2CO_3$ | Fed to maintain 3.5 V; good metal quality |
| 3-56 | 50/30/20 | 1030 - 1040 | 53.6 | 30:00 | $Nd_2O_2CO_3$ | Good results obtained, decision to build 100-A cell |

## DISCUSSION OF RESULTS

### 2.1 6-Hour Experiments (Mixed Fluoride-Oxide Electrolysis)

Table I lists the results of the 6-hour experiments obtained in the 20-A cell. A bath composition of 60 wt% $NdF_3$, 20 wt% $CaF_2$, and 20 wt% LiF generally was used for these tests, with a few exceptions. In Experiment # DOE-Nd-3-10, the metal coalesced and current efficiency (87.3 %) was evidently improved by increasing the calcium fluoride concentration. In other experiments, the current efficiencies generally ranged between 45 % to 75 %.

Cell temperature had an effect on the occurrence of anode effects. At a temperature range of 910 °C to 930 °C, normal anode effects did not occur. When a normal anode effect took place, the cell current dropped rapidly to low values while the voltage increased to maximum capacity of the power supply (40 V). During Experiment # DOE-Nd-3-18 with a cell temperature of 850 °C, anode effects did occur. The anode effects were caused by the reduction in solubility and dissolution rate of $Nd_2O_3$ at lower temperature.

Current voltage curves were taken for several experiments. Figure 3 is an example of a pair of curves taken at the beginning and end of Experiment # DOE-Nd-3-20. A transition from an all-oxide electrolysis to one also involving the oxidation of fluoride was observed when the cell voltage was increased to above 6 V. At a voltage below 3.5 to 4.0 V, all-oxide electrolysis

was occurring (only CO and $CO_2$ gases evolved). As the voltage was increased above 4 V, however, a voltage increase resulted in a relatively small increase in current. This indicated the sliding into a mixed oxide-fluoride oxidation range. Figure 5, recorded during Experiment # DOE-Nd-3-23, illustrates this effect. At voltages below 3.5 V, only CO and $CO_2$ gases were observed. As the potential was increased above 3.5 V, carbon-fluorine compounds were seen in the off-gas at increasing concentrations, while carbon oxide contents decreased. The off-gas composition was also recorded over a 6-hour run in Experiment # DOE-Nd-3-20. Several gas samples were taken at 90 minute time intervals while the cell voltage was maintained at approximately 6 V. The carbon oxide and carbon fluoride gas compositions did not change significantly during the run.

After it was decided that zero emissions of C-F compounds would be desirable, subsequent experiments (from Experiment # DOE-Nd-3-22 on) were conducted accordingly. In this test, a cell voltage of 3.5 V was maintained, i.e. a voltage at which no C-F compounds would be emitted. However, due to the low dissolution rate of $Nd_2O_3$, the cell current dropped to 3.5 A over the duration of the run. This current was too low to yield an adequate production rate.

## 2.2 6-Hour Experiments (All-Oxide Electrolysis)

Table II lists the cell results from 6-hour experiments (Experiments # DOE-Nd-3-24 to DOE-Nd-3-59) in which conditions were employed that allowed only carbon oxide to form at the anode. During these tests the cell voltage was set at 3.5 V. The feed added to the cell was more reactive which led to higher dissolution rates. $Nd_2O_2CO_3$ was the feed of choice and was prepared by partially decomposing $Nd_2(CO_3)_3$ in a furnace at 500 °C for 24 hours. Gas samples taken during all experiments did not contain any C-F compounds. A current of 10 A was maintained for an anode current density of 0.08 A/cm$^2$ (with the exception of experiments where the circular anode was employed which experienced a current density of 0.03 A/cm$^2$). A temperature of 915 °C to 920 °C was used during Experiments # DOE-Nd-3-24, 27, 28, 29. A current of 10 A could not be maintained in these experiments. Therefore, the temperature was increased, to slightly above the melting point of neodymium (1020 °C), to improve dissolution of the partially decomposed carbonate. The bath composition was shifted to higher concentration of $CaF_2$ which improved metal coalescence in the collector cup. Metal coalescence was also improved by switching to a BN cup which was electrically insulated.

Dark-layer formation at the cathode surface below the electrolyte level caused problems during most experiments. The problem was solved, or at least minimized, by employing the circular anode with the high-low oxide-concentration concept (Experiments # DOE-Nd-3-51, 52, 53, 54, 58, 59). Feed was added outside the circular anode (high oxide concentration region) while the electrolyte inside the anode was depleted (low oxide concentration region) by the electrochemical action. Dark-layer formation on the cathode seemed to be related to the dissolved oxide concentration in the electrolyte. A sample of the dark layer from one experiment was analyzed and contained a Nd-O-F compound.

## 2.3 30-Hour Experiments (Mixed Fluoride-Oxide Electrolysis.

Table III lists the results of the 30-hour experiments obtained in the 20-A cell, with anode gas compositions indicating mixed fluoride-oxide electrolysis. Three tests were completed with slightly varied bath compositions and at a temperature of 925 °C. An experimental duration of 30 hours was achieved in each experiment. The feed added to each test was a mixture of $Nd_2O_3$ and $NdF_3$ in a ratio corresponding to 20 % C.E. for $Nd_2O_3$ and 50 % C.E. for $NdF_3$. This feed ratio was selected based on off-gas analysis results from the 6-hour experiments.

Current efficiencies for Experiments # DOE-Nd-3-12, 3-14 and 3-15 could not be calculated due to the extensive intermixing of the metal product and the electrolyte. A fine dispersion of NdFe alloy in the electrolyte was observed.

## 2.4 30-Hour Experiments (All-Oxide Electrolysis)

Table IV lists the results of the 30-hour experiments obtained in the 10-A all-oxide electrolysis cell. Electrolysis Experiments # DOE-Nd-3-25 and 3-26 employed a bath composition of 60 wt% $NdF_3$, 20 wt% $CaF_2$ and 20 wt% LiF at a temperature between 915 and 940 °C. In Experiment # DOE-Nd-3-25 with a electrolysis duration of 30 hours, $Nd_2(CO_3)_3$ was fed to the cell. This allowed for a current of 10 A (ACD = 0.03 $A/cm^2$) to be passed continuously at a cell voltage of 3.5 V for the entire duration of the run. A poor current efficiency of only 11.7 % was obtained. In a second experiment, Experiment # DOE-Nd-3-26, $Nd_2O_3$ was fed to the cell instead of the more highly soluble $Nd_2(CO_3)_3$ compound. The run had to be cut short of the 30-hour goal (15 hours) because the current decreased at a fixed cell voltage of 3.5 V due to poor dissolution of the $Nd_2O_3$ . The current efficiency could not be calculated due to intermixing of metal and electrolyte.

Two successful runs (Experiments # DOE-Nd-3-55 & 56) completed in the 10-A cell are also represented in Table IV. Partially decomposed neodymium carbonate, $Nd_2O_2CO_3$, was fed to the cell to maintain a current of 10 A at 3.5 V. The electrolyte composition was shifted to be richer in calcium fluoride and leaner in neodymium fluoride (50 wt% $NdF_3$, 30 wt% $CaF_2$, 20 wt% LiF). Metal coalescence was improved. The temperature of the electrolyte was increased to the 1030 °C - 1040 °C range (slightly above the melting point of neodymium, 1020 °C) to improve alloying at the cathode. This action reduced the tendency to form dark-layer deposits at the cathode by reducing the activity of the neodymium metal. Back reaction with the electrolyte was minimized. Current efficiencies of 56.3 % and 53.6 % were obtained during the two 30-hour runs. Good metal coalescence was observed.

The goal to complete two 10-A 30-hour cell runs with current efficiencies above 50 % and good metal coalescence was met. Consequently it was decided to build and operate a 100-A cell.

## ELECTROLYSIS IN 100-A CELL

### 3.1 Cell Design

#### 3.1.1 Furnace

A rectangular furnace with the dimension 36" L x 32" W x 30" H was designed and assembled, using commercial Thermcraft heating elements. The furnace could accommodate a vessel 15" in length and 11" wide, inserted to a depth of 18 inches. A total of seven 220 V heating elements were installed in the furnace box providing a total heating capacity of 2 KW. A furnace control system was purchased to operate the furnace. The control system was outfitted with AC ammeter, temperature display (both process and overtemperature control) and programmable controller with ramping and soaking functions. Figure 8 shows the cell in operation, with the blue furnace box.

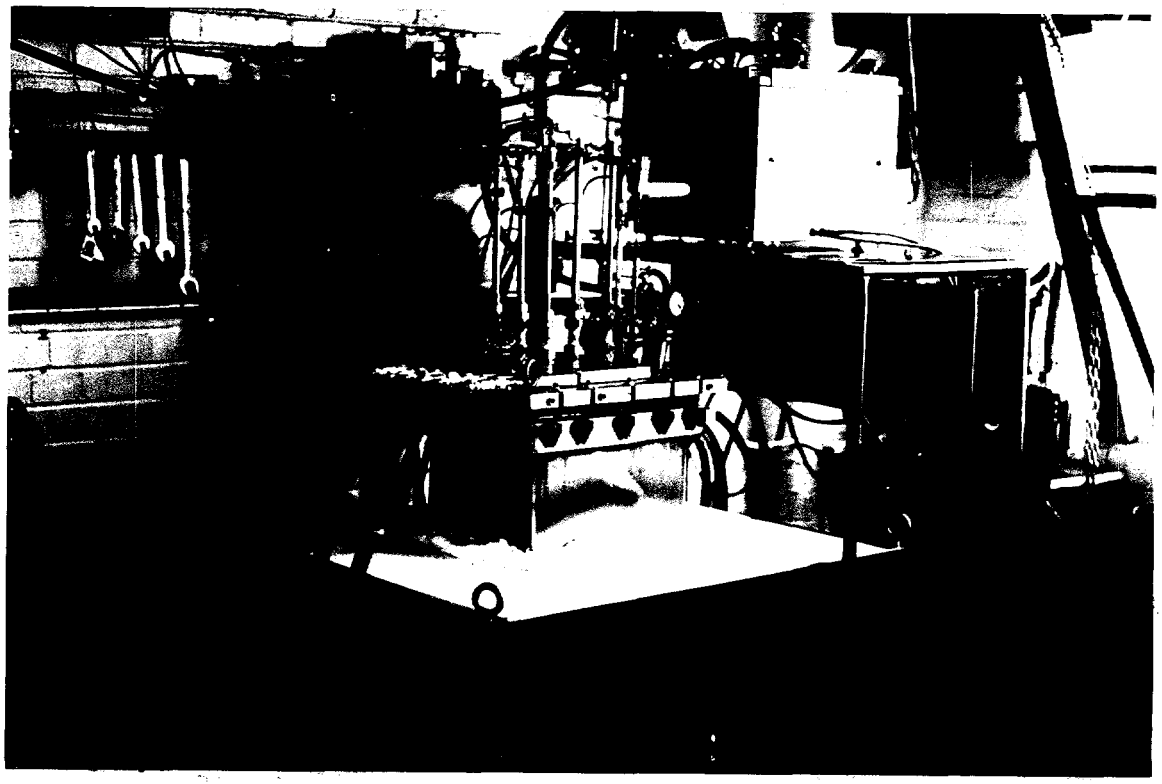

**Figure 8** 100-A electrolysis set-up

### 3.1.2 Inert-Atmosphere Vessel

An Inconel 600 inert-atmosphere vessel to contain the electrolysis cell was designed and assembled. The vessel consisted of several parts: bottom (rectangular box, open on top) with water-cooled top part; and a water-cooled lid, with water-cooled anode cover plate and three water-cooled cathode cover plates. The bottom was constructed out of ⅜" Inconel plate and had inside dimensions of 13½" L x 9½ " W x 29½" H; a water-cooled jacket was placed near the top to cool the sealing zone between the top of the vessel box and the lid. The water-cooled lid and anode and cathode cover plates were constructed out of 1-inch thick Inconel plates. Holes were drilled to allow for the passage of cooling water through the interior of the plate. Figure 8 also shows the vessel into which the electrolysis cell was placed.

### 3.1.3 Tapping Vessel

A water-cooled vacuum tapping vessel was designed and built for extracting molten neodymium-iron alloy. It is shown in preparation for a tapping operation in Figure 9.

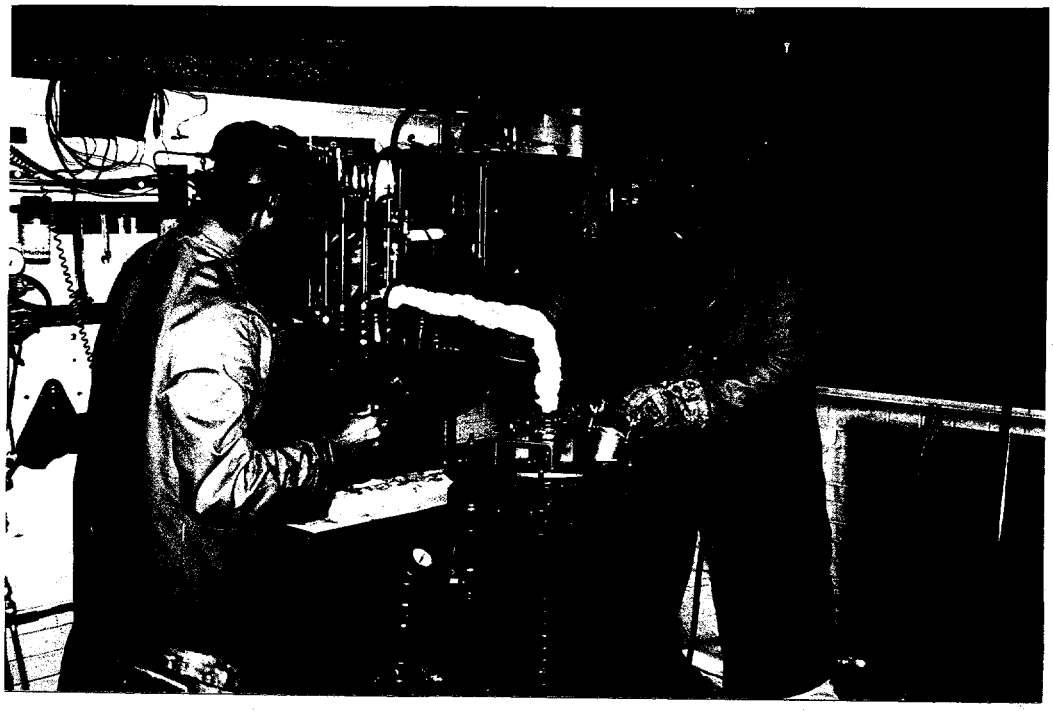

**Figure 9** Preparation of tapping vessel for operation

In experiments of extended duration, alloy must be periodically removed due to the constraints of the collector cup size. The tapping vessel was built large enough to also handle the electrolyte volume present in the electrolytic cell. The electrolyte could be tapped from the cell at the conclusion of the experiment for reuse. Stainless tubes, ⅜" in diameter, were employed as tapping pipes. One end of the tapping pipe was attached to a flange which could be secured to the top of the tapping vessel while the other end extended through the lid of the Inconel vessel into the electrolyte or metal. The tapping pipe was heated with DC current which was supplied from a 250 A AC/DC welding unit. After backfilling the vessel with argon, vacuum was applied to create an underpressure. The molten liquid was siphoned from the electrolysis cell into a mold placed in the tapping vessel

### 3.1.4 Feed System

A feed system to add solid neodymium oxide or carbonate was designed and assembled. It could be controlled to feed based on either voltage or current signals from the electrolytic cell. A commercially available screw feeder, AccuRate Model # 300, with ¼-inch diameter screw, was supported above one end of the Inconel vessel on a movable cart. An alumina tube attached to the end of the screw extended through the lid and into the cell area. Feed was passed down the tube and into the molten bath. The control system turned the feeder on and off. The arrangement is shown in Figure 8 and more clearly in Figure 10.

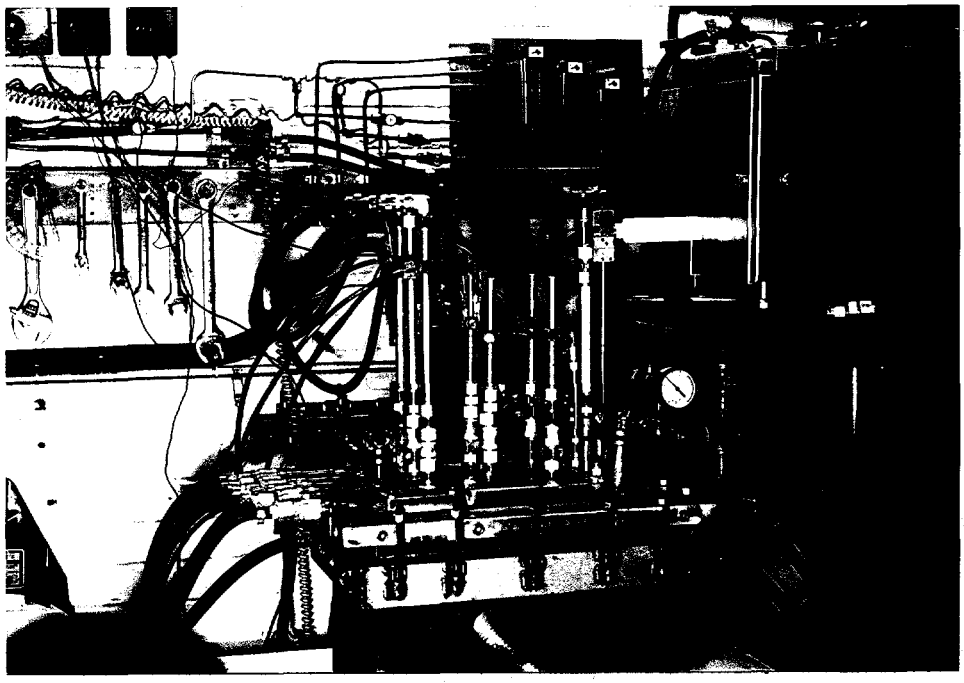

**Figure 10** Arrangement to add cell feed

### 3.1.5 Electrolysis Cell

An electrolysis cell was designed, as shown in Figure 11. With the inside dimensions of 8" W x 12" L x 18" H, it was built slightly smaller than the Inconel vessel, and it could be placed inside this vessel. Mild steel, ½ inch in thickness, was employed to construct the cell. The sides of the cell (in later 100-A experiments) were fitted with ¼-inch thick boron nitride plates, to eliminate any current passing from anode to sidewall, then to cathode. With the use of the plates, all current was forced to pass only through the electrolyte between anode and cathode. This measure, incidentally, will not be necessary in larger cells when cathodes are placed between two stacks of anodes and not adjacent to a cell wall.

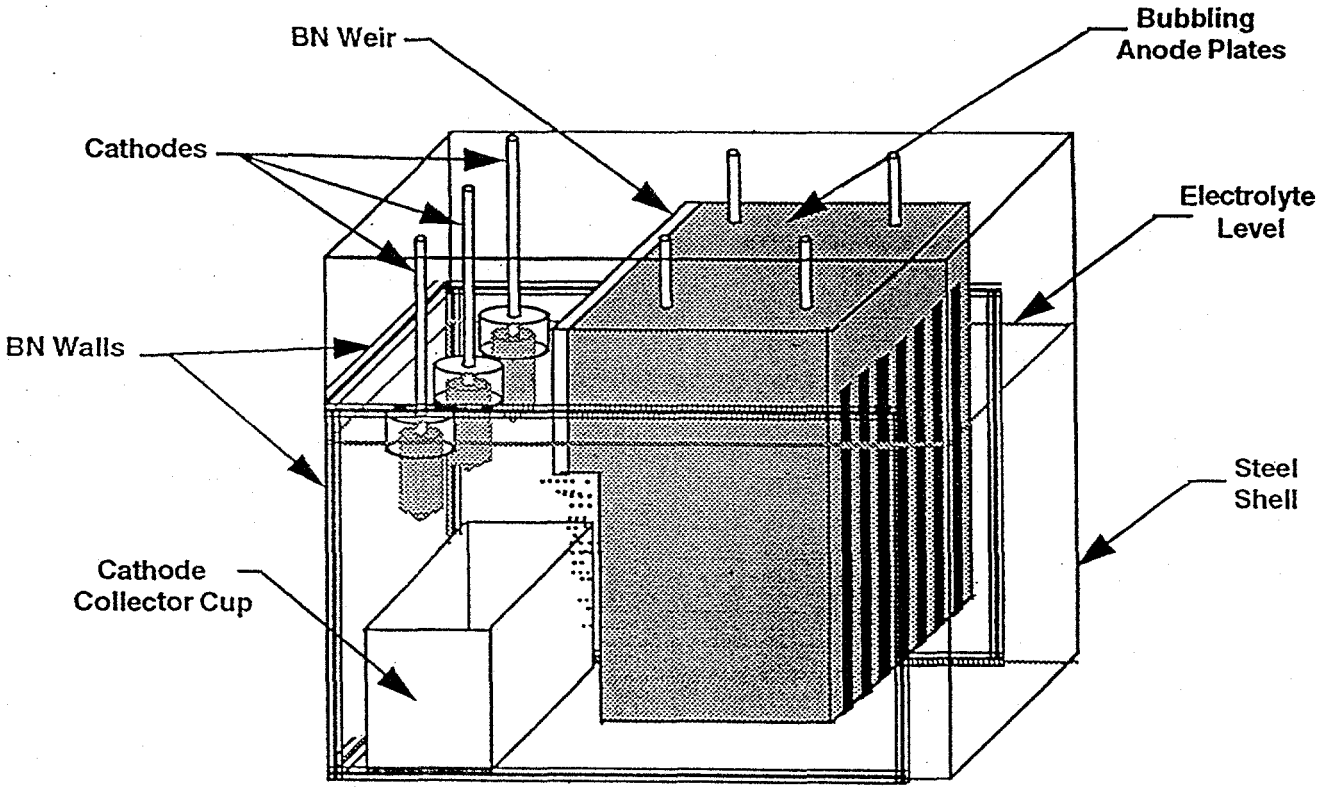


**Figure 11** 100-A cell design

A graphite anode with outside dimensions 5" W x 6.5" L x 10" H was placed 3 inches from one end of the cell. The anode was constructed of 7 plates ½" in thickness to maximize the surface area. The plates were parallel to the 12" length side of the cell. A weir constructed out of graphite or boron nitride, with dimensions 6.5" L x 5" H x 1/2" thick, was attached to one side of the anode perpendicular to the anode plates. The weir faced the three cathodes and served to stagnate the electrolyte above the collector cup. Feed added to the cell dropped on the side opposite the weir.

Three iron cathodes, 1¼ inch in diameter, were placed at one end of the cell. Inverted cups of boron nitride were attached above the cathodes. The cathodes were immersed to a level such that the boron nitride sleeve bottom was just under the bath surface. The trapped space inside the boron nitride cup was purged with argon.

A collector cup constructed out of iron or boron nitride was placed below the cathodes to collect neodymium-iron alloy. The cup dimensions were 2¼" W x 6½" L x 3¼" H for extended duration experiments (96 hours) and 1¾" W x 6½" L x 2¾" H for shorter tests of 15 to 30 hours duration. The larger cup only had to be tapped once a day.

## 3.2 100-A Electrolysis Experiments (All-Oxide Electrolysis)

### 3.2.1 6- to 30-Hour Electrolysis Experiments

Experimental Procedure

Neodymium fluoride (50 wt%), 95 % $NdF_3$ provided by Rhône-Poulenc, lithium fluoride (20 wt%), 99.0 % pure LiF purchased from Foote Mineral, and calcium fluoride (30 wt%), 99.95 % $CaF_2$ supplied by Alfa AESAR, were weighed (29.5 kg to 32.0 kg), mixed, and placed into the 8" W x 12" L x 18" H steel cell along with the collector cup. The collector cup (1¾" W x 6½" L x 2¾" H) type varied as experimentation progressed, from solid iron to solid iron lined with boron nitride, to solid boron nitride (weighted with iron). Also, the mild steel shell was modified and equipped in later tests with boron-nitride-lined walls. The water-cooled lid was assembled with all the appropriate electrochemical and physical connections. One graphite anode consisting of seven plates was attached to four stainless steel bars with threaded connections. The weir was attached to the side of the anode between the anode and cathode. The weir was constructed out of graphite in initial testing and of boron nitride in later experiments. Three cathodes, 4 inches in length and 1¼ inch in diameter, along with three boron nitride cups were attached to stainless steel tubes. The cathodes protruded 3 inches out of the cups (1 inch remained inside the cup). Cathode material in initial experiments was 1010 steel. However, in later test when metal quality became important, high-purity iron was employed. The charged cell was placed into the Inconel vessel and the vacuum-tight lid was installed. The electrolyte was vacuum-dried for 24 hours at a temperature of 500 °C to insure excellent starting conditions. After drying, the cell was heated to 1020 °C to 1040 °C. The anode was lowered by 7 inches into the electrolyte, for a nominal anode current density of 0.03 A/cm$^2$ at 100 A. The cathodes were lowered just enough to immerse the inverted cup edges. When three cathodes were immersed 3 inches, a current density of 0.44 A/cm$^2$ was established, which increased to approximately 0.60 A/cm$^2$ as cathode metal was consumed. For 30-hour runs, the cathodes were changed once after 15 hours. The cathodes were not changed for shorter experiments (15 hours and less). The feeder was assembled, charged with feed ($Nd_2O_2CO_3$, prepared from $Nd_2(CO_3)_3$ supplied by Rhône-Poulenc by heating to 500 °C for 24 hours, or $Nd_2O_3$, a 95 % product also supplied

by Rhône-Poulenc, and also heated to 500 °C for 24 hours), and put into position above the cell. The feeder control system was set to maintain a current of 100 A at a constant cell voltage. DC power was applied to the cell. The DC power source was set on constant voltage of 3.5 V to 4.25 V, to establish a current of 100 A. The feeder turned on when the current decreased to 99 A and shut off at 101 A in a cycling fashion. The duration of the experiments varied between 6 and 30 hours.

Neodymium-iron alloy was produced at the cathodes and dripped into the collector cup. Vacuum-tapping of the neodymium-iron alloy for 30-hour experiments was completed at 15 and 30 hours to avoid a collector cup overflow. In experiments of shorter duration, the alloy was allowed to solidify in the collector cup. The electrolyte was tapped from the cell at the conclusion of each experiment. Gas samples were taken periodically to insure that no C-F compounds were present. Metal samples were sent to Rhône-Poulenc for analysis.

Experimental Results (6- to 30-Hour Electrolysis Experiments)

Table V lists the results obtained in the 100-A cell for 6- to 30-hour experiments. Experiment number, collector cup type, anode weir type, current efficiency, duration and remarks about cell conditions are presented in this table.

**Table V.** 6- to 30-hour electrolysis results in 100-A cell

| Exp # | Collector cup | Anode | C.E % | Time (hr) | Remarks |
|---|---|---|---|---|---|
| 3-60 | iron: not isolated | graphite weir | 41.5 | 10 | failure of furnace elements, metal recovered in lumps |
| 3-61 | iron: not isolated | graphite weir | ND | 4.25 | anode rods warped causing anode to short to side wall |
| 3-62 | iron: not isolated | graphite weir | 42.8 | 10 | metal recovered in lumps |
| 3-63 | iron: not isolated | no weir | ND | 8 | no metal recovered |
| 3-64 | iron: not isolated | graphite weir | ND | 10 | metal intermixed with electrolyte in flat layers |

| Exp # | Collector cup | Anode | C.E % | Time (hr) | Remarks |
|---|---|---|---|---|---|
| 3-65 | iron: BN isolated | graphite weir ext. to bottom | ND | 10 | metal intermixed with electrolyte in flat layers |
| 3-66 | BN-lined iron | graphite weir ext. to bottom | 55.7 | 10 | metal recovered as one ingot, some entrained electrolyte |
| 3-67 | BN-lined iron | graphite weir | 63.4 | 10 | metal recovered as one ingot, some entrained electrolyte |
| 3-68 | BN-lined iron | graphite weir | 23.9 | 6 | metal intermixed with electrolyte |
| 3-69 | BN-lined iron | graphite weir | 70.8 | 10 | anode fins reduced to 5" in length |
| 3-70 | BN-lined iron | graphite weir | 59.6 | 10 | metal intermixed with electrolyte |
| 3-71 | solid BN lined iron | graphite weir | 64.7 | 10 | some intermixing near top of ingot |
| 3-72 | solid BN lined iron | graphite weir | 65.8 | 10 | high-low cell condition did not occur |
| 3-73 | | | | | tapped metal from exp. 3-71, 3-72 to test tapping equipment |
| 3-74 | solid BN lined iron | graphite weir | 62.1 | 10 | electrolyte mixed, high-low cell condition did not occur |
| 3-75 | solid BN lined iron | graphite weir | 29.4 | 15 | electrolyte mixed during run, metal spilled during stirring |
| 3-76 | solid BN lined iron | graphite weir | ND | 30 | no metal observed in cell after 30 hrs. cell current 50 A |
| 3-77 | solid BN lined iron | graphite weir | 69.8 | 10 | $Nd_20_3$ derived from $Nd_2(CO_3)_3$ employed as feed |
| 3-78 | solid BN | graphite weir | 67.2 | 10 | metal intermixed with electrolyte near surface |
| 3-79 | solid BN | graphite weir | ND | 8 | BN liner broke free from iron collector cup during run |
| 3-80 | solid BN | graphite weir | ND | 4 | feeder plugged, test aborted |

| Exp # | Collector cup | Anode | C.E % | Time (hr) | Remarks |
|---|---|---|---|---|---|
| 3-81 | solid BN | BN weir | 65.3 | 6 | metal recovered as a solid ingot, feeder electrical short |
| 3-82 | solid BN | BN weir | 64.3 | 10 | metal recovered as a solid ingot |
| 3-83 | solid BN | BN weir | 62.7 | 10 | metal recovered as a solid ingot |
| 3-84 | solid BN | BN weir | 60.2 | 15 | metal recovered as a solid ingot |
| 3-85 | solid BN | BN weir | ND | 15 | metal blew out of collector cup during tapping |
| 3-86 | solid BN | BN weir | 45.7 | 15 | metal tapped from cell and recovered as a solid ingot |
| 3-87 | solid BN | BN weir | 53.7 | 30 | metal tapped from cell twice and recovered as solid ingots |
| 3-88 | solid BN | BN weir | 52.3 | 10 | BN lined iron cell, dark layer formed on back of cathodes |
| 3-89 | solid BN | BN weir | 57.9 | 15 | BN cell, high-purity R-P iron cathode material, 0.038 wt% Mn, 0.089 wt% C |
| 3-90 | solid BN | BN weir | ND | 10 | clean-up run, iron cell |
| 3-91 | solid BN | BN weir | ND | 15 | $Nd_2O_3$ fed instead of $Nd_2O_2CO_3$ to reduce C in alloy, R-P cathodes, BN cell, analysis: 0.170 wt% C |
| 3-92 | solid BN | BN weir | 51.6 | 30 | $Nd_2O_3$ fed instead of $Nd_2O_2CO_3$, high-purity cathodes (0.04 C), BN cell |
| 3-93 | solid BN | BN weir | 56.8 | 10 | $Nd_2O_2CO_3$ fed, H-P Fe cathodes temp reduced to lower C in alloy, cathodes scraped hourly, BN cell |
| 3-94 | solid BN | BN weir | ND | 10 | clean-up run, iron cell |
| 3-95 | solid BN | BN weir | ND | 18 | 96-hour run attempted, dark layer formed on cathodes, cell over-fed |
| 3-96 | solid BN | BN weir | ND | 10 | clean-up run, iron cell |

| Exp # | Collector cup | Anode | C.E % | Time (hr) | Remarks |
|---|---|---|---|---|---|
| 3-97 | solid BN | BN weir | ND | 8 | $Nd_2O_2CO_3$ + 5 wt% $Fe_2O_3$ fed to BN cell, metal BBs recovered, lost furnace element |
| 3-98 | solid BN | BN weir | ND | 10 | clean-up run, iron cell, failure to clean-up electrolyte |
| 3-99 | solid BN | BN weir | 52.3 | 10 | clean-up run, iron cell |
| 3-100 | solid BN | BN weir | ND | 6 | clean-up run, iron cell |
| 3-101 | solid BN | BN weir | 33.0 | 10 | $Nd_2O_2CO_3$ + 0.5 wt% $Fe_2O_3$ fed to cell, dark layer formed at cathode, cell voltage increased to 4.25 V |
| 3-102 | solid BN | BN weir | 47.6 | 10 | operation at 4.25 V eliminated dark layer at cathode |
| 3-103 | solid BN | BN weir | ND | 6 | clean-up run |
| 3-106 | solid BN | BN weir | 53.2 | 8 | $Nd_2O_3$ fed to cell (not from carbonate), cell ran without problems |
| 3-107 | solid BN | BN weir | ND | 8 | electrolyte clean-up run |

Table VI lists analytical results (in wt%) for two metal product samples and a cathode metal sample (Experiment # DOE-Nd-3-89), analyzed by Rhône-Poulenc.

**Table VI.** Metal analysis results from 6- to 30-hour experiments (in wt%)

| Exp# | Fe | Pr | Si | Mg | Al | Mn | Ca | C | O | N |
|---|---|---|---|---|---|---|---|---|---|---|
| 3-84 * | 20.79 | 0.972 | 0.038 | <0.01 | <0.01 | 0.274 | <001 | 0.097 | 0.010 | 0.001 |
| 3-89+ | - | - | - | - | - | 0.038 | - | 0.089 | - | - |
| 3-92 * | 26.40 | 1.06 | <0.01 | <0.01 | 0.014 | 0.094 | 0.015 | 0.065 | 0.025 | 0.002 |

* balance Nd + Mn and C determined

### 3.2.2 96-Hour Experiments

Experimental Procedure

The same procedures, with a few exceptions, were used for the 96-hour experiments as described in the 6- to 30-hour experimental procedures. The steel shell was lined with boron nitride for all experiments. A solid boron nitride collector cup with size 2¼" W x 6½" L x 3¼" H was employed to collect 24 hours of product. A boron nitride weir attached to the anode was used in all tests. High-purity iron for the cathode material was employed to improve alloy quality. The cathodes were changed once every 12 hours. Metal was tapped from the cell every 24 hours for a total of four metal taps. The duration of the test was extended to 96 hours.

Experimental Results (96-Hour Electrolysis Experiments)

Table VII lists the results obtained in the 100-A cell for the 96-hour experiments. Experiment number, collector cup type, anode weir type, current efficiency, duration and remarks about special cell conditions are presented in this table.

**Table VII.** Results from 96-hour electrolysis experiments in 100-A cell

| Exp # | Collector cup | Anode | C.E % | Time (Hr) | Remarks |
|---|---|---|---|---|---|
| 3-104 | solid BN | BN weir | 48.5 | 91 | 3 metal taps completed, no dark layer formed at cathodes, test discontinued due to furnace element failure |
| 3-105 | solid BN | BN weir | 57.5 | 48 | 96-hour attempted, Fe cell leaked electrolyte, one metal tap completed |
| 3-108 | solid BN | BN weir | 52.7 | 96 | 96-hour run complete with four metal taps |
| 3-110 | solid BN | BN weir | 62.6 | 96 | 96-hour run complete with four metal taps |
| 3-112 | solid BN | BN weir | 61.2 | 96 | 96-hour run complete with four metal taps |

Table VIII lists analysis data obtained with metal from the second tap of Experiment # DOE-Nd-3-104. Weight % of elements analyzed are listed in this table.

**Table VIII.** Metal analysis data from 96-hour experiment

| Exp | Fe | Pr | Si | Mg | Al | Mn | Ca | C | O | N |
|---|---|---|---|---|---|---|---|---|---|---|
| 3-104 | 27.0 | 0.948 | <0.01 | 0.010 | 0.24 | 0.085 | <0.01 | 0.048 | 0.004 | 0.001 |

balance Nd

### 3.3 Discussion of Results (100-A Cell Experiments)

#### 3.3.1 6- to-30 Hour Electrolysis Experiments.

Table V lists the results obtained in the 100-A cell for experiments of 6 to 30 hours duration. In initial experiments, an iron collector cup resting on the bottom of the steel shell was used. Metal from these experiments (DOE-Nd-3-60 to 63) was recovered as lumps and intermixed electrolyte-metal product. A slight improvement in the metal coalescence was observed when the iron collector cup was isolated from the large steel cell by means of boron nitride parts. The metal was recovered in a flat layer with metal-electrolyte bands present in Experiments # DOE-Nd-3-64 and 65. No current efficiency values could be calculated due to the intermixing. The reason for the slight improvement in metal coalescence was ascribed to the fact that less iron surface was in electrical contact with the molten Nd-Fe alloy. The tendency for neodymium to be oxidized out of the alloy molten pool and to establish equilibrium by reducing neodymium at the pure iron collector cup and cell walls, i.e. to act in a corrosion couple mode, was reduced. To decrease this tendency further, the metal was isolated from the iron collector cup, using boron nitride plates to line the inner surfaces of the iron cup. The coalescence was improved with a small amount of entrained electrolyte present throughout the ingot (Experiments # DOE-Nd-3-66 to 70). A solid boron nitride collector cup was then employed and coalescence was improved again, with only a slight amount of entrained electrolyte near the surface of the ingot. A solid ingot was finally recovered from the 100-A cell when the graphite weir was replaced with boron nitride (Experiment # DOE-Nd-3-81). In all experiments, the graphite weir showed a lot of wear due to electrochemical action. The generation of gas bubbles near to the cathodes and collector cup caused stirring of the electrolyte which led to the formation of metal-electrolyte intermixed product. With the use of the boron nitride weir, the formation of gas bubbles was eliminated near the cathodes and the collector cup. For the remaining experiments, attention was paid to obtaining high current efficiencies and excellent metal quality, and to the vacuum-tapping of Nd-Fe alloy. Current efficiencies in the 50 % to 70 % range were obtained. Tapping procedures were modified to insure successful extraction of the Nd-Fe alloy in preparation for the 96-hour extended test. Gas analysis taken in all experiments showed no C-F compounds.

Table VI lists analytical results obtained on metal samples from the 6- to 30-hour experiments. In Experiment # DOE-Nd-3-84, the metal quality was excellent except for the high value of

0.274 wt% Mn. This concentration was high because 1010 steel with fairly high concentration of Mn was used as the cathode. High-purity cathode material was employed in Experiments # DOE-Nd-3-89 and 92 and acceptable levels of Mn were reported for the Nd-Fe alloy.

### 3.3.2 96-Hour Electrolysis Experiments

Table VII lists the results obtained in the 100-A cell for experiments of 96 hours in duration. In Experiments # DOE-Nd-3-104 and 105, furnace element failure and a leaking electrolytic cell led to early shut-down of the tests. Three successful 96-hour tests were completed. In each of the Experiments # DOE-Nd-3-108 and 110, metal was tapped successfully four times, yielding current efficiencies of 52.7 % and 62.6 %, respectively. In these two tests, $Nd_2O_2CO_3$ was employed as feed. 99.8 % oxide utilization was obtained for Experiment # DOE-Nd-3-110. Experiment # DOE-Nd-3-112, with a current efficiency of 61.2 %, employed $Nd_2O_3$ as feed to the cell instead of $Nd_2O_2CO_3$. This cell also operated smoothly, with an oxide utilization of 92.9 %, as not all of the oxide dissolved.

The metal product from Experiment # DOE-Nd-3-108 is pictured in Figure 12. One metal sample was taken for analysis from tap # 2 of Experiment # DOE-Nd-3-104. Table VIII lists the results from an analysis performed at Rhône-Poulenc. Metal quality was excellent for magnetic alloy application.

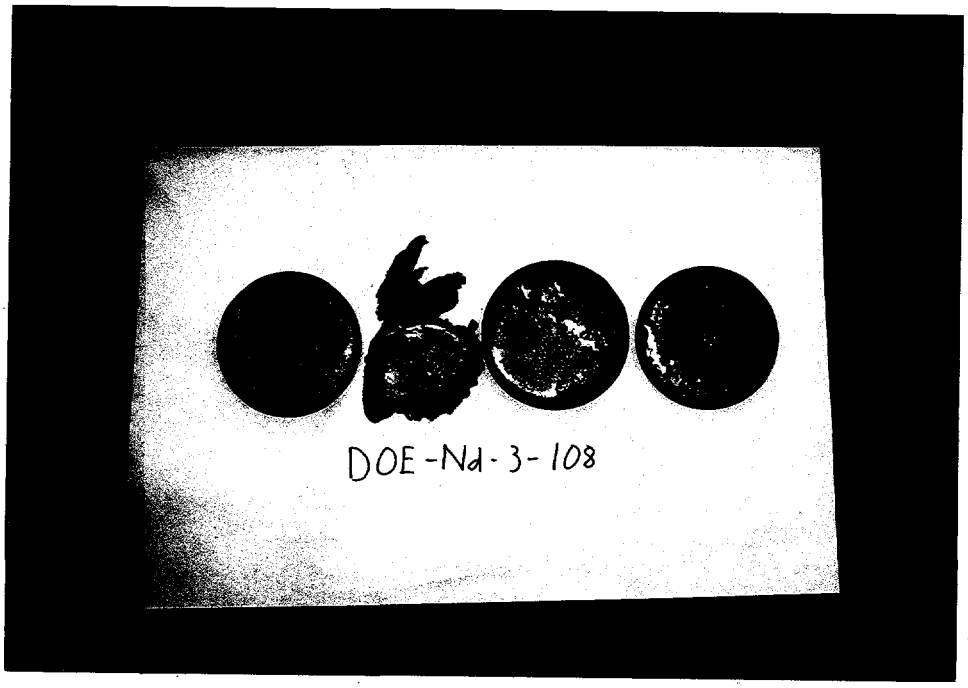


**Figure 12** Metal product from 96-hour electrolysis in 100-A cell

## PILOT CELL DESIGN CONCEPT

### 4.1 Conceptual Design

A conceptual design of a 10,000-A pilot cell was completed. The cell contains four anode banks, with each bank containing 22 plates 12" W x 30 " L x 1" T, to be immersed 24 inches into the electrolyte. The current density at the anode plates is 0.03 A/cm$^2$ at a cell current of 10,000 A. The anodes have a weir attached to one side to direct the flow of electrolyte. Two rectangular cathodes are placed between anode banks. The size of the cathodes is 48" L x 18" W x 6" T and they are immersed 12 inches into the electrolyte for a current density of 0.5 A/cm$^2$ at 10,000 A. The cathodes are surrounded by sleeves which are purged with inert gas if necessary. A collector pan situated on the bottom of the cell under the cathodes collects molten alloy. The dimensions of the pan are 108" L x 12" W x 12" H. This size pan is capable of containing a 3-days production of alloy at 70 % CE. The cell itself is constructed out of 1" thick steel plates and has inside dimensions of 9' 8" L x 5' 8" W x 4' H. The steel shell is surrounded by 12 inches of insulation. A 1/4" thick outer steel shell contains the insulation. The lid with appropriate holes and fittings contains 12 inches of insulation to contain the heat. The thickness of the insulation inside the lid can be varied to maintain a proper heat balance during electrolysis. Four feeders located by each anode provide feed to the cell. A tapping port located at one end of the cell provides access to the molten alloy for vacuum-tapping. The depth of the electrolyte is 36 inches. If a bath composition of 50 wt% $NdF_3$/30 wt% $CaF_2$/20 wt% LiF is employed, the total weight of the electrolyte is 13,000 kg (6,500 kg $NdF_3$, 3,900 kg $CaF_2$, 2,600 kg LiF). Figure 13 illustrates a top view of this 10,000-A cell, Figure 14 a side view.

At an average current efficiency of 65 %, an amount of 102,000 kg neodymium is deposited in a 12-month period of uninterrupted operation. With a cell voltage of 3.5 V, the energy consumption is 3.0 kWh per kg Nd produced.

### 4.2 Estimated Cost of 10,000-A Cell

A cost estimate for the 10,000-A pilot cell was completed with the assistance of J. Donald Talbot. The cost estimate is shown below:

| | | | |
|---|---|---|---|
| <u>Steel Fabrication</u> | | | |
| Steel Sheets - 1" inside, ¼" outside | | | |
| | Materials | $5,700 | $0.05/Pound |
| | Labor | $10,000 | Estimate - 2m x 10d |
| Steel Roof- ¼" Thick Inconel - | Material | $5,000 | $6.00/lb |
| | Labor | $2,800 | Estimate - 2m x 4d |
| Structural - Materials | | $1,500 | $1.00/Pound |
| Labor | | $2,100 | Estimate - 2m x 3d |
| Electrode Support Structure | | $1,000 | $1.00/Pound |
| Labor | | $1,400 | Estimate - 2m x 2d |
| Metal Pan - Boron-Nitride-Coated Steel | | $5,000 | Very crude estimate |

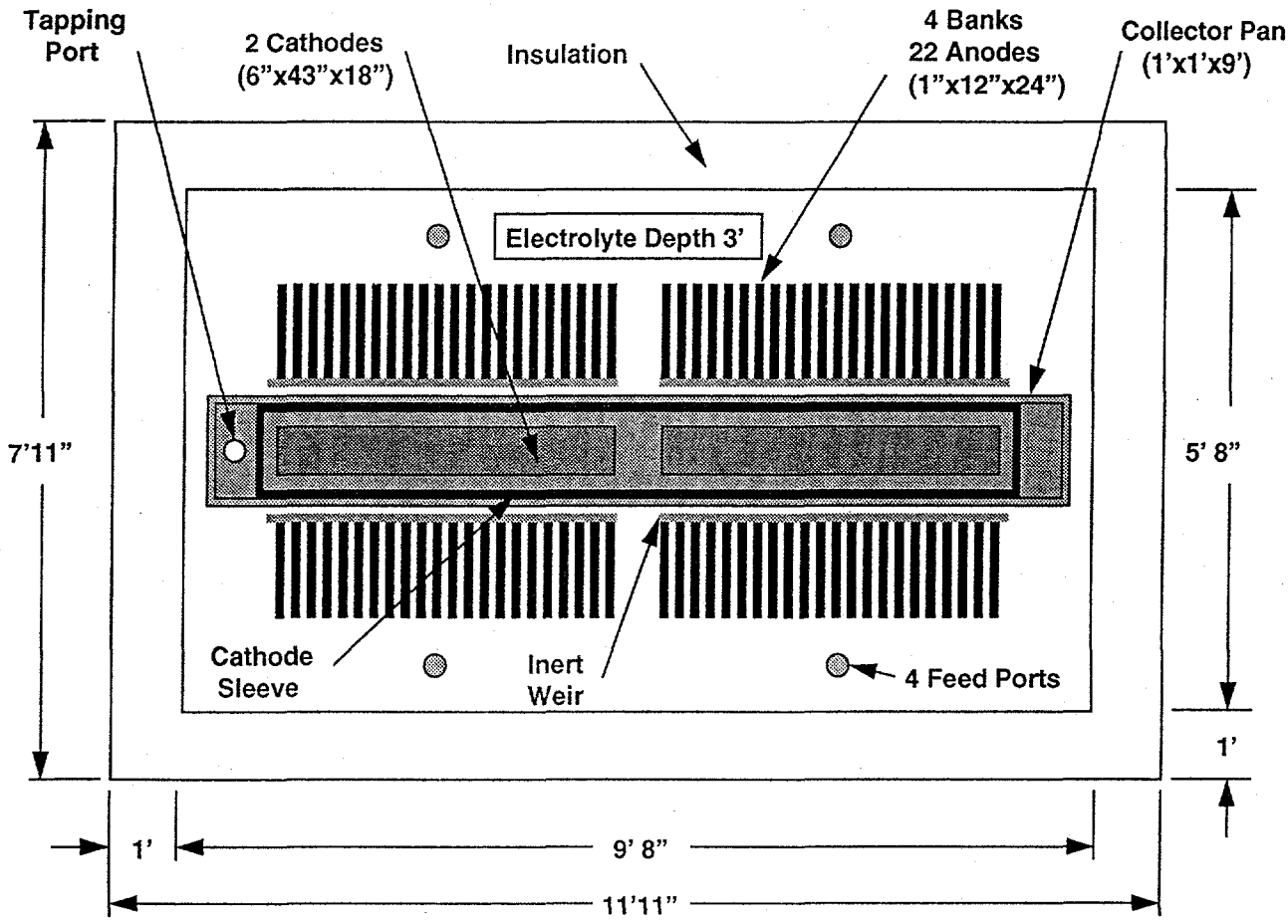


**Figure 13** Top view of 10,000-A pilot cell

| | | |
|---|---|---|
| <u>Anode & Cathodes</u> | | |
| Anode Blocks-88 plates 12" W x 30" L x 1" T | $5,000 | Quote to EMEC |
| Anode cutting & drilling | $1,400 | Estimate-2m x 1/2d/assembly |
| Steel Spacer @ 2' x 1' x 1"-drilled | $4,000 | $0.50/Pound + drilling allowance |
| Anode Assembly | $1,400 | Estimate - 2m x 1/2d/assembly |
| Cathodes - Iron 3" x 2" x 43" | $ 500 | $0.75/Pound |
| Miscellaneous Hangers | $1,000 | Estimate |
| <u>Refractories</u> | | |
| Roof Gunting-Hanger welding & preparation | $ 900 | Estimate - 2m x 1d + hangers |
| Gunning 100 sq. ft. @ 8" thick | $2,500 | $25/sq. ft. |
| Brick Work-Mat'ls 700 hard-1400 insul. Brick | $3,000 | Estimate |
| Labor | $3,500 | Estimate - 5m x 2d |
| Loose Brick for roof-Material | $1,000 | Estimate |
| Loose Brick for roof-Roof | $ 500 | Some cutting may be required |
| Insulating Batt for shell to roof joint | $1,000 | Estimate |

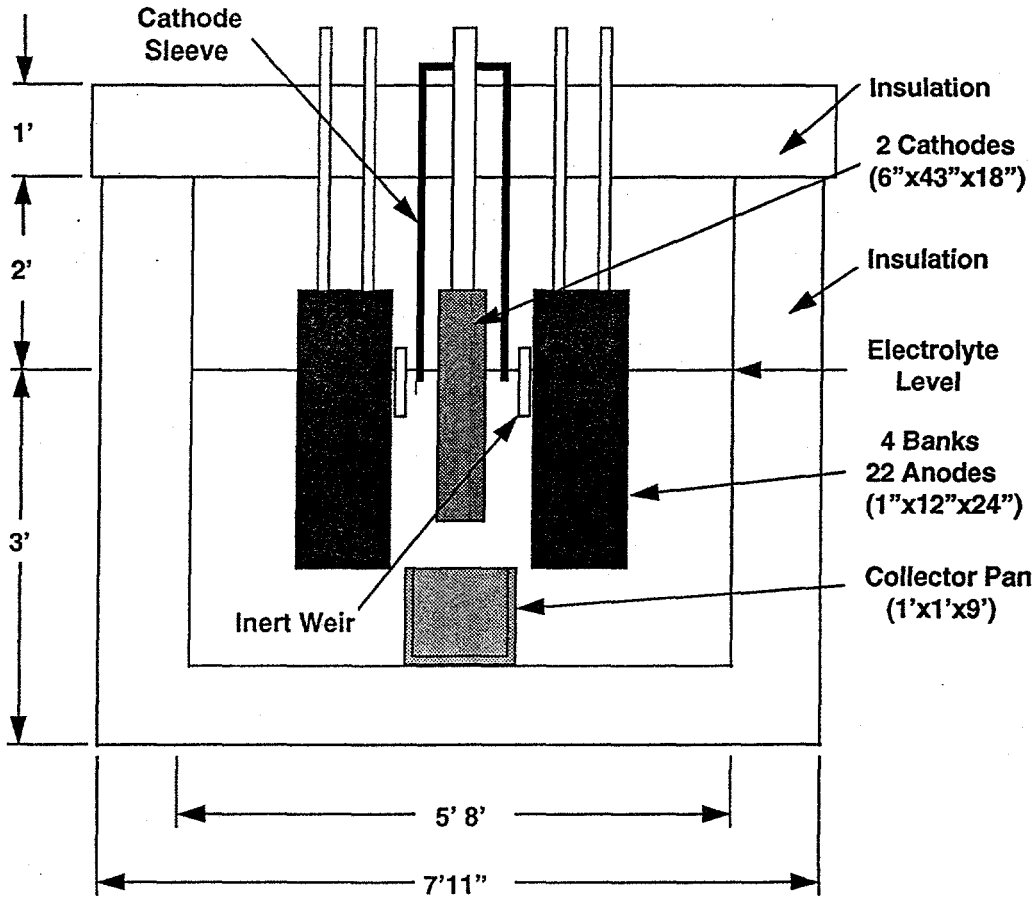


**Figure 14** End view of 10,000-A pilot cell

| | | |
|---|---|---|
| Heaters | | |
| Heating Materials-4 @ 6 kw, Incoloy sheath w/integral controls | $10,000 | Catalog information |
| Round-off | $ 800 | |
| **Electrolytic Cell Total** | **$71,000** | |

### 4.3 Estimated Cost of 10,000-A Pilot Plant

A cost estimate was also completed for the pilot plant installation. This estimate, shown below, is based on an installation in an existing building near our laboratory.

| Equipment Costs | | | Total $ 213,000 |
|---|---|---|---|
| Name | Description | Cost | Basis |
| Fork Truck | Elect. 5000 lb/cp | $9,000 | Rent for 6 mo. |
| Drum Furnace | 8" gun.insul.,w/5 heat pan 80K | $15,000 | Estimate |
| Drum Dry Air Purge | Air Line-Desiccant Dryer-10 CFN | $1,500 | Estimate |
| Drum Handlers (2) | 55 gal. drum 1 ton cap. | $3,000 | McMaster-Carr |
| Material Handler | Drott crane type 2 ton cap. | $20,000 | Rent for 6 mo. |
| Vibrating Screen | Sweco 24" Dia., 2 hp, 1 deck | $5,000 | Quote |
| Tote Bin | Cap.-2000 lbs, 60 deg slp. | $5,000 | Estimate |
| Feeders (4) | Accu-Rate | $25,000 | Quote |
| Electrolytic Cell | 10,000 A | $71,000 | Estimate |
| Rectifier | 10,000 A @ 25 V | $22,500 | Per Wesco |
| Baghouse | 2000 CFM @ 6"w.g. | $6,000 | Quote |
| Ductwork | 50' of 6"/50' of 4" fl hose | $6,000 | Installed cost |
| Hoods/Transitions | 12 ga sheetmetal | $3,000 | Estimate |
| Vacuum Tap. sys. | Lines,values and vac.vessel | $8,000 | Estimate |
| Receiving Mold | Once/Shift 3/4 cu.ft. | $2,000 | Estimate |
| Welding machine | Elec. 300 A Ind. type | $3,000 | Mean's Const Cost |
| Vacuum Pump | Single Stage-100 CFM | $5,000 | Quote |
| Computers/Control | epuip.-mostly use existing | $3,000 | Estimate |
| **Construction Cost** | | | **Total $ 102,525** |
| Structural | Building Wall to isolate area | $1,000 | Hang Plastic |
| | Widen 1 door for equip. access | $10,000 | Guesstimate |
| | Pour 8 piers for platform, basin for cool tower | $0 | None required |
| | Platform-5'H x 3' W (3 sides) | $6,000 | 1.5 tons @ $4000/T |
| | Grating, Handrail/Steps | $4,000 | Recent prices |
| | General Clean up/Repair | $4,800 | 5x4 days @$30/mh |
| | Painting of facility & Build offices | $0 | Deleted |
| Set Equipment | 15 ton crane + 5 ironworkers for 3 days | $7,500 | 3 days @ $50/mh $500/day for crane |
| Pipefitting | Labor & Materials | $15,975 | 7.5% of equip. costs |
| Electrical | Labor & Materials | $53,250 | 25% of equip. costs |
| | | Project Sub-Total | $ 315,525 |
| | | Contingency, 10 % | $ 31,553 |
| | | Round-Off | $ 2,922 |
| (Estimated accuracy ± 20 %) | | Project Total | $ 350,000 |

## SUPPORTING EXPERIMENTATION

### 5.1 Metal Solubility

#### 5.1.1 Experimental Procedure

Experiments were conducted to find the extent of neodymium metal solubility in various electrolyte compositions. A hydrogen evolution test, used in past studies to quantify dissolved metal in electrolyte, was used as an analysis tool. A charge of electrolyte (400 g) and of Nd/Fe alloy (60 to 100 g) was packed in a molybdenum crucible. The filled crucible was placed into a sealed Inconel vessel. A vacuum was applied, and the sample was heated to 500 °C overnight to remove moisture. The system was backfilled with argon and the temperature increased to 900-1000 °C where it was held for the duration of the test. Bath samples were drawn from the electrolyte melt by using a quartz tube pipette at timed intervals. The cooled samples were then crushed by mortar and pestle in an argon filled glove bag. The weighed samples were analyzed for reactive metal content by measuring the amount of hydrogen evolved upon exposure to acid. The results are given in Table IX, the metal content taken as neodymium producing 1.5 moles $H_2$ per mole Nd.

**Table IX.** Metal contents determined in various electrolytes

| Exp.# | Temp.°C | Electrolyte Composition | Wt% Nd 60 min | Wt% Nd 120 min | Wt% Nd 180 min |
|---|---|---|---|---|---|
| 4-1 | 930 | 60-20-20 | - | 0.17 | 0.22 |
| 4-2 | 950 | 65-20-15 | 0.21 | 0.25 | - |
| 4-3 | 1000 | 70-20-10 | 0.15 | 0.19 | - |

Electrolyte components $NdF_3$, $CaF_2$, and LiF, respectively, in wt%

After Experiment # DOE-Nd-4-1 cooled, the crucible was sectioned and a piece of dark layer above frozen metal was analyzed. As suspected, the dark layer adjacent to the metal contained a higher amount (0.78 wt.%) of dissolved metal than the timed samples taken from the bulk electrolyte.

Discussion

The metal solubility values were relatively low. Changes in electrolyte composition did not have any significant effect (content of $Nd_2O_3$, however, may play a role). If one considers the higher atomic weight of neodymium compared to aluminum, similar, or slightly more favorable, conditions exist as in the Hall-Héroult process. The metal solubility, therefore, should not prevent one from achieving good current efficiency values.

## 5.2 Oxide Dissolution

### 5.2.1 Experimental Procedure

Visual observations were made of electrolysis feed dissolution in selected electrolyte compositions. The electrolyte was melted in a graphite crucible at 930-940 °C. Then neodymium oxide or partially decomposed neodymium carbonate ($Nd_2O_2CO_3$) was added in 0.25 wt.% increments. The dissolution behavior and the resulting bath clarity were observed after each addition. Stirring was used to enhance the visibility of settled particles. Once electrolyte remained cloudy after an addition, the solubility was assumed to be slightly less than the total amount added. The temperature was raised to 1000 °C and additions were continued.

### 5.2.2 Results -- Dissolution

Dissolution times were similar for oxide and carbonate compound, in all bath compositions. Differences were observed in the dissolution behavior. With the oxide, some added material floated on top, some sank in lumps. The partially decomposed carbonate floated longer on top and dispersed readily. The greater tendency to sink in lumps may indicate greater difficulties in dissolving the oxide, particularly with insufficient electrolyte movement.

### 5.2.3 Results -- Solubility

Solubility values obtained from the observation of dissolution are expressed in Figure 15. Note that the formula weight for $Nd_2O_2CO_3$ (FW 380.5) is larger than that of $Nd_2O_3$ (FW 336.5).

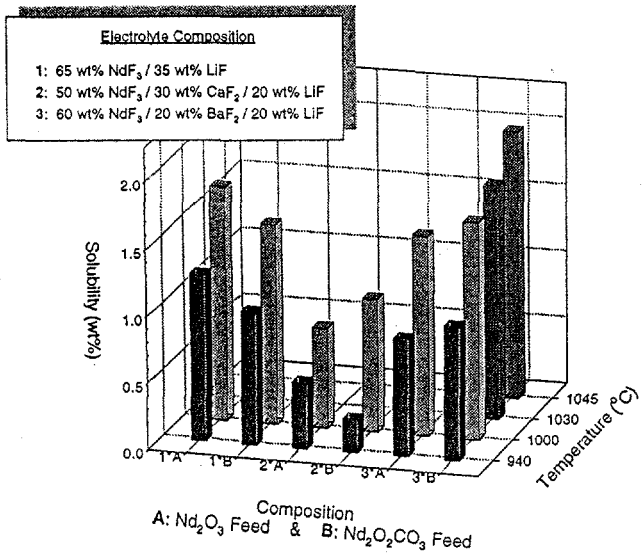


**Figure 15** Results of oxide dissolution studies

## 5.3 Characteristics and Treatment of Cell Off-Gases

### 5.3.1 Introduction

Emission of perfluorinated carbon compounds such as $CF_4$ and $C_2F_6$ into the atmosphere is environmentally unsound. Experimental studies of reactions to treat the off-gases were conducted, for the case that overriding advantages suggest the operation of the neodymium oxide electrolysis in a mode in which carbon tetrafluoride and possibly other fluorine-containing compounds, such as $COF_2$ and $C_2F_6$, are formed.

In analogy to the electrolysis of aluminum oxide in the Hall-Héroult process, carbon anodes are expected to produce primarily carbon dioxide, according to

$$2\ Nd_2O_3 + 3\ C \dashrightarrow 4\ Nd + 3\ CO_2\ .$$

The carbon dioxide can react with reactive metal in the electrolyte to form CO, this reaction resulting in current efficiency losses.

During neodymium oxide electrolysis, perfluorinated carbon compounds may form (at higher cell voltages) along with carbon dioxide. Significant amounts of $CF_4$ also form in industrial aluminum electrolysis when the so-called anode effect occurs at low oxide contents. As discussed elsewhere in the report, we did not always observe the characteristic steep voltage increase in the case of neodymium oxide electrolysis, although more positive electrode potentials are evidently (and thermodynamically) required for the formation of $CF_4$. The analysis of gas samples usually indicated the presence of a mixture of CO, $CO_2$, $CF_4$, and $C_2F_6$ at higher cell voltages.

A reaction with neodymium oxide according to

$$2\ Nd_2O_3 + 3\ CF_4 \dashrightarrow 3\ CO_2 + 4\ NdF_3$$

consumes $CF_4$ and neodymium oxide. The neodymium fluoride product can be fed to the electrolysis cell, thereby making up any losses of fluorine. Treatment involving the use of $Nd_2O_3$ as feed would be facilitated by the fact that only a part of the (mixed) off-gases, and thus only a minor portion of the feed, needs to react.

### 5.3.2 Experimental Procedures for Study of Off-Gas Treatment

Experiments were conducted to ascertain the feasibility of reacting the $CF_4$ in the anodic gas with neodymium oxide. A weighed quantity of neodymium oxide was placed in an alumina or Inconel tube which was sealed and inserted into the heating zone of a furnace. The tube, connected to a gas recirculator, could be evacuated and backfilled with pure $CF_4$ gas. First, the $Nd_2O_3$ was exposed to a vacuum for a period of 24 hours at a temperature of 600 °C, to remove moisture from the sample. The system was backfilled with $CF_4$ and the gas recirculator activated for a period of 2 to 6 hours, depending on experimental objectives. The temperature was increased to 1000 °C for the duration of the test. A bottle placed in-line with the recirculator was used to obtain gas samples. Gas samples were analyzed on site by gas chromatography. Figure 16 represents the $CF_4$ recirculating apparatus.

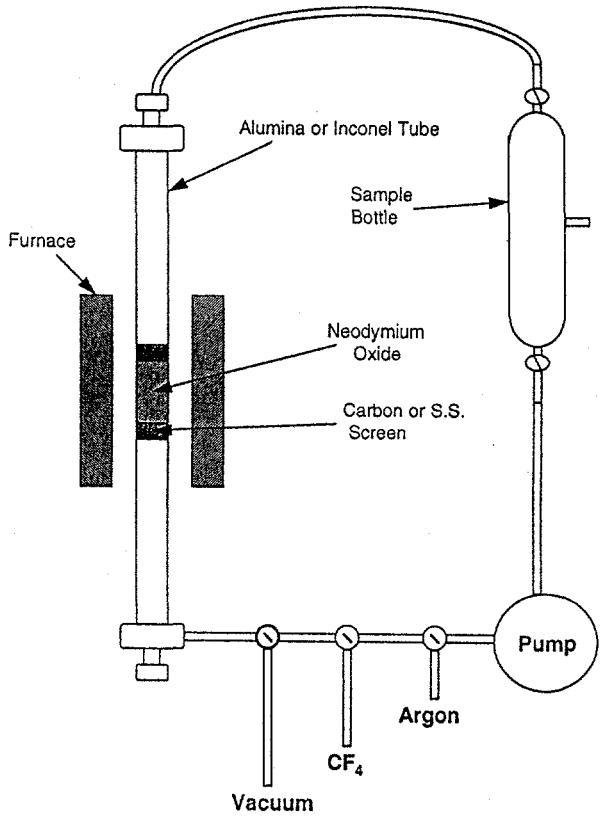


**Figure 16** Gas treatment apparatus

### 5.3.3 Results of Study of Off-Gas Treatment

Timed samples were taken and analyzed during selected tests. Typically the $CF_4$ concentration was reduced from 100 % to <1 % within a period of 1 hour. Analytical results indicated that the $CF_4$ reacted almost quantitatively to form $CO_2$. Experiment # DOE-Nd-4-6 showed that most $CF_4$ reacted in the first 15 minutes to form 73.1 % $CO_2$. Graphical results are reported in Figure 17.

### 5.3.4 Discussion

Although generally considered an nonreactive compound, $CF_4$ reacted extensively at acceptable rates in the high-temperature treatment investigated. Fluorine values could be recycled to the electrolysis process as $NdF_3$, along with unreacted neodymium oxide. Efficient capture of the off-gases would be necessary, however, and the treatment would not be inexpensive.

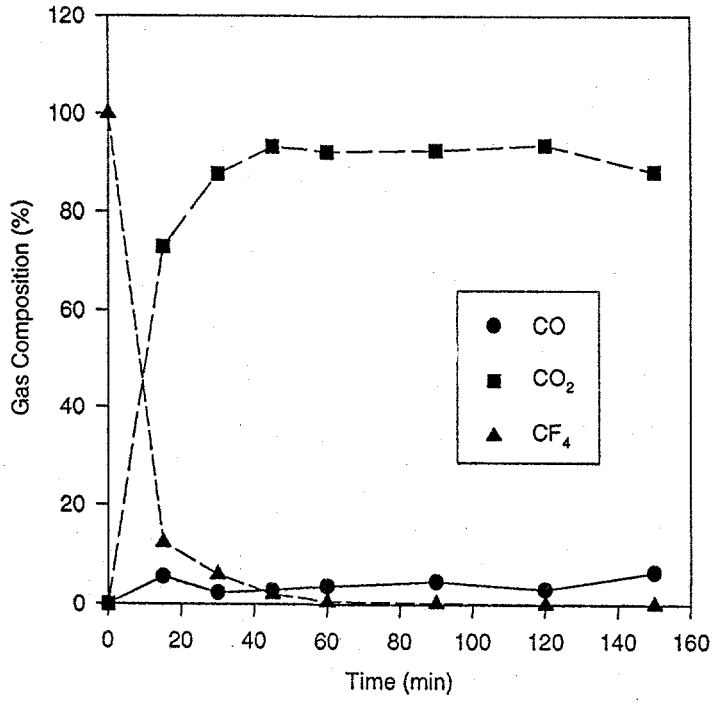


**Figure 17** Reaction of $CF_4$ with $Nd_2O_3$ as a function of time

### 5.4 Anode Effect Studies

The anode effect is well known from the industrial aluminum electrolysis. Hall-Héroult cells are arranged electrically in series, with the same current value maintained in each cell. When the oxide concentration becomes too low in a cell, its voltage increases to high values of typically 20 V. At anode effect, the surface of the anode and its wetting characteristics change. The current then passes through a gas layer with high electrical resistance. To extinguish the anode effect, aluminum oxide is added to the electrolyte and the surface layer is disturbed by various means. Perfluorinated carbon components are emitted during anode effect.

Indications for an incomplete or partial anode effect at lower voltages were found in the literature [22]. Figure 18 is reproduced from this publication of Japanese authors (Santoku Metal Industry Co.). At an anode potential of about 2.5 V, the current started to increase, but this increase was temporarily interrupted by a decrease at 3.0 V. Subsequently the current increased to markedly higher values before another decrease occurred. The authors ascribe a critical current density of 0.16 A/cm$^2$ to the discharge of $O^{2-}$, a second critical current density of 1.6 A/cm$^2$ to $F^-$ discharge.

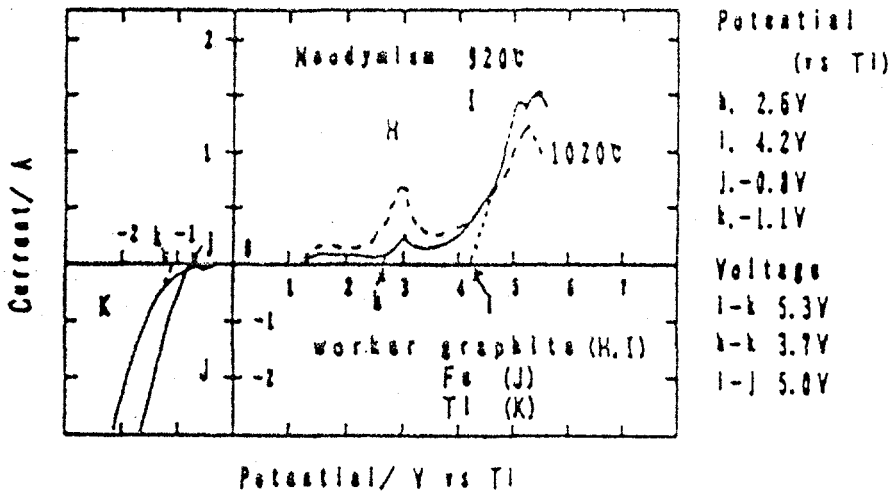


Fig. 5. Polarization curves in neodymium electrolyte (72wt.% $NdF_3$–15wt.%LiF–12wt.%$BaF_2$–1wt.%$Nd_2O_3$) at 920 °C (——) and 1020 °C (– – –).

**Figure 18** Polarization curves from literature [22]

Reproducing the conditions of [22], we obtained the current-voltage curves of Figure 19. The electrolyte composition was 72 wt% $NdF_3$, 12 wt% $BaF_2$, 15 wt% LiF, 1 wt% $Nd_2O_3$. The cell voltage was scanned from the open-circuit value at the rate of 50 mV/sec. At 1,020 °C, the current reached almost 50 A, then dropped to nearly zero, as typical for a "hard" anode effect. At 925 °C, the drop occurred at a lower critical current of about 30 A, but dropped only to a value of 10 A and rose again, before displaying the "hard" anode effect at 45 A. It appears that the first drop was not observed at the higher temperature. At both temperatures, a minor aberration was observed at low values. To study the correlation with the emission of C-F-containing gases, the current was arrested for 3 minutes in some experiments, at conditions indicated in Figure 19 as Points A, B and C. A content of 0.6 % $CF_4$ and 13.1 % $CO_2$, no $C_2F_6$ (CO not determined due to instrumental difficulties) indicated some formation of $CF_4$ at higher voltages at 1,020 °C. No such emission was observed for 925 °C before the first critical current was observed, but at Point C the gas contained 2.8 % $CF_4$, 6.9 % $C_2F_6$, 7.7 % $CO_2$ (CO not determined, balance argon).

These results seem to confirm that the evolution and emission of perfluorinated carbon compounds has to be expected when practicing "high-voltage" electrolysis of neodymium oxide.

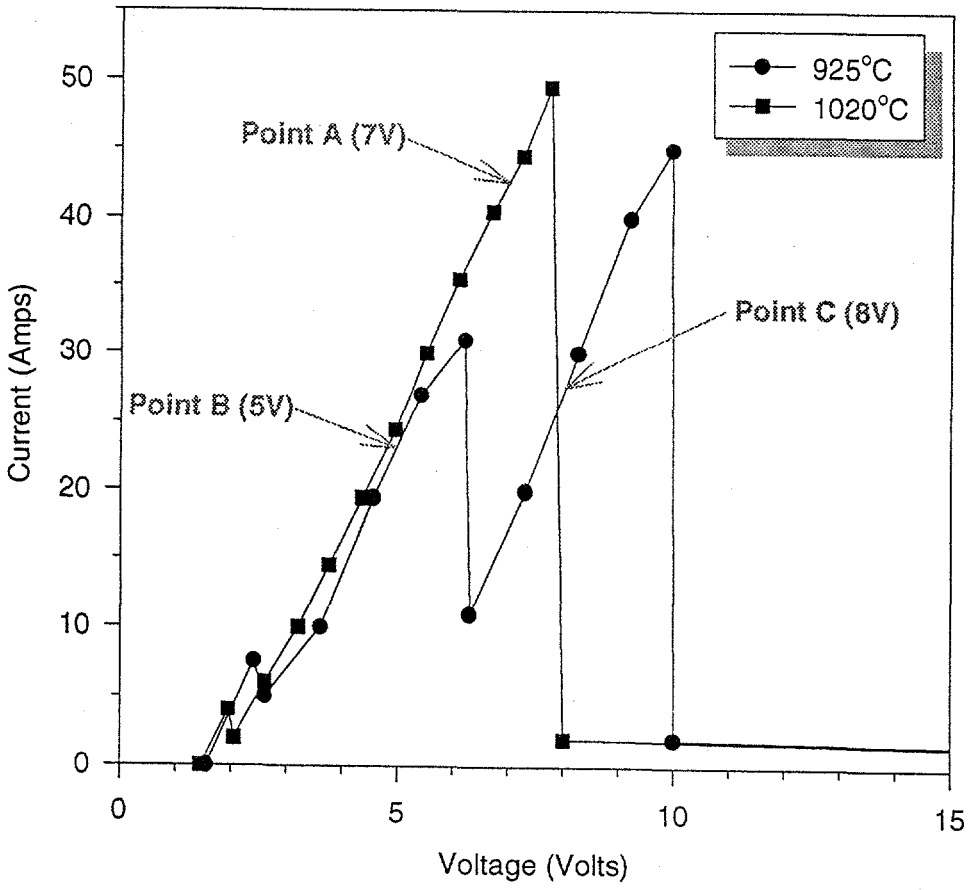


**Figure 19** Current-voltage curves showing partial anode effect (Experiment # DOE-Nd-3-113)

## 5.5 Flow Modeling

Electrolyte circulation is the main component affecting convective mass transport within the electrolysis cell. We found that for the present system, its optimization of electrolyte movement plays a very important role in maximizing cell performance. While direct observation of flow in the enclosed high-temperature cell is impossible, room temperature models can be substituted to study critical elements. This technique has been used to study phenomena in Hall cells, often combining an aqueous phase with an organic liquid of different density to a two-phase system, one phase simulating the electrolyte, the other the molten metal. Bubble-induced electrolyte flow (caused by density differences due to the bubble volume) can be simulated by bubbling gas through porous metal or graphite plates simulating the electrodes. Resulting flow patterns can be made visible by suspension of solid particles or, as was done in our case, by injecting dyed liquids.

### 5.5.1 Cell Flow Characterization

This experimentation was performed to answer some questions about flow patterns in the 100-A cell, in view of their effect on cell performance. Reduced mass transport at the cathode surface led to cleaner metal deposition. Also reoxidation of neodymium and scum formation was reduced at the metal collection sump when mass transport rates were reduced by keeping the electrolyte as stagnant as possible. On the other hand, vigorous electrolyte movement in the anode area is desirable to foster dissolution of neodymium oxide and its transport to the active anode areas.

Flow conditions were hence simulated in a room-temperature plexiglass model. Transparent plexiglass plates, ⅜" thick, were used for the container walls, so that the inside dimensions would match the working electrolysis cell on a 1:1 scale. In order to duplicate the actual flow conditions, a bubbling anode was constructed. One-half inch thick graphite plates were cut and machined to the same specifications as the actual anode plates. Next, three holes of ⅛" diameter were drilled down into each graphite plate to about one inch from the bottom. Each hole was threaded and fitted with a hollow and headless bolt which in turn was used as a hose connection. Pressurized argon introduced into the holes caused bubbling at the surface of the graphite due to the inherent porosity of the material. Some preliminary testing was conducted varying the location of the holes in the plate so that a suitable bubbling pattern could be achieved. Anode wear and visual observations made during actual electrolysis indicated that the majority of gas evolution occurred at the front of the anode. Taking this into account, the configuration shown in Figure 20 was established and seven test plates fashioned in a similar manner. The seven ½" graphite plates were fastened together with ½" graphite spacers between each plate. The leading edge of the anode protruded about ½" from the rest of the anode plate. This is where the BN weir was attached to direct oxygen flow away from the cathode region. Connections were made between the plates (21 holes) and the argon cylinder by using Masterflex tubing. The main line was split into three lines using tees. Three valves were used to increase or decrease flow to the front, middle, or rear sets of holes (7 each) as needed. The anode arrangement was suspended from the side of the tank so that one inch remained between the

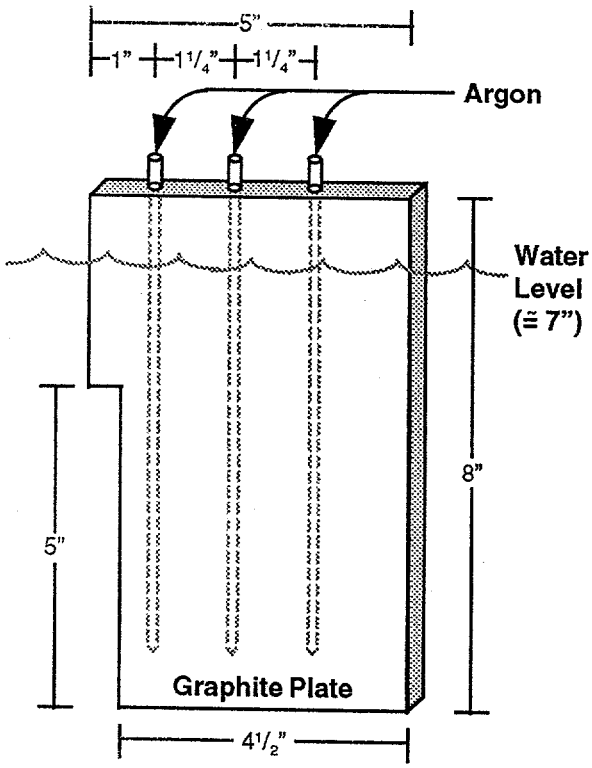


**Figure 20** Graphite plate configuration for flow modeling

bottom of the cell and the base of the anode. A plexiglass cathode collector cup arrangement was constructed and placed in the model cell in front of the anode (Figure 21). Due to changes in the actual electrolysis cell, a bigger cathode cup replica was needed after a few tests. Once the anode was suspended, and the cathode cup was positioned, the cell was filled with water. Two dye-filled 10-ml burettes were placed in the cell at each end. The burette suspended over the cathode cup contained red dye, while the burette positioned behind the anode contained green dye. The cell was not touched for a few minutes so that everything was allowed to equilibrate.

**Figure 21** 100-A cell flow model

Pressurized argon was introduced into the anode causing bubbling at the surface. Due to the hole configuration and the in-line flow control valves, most bubbling occurred at the front (facing the cathode) of the anode, as observed in the actual electrolysis cell. Depending on the test conditions, the dye could be added before flow began, or after flow patterns had already been established. All of the tests were videotaped at critical moments so that the observations could be documented and replayed.

The first tests were conducted representing standard cell configuration. These tests showed a sweeping circular flow (clockwise) from the top of the anode along the bottom of the cell

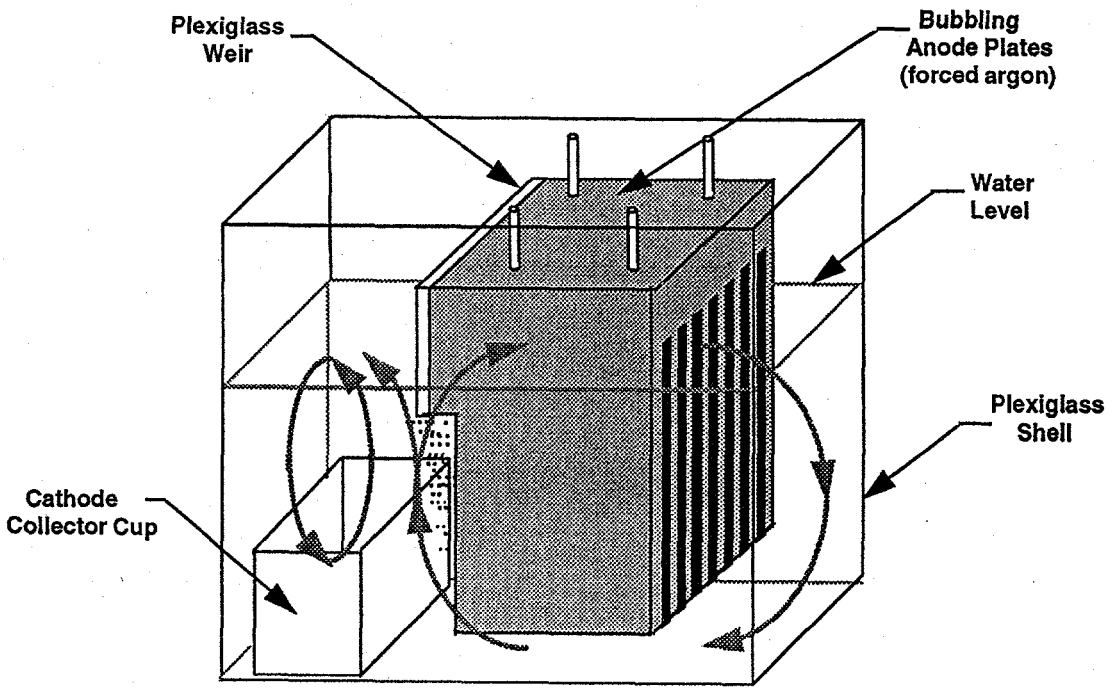


**Figure 22** Flow patterns that develop in the electrolysis cell

in the anodic region. As the bulk flow passed the front of the anode, it appeared to split into two currents at the weir; one continuing in the clockwise direction through the anode, and the other forming a counter-clockwise flow in front of the weir, above the cup, in the cathodic region (Figure 22). When the dye was added before the flow was initiated, the red dye would settle into the cathode collector cup. Once the flow was initiated, the counter-clockwise current above the cup was strong enough to diffuse the dye in the cup, into the bulk flow in only a few seconds. Any dye added to the cathode after the flow patterns had developed could immediately be seen diffusing into the bulk flow above the cup. Testing of the model in the standard configuration continued when the larger cathode cup was employed. Basically, the same two flow patterns still existed, but the counter-clockwise cathodic flow was not as pronounced.

### 5.5.2 Cell Flow Optimization

Further testing was conducted to examine the effect of changes in the model configuration on the flow patterns. Additional weirs were added and tested in different locations to redirect the bulk flow away from the cathodic region of the model. Two tests were conducted using a ¾" angle-iron segment resting on the bottom of the model as a weir. The typical flow pattern did not seem to be affected, neither with the ¾" weir at the base of the anode nor at one inch from the base of the anode.

A larger customized weir was placed in the bottom of the model and tested as well. This weir had a 1½" straight vertical segment with an additional ¾" length bent at a 30° angle (from vertical) toward the anode. This was designed to direct the sweeping flow off the bottom of the cell and to redirect it back into the anode cavity, before it entered the cathodic region of the cell. Once again, this weir showed minimal improvement over the standard flow patterns observed with no secondary weir in place.

The height of the tested (secondary) weirs placed in front of the anode was limited because of possible interference in the conductive path between the cathode and anode. Attempts to divert the flow by placing obstacles in front of the anode failed because the current appeared to bypass the secondary weirs and still effect the flow above the cathode cup.

An effort to alter the flow by positioning a different weir in another location was undertaken. Testing resumed with the idea that the flow could be redirected by placing an obstacle in back of the anode. Since the smaller cathode cup still remained from the earlier flow tests, it was utilized as a weir in the final flow tests. The small cup was positioned behind the anode and the red and green dye were added to the water at their respective locations. Pressurized argon was introduced to the anode and bubbling began. Some of the green dye, added behind the anode, was immediately swept into the small crucible, and the clockwise flow in the anodic region was not nearly as pronounced as in previous tests. As a result, the red dye entered into the cathode area and collector cup did not dissipate nearly as fast as in other tests without the "rear" weir. The small cathode collector/weir was altered once more by adding a vertical plate to the top of the cup on the side closest to the anode. This addition further isolated, temporarily, the liquid flow at the cathode from flow in the anode area (Figure 23). The test was repeated in the model to verify this observation.

Time did not permit to test successful model cell configurations in the actual electrolysis cell. A videotape featuring critical moments from all of the flow tests (1 hr:40 min) as well as an edited videotape (30 min) of the raw experimental footage is available.

### 5.6 Materials Studies

Neodymium ferrite ($NdFeO_3$) may be a useful material for cell components such as side walls, barriers, or collector cups. It would not introduce any impurities into the system. The materials study entailed calcination of reactant powders, phase confirmation of product powder, developing a sintering schedule, calculation of a theoretical density, and dense product conductivity measurements.

$NdFeO_3$ powder was obtained by mixing the raw materials, $Nd_2O_3$, 95 %, Rhône-Poulenc and $Fe_2O_3$, 99 %, EM Science, in a 1 : 0.47 ratio, overnight in a ball mill. The mixture was then calcined by heating to 1400 °C at a rate of 120 °C per hour and holding for 6 hours. After grinding the powder to -100 mesh, a small portion was sent for XRD analysis and was verified to be completely reacted to the $NdFeO_3$ phase.

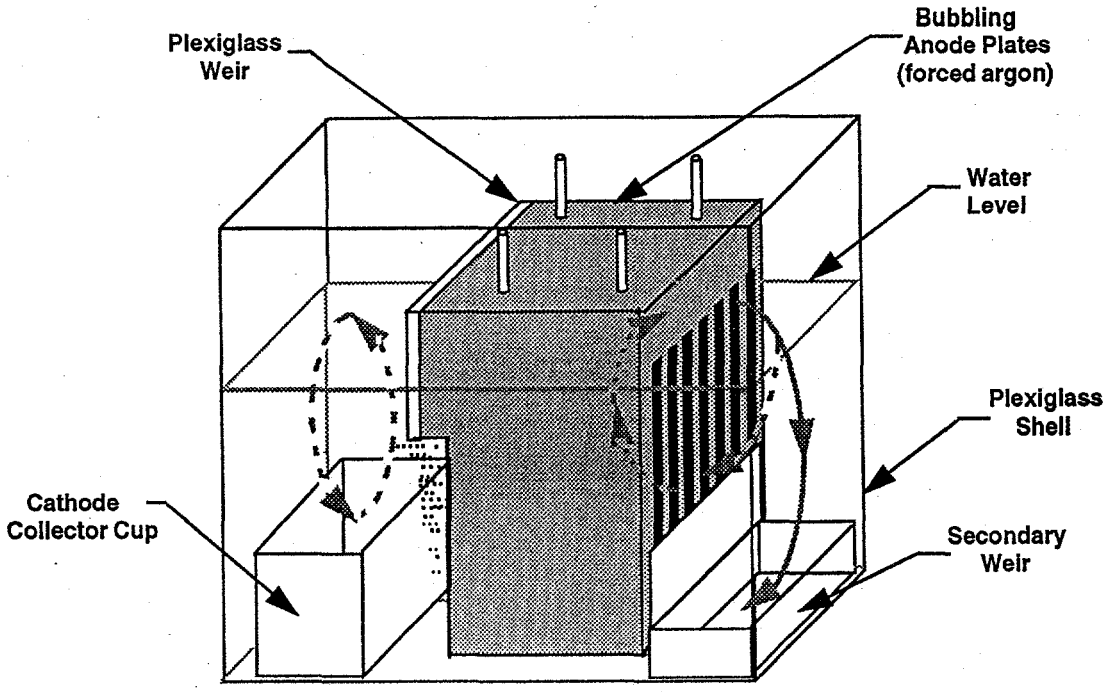


**Figure 23** New flow patterns in the model utilizing the weir behind the anode

The remainder of the powder was mixed with a binder, a 0.5 % addition of PEG 1000. Samples were uniaxially pressed at 25,000 PSI and sintered as follows:

heating from room temperature to 500 °C at 60 °C per hour
6-hour hold
heating from 500 to 1500 °C at 360 °C per hour
7-hour hold
cooling from 1500 °C to room temperature at 360 °C per hour

The maximum sintering temperature was limited to 1500 °C due to furnace capabilities. With this limitation, a density of 6.00 g/cm$^3$ was obtained based on Archimedes' method. After an open pore volume calculation, it was found that the theoretical density of the material is 6.42 g/cm$^3$.

The electrical conductivity of a 93.5 % dense pellet was measured using a two-point probe technique at temperatures between 600 and 1000 °C. The results, shown in Figure 24, reveal that it has a fairly high resistance.

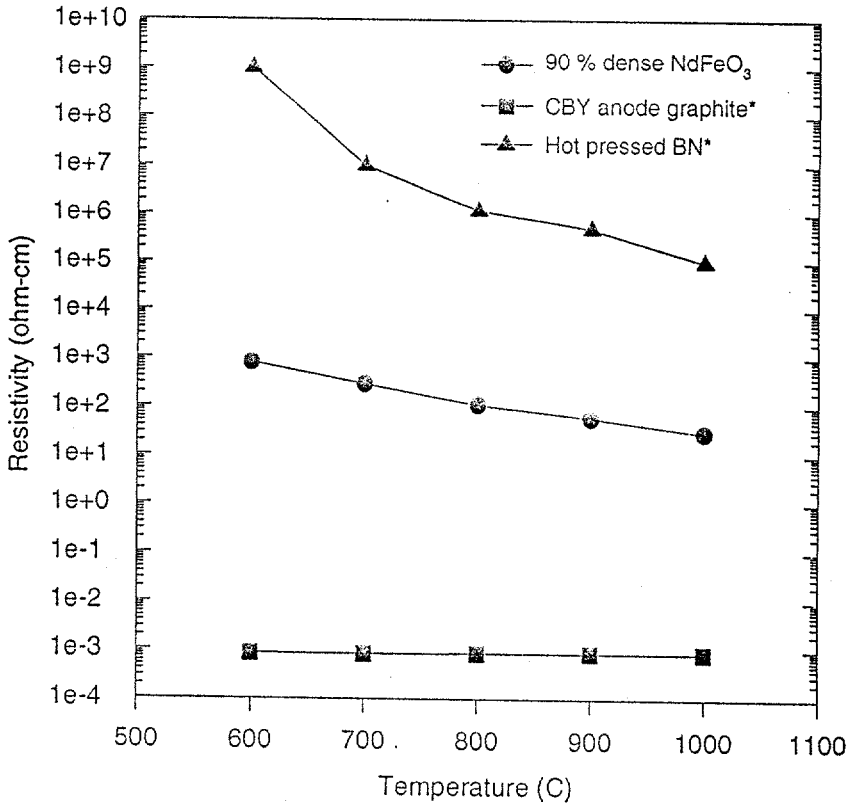


* Data provided by UCAR Carbon Company Inc.

**Figure 24** Resistivity data for $NdFeO_3$, boron nitride and anode graphite

# DISCUSSION

## MAIN FACTORS DISTURBING ELECTROLYSIS

### Anode Effect

The term "anode effect" is used in molten salt electrolysis to describe a phenomenon associated with a substantial rise in electrode potential. When the oxide concentration in aluminum electrolysis, for example, is not sufficient to maintain a normal oxidation of the carbon to carbon dioxide, carbon fluorides form on the electrode surface, whose wetting characteristics change to cause decreased wetting by electrolyte. A gas film forms on the surface and potentials of 20 to 30 V are necessary to conduct the direct current through this film. A similar phenomenon can occur in the electrolysis of neodymium oxide.

Current-voltage characteristics and analysis of cell gases indicate that with $NdF_3$-LiF electrolytes there exists the possibility to avoid a "hard" anode effect corresponding to a critical current for the oxidation of $O^{2-}$ species and to operate smoothly in a region of relatively moderate potential (voltage) in which $CO_2$, CO and perfluorinated carbon compounds ($CF_4$ and $C_2F_6$) are formed. Literature data seems to indicate that such a regime has been found advantageous by others to conduct a commercial neodymium oxide electrolysis.

We found it desirable and possible to conduct the electrolysis in a low-voltage regime, thereby avoiding anode effects and the formation of perfluorinated carbon compounds. Environmental aspects favoring this concept are discussed below.

### Scum Formation

Neodymium metal interacting with electrolyte was observed to form scum. This scum formation was more severe when the oxide content in the bath was increased, and it was particularly pronounced in the presence of moisture. It can be controlled to a significant extent by keeping mass transport at the surface of liquid metal products as low as possible.

Solidified scum was found to contain neodymium metal. It is possible that this metal forms on cooling by disproportionation of a subvalent neodymium species.

Sludge formation observed during the reduction of tantalum [23] has been ascribed to the disproportionation of lower-valent complexes that formed when fluoride had been added to the chloride electrolytes and a tantalum anode was used. A suspension of metallic tantalum contributed both to the formation of sludge and the formation of metal dendrites growing out from the electrodes at the surface of the electrolyte. It is conceivable that a similar situation exists in our system.

### Cathode Deposits

Neodymium metal tends to dissolve into the electrolyte. It appears that dark layers adjacent to the solid cathode may form in conjunction with metal dissolution. The effect can be diminished by forming a neodymium alloy at the cathode and by keeping convection at the cathode surface low.

Deposition of solid, dendritic or dispersed neodymium with a high surface area is to be avoided. Such deposits can form on any cathode substrate, but are expected to be particularly numerous when reduced incoherent impurity deposits become reduction sites for neodymium.

Solid carbonaceous deposits can form by reduction of anode gases at the cathode. A particularly sensitive area is the vicinity of the three-phase boundary of solid cathode, electrolyte and cell gas above the electrolyte. Significant operational improvements have been achieved by shielding the cathode in this area with an electrically non-conductive material such as boron nitride.

## PATH TO HIGH CURRENT EFFICIENCIES

Current efficiency losses occur when neodymium metal dissolves into the electrolyte and then is reoxidized at the anode or, more likely, by anode products. The true mechanism may involve the formation of subvalent species rather than a physical dissolution of reactive metal, and the oxidation of such species.

Scum formation and metal dissolution or formation of subvalent species are suspected to be related. At low oxide content, less scum formation has been observed. When high current efficiencies were obtained initially, high concentrations of fluorocarbon compounds were found in the off-gases. We learned, however, to operate in a low-voltage regime and to achieve current efficiencies exceeding 60 % by controlling the electrolyte flow in the cell to keep agitation and oxide content as low as possible in the cathode area.

Current efficiency losses are less if no pure neodymium is exposed to the electrolyte. Neodymium in neodymium-iron alloy has a reduced activity and, thus, a reduced tendency to dissolve into the electrolyte.

## ENVIRONMENTAL IMPLICATIONS

When operating a neodymium oxide electrolysis in a way that perfluorinated carbon compounds are produced at the anode, a cumbersome treatment of the off-gases is required. Intuitively, one may expect, though, that the emission of perfluorinated carbon compounds (PFCs) by a relatively low-volume process such as rare earth electrolysis is insignificant compared to amounts emitted, e.g., by the aluminum industry during periods of anode effect.

This, however, may not be the case. Assuming the evolution of an average of 16 % of carbontetrafluoride in the anode gases during anode effect [24], an average period of 2.5 minutes for any cell to be on anode effect, a frequency of an anode effect every other day, and a current efficiency of 91 %, 0.73 kg $CF_4$ per t of aluminum produced are emitted [25]. An aluminum smelter producing 250,000 t of aluminum annually, therefore, would emit 180 t of $CF_4$ per year. The aluminum industry is undertaking great efforts to reduce this emission by reducing frequency and duration of anode effects, and values of 0.054 kg $CF_4$ per t of Al have been measured in a 180 kA potline [24]; the corresponding total emission for a plant producing 250,000 t/yr aluminum would be 13 t $CF_4$ per year. A 1000 t/yr neodymium electrolysis using carbon anodes with a content of fluorocarbons equivalent to, e.g., 20 % $CF_4$ in the anodic off-gases, and operating at a current efficiency of 75 %, would produce 120 t of $CF_4$. This is about ten times more $CF_4$ than emitted by a modern aluminum smelter.

The uncontrolled emission of such high amounts of potent greenhouse gases may not be tolerated. Sealing of the neodymium electrolysis cell and treatment of the gases to destroy the fluorocarbon compounds, probably at high temperatures, is possible but would hardly be practical as long as an alternative exists. This alternative is low-voltage electrolysis with zero emission of fluorocarbon compounds.

## CONCLUSIONS AND RECOMMENDATIONS

The goal of Phase II to develop a commercially attractive neodymium oxide electrolysis at the pre-pilot stage has been met. The electrolysis of neodymium oxide continues to show promise for implementation as a low-cost process to produce high-quality neodymium or neodymium-iron alloy.

With the decision by the U. S. Department of Energy not to fund the initially projected pilot cell work in Phase III, an opportunity to establish an advanced, environmentally favorable technology in this country, may have been lost. The tendency to rely on foreign technology and suppliers could have been counteracted.

We recommend that the adaption of our process to the preparation of misch metal, another product of increasing commercial value, be investigated.

# REFERENCES


[1] C. O. Bounds, private communication (1997).

[2] Neomet, no reference available.

[3] H. Tamamura, several patents, see [13] [16].

[4] R. A. Sharma, "Neodymium Production Processes", Journal of Metals, February 1987, pp. 33-37.

[5] W. G. Moffatt, Binary Phase Diagram Handbook, General Electric Company (1976).

[6] M. F. Chambers and J. E. Murphy, "Electrolytic Production of Neodymium Metal from a Molten Chloride Electrolyte", Bureau of Mines Report of Investigations, RI 9391 (1991).

[7] E. S. Shedd, J. D. Marchant, and T. A. Henrie, "Electrowinning and Tapping of Lanthanum Metal", Bureau of Mines Report of Investigations, RI 6882 (1966).

[8] E. Morrice and T. A. Henrie, "Electrowinning High-Purity Neodymium, Praseodymium, and Didymium Metals from their Oxides", Bureau of Mines Report of Investigations, RI 6957 (1967).

[9] E. Morrice, E. S. Shedd, and T. A. Henrie, "Direct Electrolysis of Rare-Earth Oxides to Metals and Alloys in Fluoride Melts", Bureau of Mines Report of Investigations, RI 7146 (1968).

[10] E. Morrice, E. S. Shedd, M. M. Wong, and T. A. Henrie, "Preparation of Cobalt-Rare-Earth Alloys by Electrolysis", Journal of Metals, January 1969, pp. 34-37.

[11] D. K. Dysinger and J. E. Murphy, "Electrowinning of Neodymium From a Molten Oxide-Fluoride Electrolyte", Bureau of Mines Report of Investigations, RI 9504 (1994).

[12] J. E. Murphy, Technical Discussion at Bureau of Mines, Reno, Nevada, 12 July 1993.

[13] H. Tamamura, "Process for Preparation of Neodymium or Neodymium-Iron Alloy", U.S. Patent No. 5,091,065, issued 25 February 1992.

[14] H. Tamamura, "Process for Preparing Praseodymium Metal or Praseodymium-Containing Alloy", U.S. Patent No. 5,000,829, issued 19 March 1991.

[15] H. Tamamura, "Process for Preparing Praseodymium Metal or Praseodymium-Containing Alloy", U.S. Patent No. 4,966,662, issued 30 October 1990.

[16] H. Tamamura, "Process for Preparation of Neodymium or Neodymium Alloy", U.S. Patent No. 4,966,661, issued 30 October 1990.

[17] Y. Bertaud, "Process for the Preparation of Mother Alloys of Iron and Neodymium by Electrolysis of Oxygen-Bearing Salts in a Medium of Molten Fluorides", U.S. Patent No. 4,828,658, issued 9 May 1989.

[18] K. Itoh, Y. Watanabe, E. Nakamura, M. Toyoshima, "Apparatus for Producing Neodymium-Iron Alloy", U.S. Patent No. 4,747,924, issued 31 May 1988.

[19] E. Nakamura, K. Itoh, M. Nishio, M. Sakakibara, "Process for Producing Dysprosium-Iron Alloy and Neodymium-Dysprosium-Iron Alloy", U.S. Patent No. 4,737,248, issued 12 April 1988.

[20] K. Itoh, Y. Watanabe, E. Nakamura, M. Toyoshima, "Process for Producing Neodymium-Iron Alloy", U. S. Patent No. 4,684,448, issued 4 August 1987.

[21] M. Ghandehari, "Electrolytic Production of Praseodymium", U.S. Patent No. 4,627,898, issued 9 December 1986.

[22] H. Kaneko, Y. Yamamoto, and C. Okada, Electrochemistry of Rare Earth Fluoride Molten Salts, J. Alloys and Compounds, 193, 44-46 (1993).

[23] L. P. Polyakova, E. G. Ploykov, A. I. Sorokin, and P. T. Stangrit, "Secondary processes during tantalum electrodeposition in molten salts", J. Applied Electrochemistry, 22, 628-637 (1992).

[24] R. Huglen and H. Kvande, "Global considerations of aluminium electrolysis on energy and the environment", Light Metals 1994, 373-380.

[25] A. T. Tabereaux, "Anode Effects, PFCs, Global Warming, and the Aluminum Industry", JOM November 1994, 30-34.